Seismic analyses of nuclear facilities with interaction between structure and water

Comparison between methods to account for Fluid-Structure-Interaction (FSI)

Elforsk rapport 13:79

Tobias Gasch, Luca Facciolo, Daniel Eriksson,
Cecilia Rydell, Richard Malm

April 2013

ELFORSK

Seismic analyses of nuclear facilities with interaction between structure and water

Comparison between methods to account for Fluid-Structure-Interaction (FSI)

Elforsk rapport 13:79

Tobias Gasch, Luca Facciolo, Daniel Eriksson,
Cecilia Rydell, Richard Malm

April 2013

Förord

Elforsk driver forskningsprogram kring betongkonstruktioner inom kärnkraftverk. Det finns ett behov av att både bygga upp kompetens inom området och att utveckla teknikbasen för teknisk förvaltning av byggnader och konstruktioner inom kraftindustrin. Det övergripande målet med det betongtekniska programmet är att säkerställa avsedd livslängd och hög tillgänglighet för svenska kraftverk med bibehållen säkerhet och för att kunna driva en effektiv förvaltning.

Vatten som finns i bränsle- och kondensationsbassängerna har en stor inverkan på verkningssättet hos inneslutningen vid seismiska analyser. Vattnet bidrar dels med en ökad massa som sänker strukturens egenfrekvenser, dessutom bidrar vattnet till en ökad dämpning, särskilt för höga egenfrekvenser, som motverkar rörelserna orsakade av jordbävningar. För kraftbolagen, anläggningsägarna och Strålsäkerhetsmyndigheten kan dessa resultat vara till nytta och vägledning vid utvärdering av seismiska analyser på kärntekniska anläggningar. Vidare kan resultaten användas vid utvärdering av andra dynamiska belastningar som våra kärntekniska anläggningar skall dimensioneras för vid eventuella kommande krav, såsom exempelvis explosioner, tappade komponenter, flygplanskollisioner, trombinducerade missiler etc.

Betongtekniskt program kärnkraft finansieras av Vattenfall, kärnkraftverken i Forsmark, Ringhals samt OKG i Oskarshamn, Strålsäkerhetsmyndigheten (SSM) samt av Teollisuuden Voima Oy (TVO) i Finland.

Sammanfattning

Metoder för att beakta interaktionen mellan fluider och strukturer har varit ett av de främsta forsknings- och utvecklingsområdena inom numeriska metoder under de senaste åren. Detta område tillämpas inom en rad olika tekniska problem, så som flöde i blodkärl, aerodynamik och naturligtvis interaktionen mellan byggnader och vatten. En typisk tillämpning av fluid-struktur-interaktion (FSI) inom konstruktionsanalyser av kärntekniska anläggningar, uppstår vid seismisk belastning där anläggningen inkluderar vattenfyllda bassänger i olika storlekar, så som bränsle- och kondensationsbassänger. Vattnet i dessa bassänger har en stor inverkan på strukturens verkningssätt, där det dels bidrar med en ökad massa som sänker strukturens egenfrekvenser, dessutom ger vattnet upphov till hydrostatiskt och hydrodynamiskt tryck på bassängens väggar p.g.a. vågutbredningen i fluiden. Dessutom, eftersom bassängerna har en fri vattenyta så måste även den fria ytans vågutbredning beaktas, d.v.s. sloshing. Detta medför ytterligare en icke-linjäritet i problemet, eftersom en fri yta utgör ett okänt randvillkor. Huvuddelen av denna rapport utgör en state-of-the-art sammanställning, där de begrepp som är väsentliga för FSI analyser presenteras och viktiga skillnader diskuteras. På grund av alla olika tekniska tillämpningar av FSI hos olika discipliner inom forskningsområdet, så har en stor mängd metoder utvecklats. Varje metod har sina styrkor respektive svagheter beroende på vilken tillämpning som den har utvecklats för. Fokus i denna rapport har varit att beskriva de numeriska metoder samt de kategorier av metoder som är av störst intresse för konstruktionsanalyser, såsom förenklade analytiska metoder, modeller baserade på massa-fjäder system, akustiska element, Arbitrary Lagrangian-Eulerian (ALE) och coupled Eulerian-Lagrangian (CEL).

I rapporten presenteras två numeriska beräkningsexempel, avsedda att belysa skillnader mellan de olika FSI metoderna. I den första studien, studeras sloshing av en vätskefylld tank där olika numeriska metoder jämförs mot experimentellt uppmätta vågrörelser hos den fria vattenytan. Dessutom jämförs de hydrodynamiska trycken på tankens väggar mellan de olika numeriska metoderna. Resultaten visar att de flesta analysmetoder ger mycket goda resultat avseende våghöjden jämfört med de experimentella resultaten. Det bör dock nämnas att tanken belastades av en enkel harmonisk rörelse med en frekvens som inte gav upphov till några resonansvågor i vattnet. Även när det gäller det hydrodynamiska trycket erhölls en god överensstämmelse mellan de olika analysmetoderna, dock fanns inga experimentellt uppmätta tryck att jämföra mot. Det noterades också att den huvudsakliga variationen i tryckfördelning uppstod nära den fria vattenytan, vilket indikerar att den huvudsakligen beror på det konvektiva trycket, d.v.s. orsakat av ytvågor. Detta illustrerar att finita element program som förenklat beskriver FSI analyser genom att endast inkludera den impulsiva massan inte bör användas för denna typ av analys. I det andra beräkningsexemplet, jämförs de numeriska metoderna vid olika typer av seismiska tidssignaler, d.v.s. en stor jordbävning bestående av huvudsakligen lågfrekvent innehåll vilket är typiskt för en jordbävning på USA:s västkust, samt en mindre jordbävning med relativt hög grad av högfrekvent innehåll vilket motsvarar en svensk jordbävning. En viktig iakttagelse var att den relativa ökningen av inducerade spänningar i strukturen, med respektive utan hänsyn till vattnet, var betydligt större för den svenska jordbävningen än för motsvarande

amerikanska. En möjlig orsak till detta kan vara att den svenska jordbävningen inte är tillräckligt stor för att excitera den relativt styva strukturen utan vatten, men att den orsakar signifikanta dynamiska effekter i vattnet som ger upphov till högre spänningar i betongen. Detta belyser därmed vikten av att inkludera vatten i seismiska analyser.

Summary

Methods to describe the interaction between fluids and solids has been one of the biggest focus points for the research within the field of computational engineering for the recent years. This area is of interest to a variety of engineering problems, ranging from flow in blood vessels, aerodynamics and of course the interaction between water and civil engineering structures. The typical civil engineering application of fluid-structure interaction (FSI) encountered in a nuclear facilities is obtained at seismic loading, where the nuclear facilities consists of water filled pools of various sizes, for example the spent fuel and condensation pools. These water filled pools contribute with added mass to the structure, which lowers the natural frequency of the structure as well as hydrostatic and hydrodynamic pressure that acts on the walls of the pool due to wave propagation in the fluid. In addition, as the pools also have a free water surface towards the environment of the structure, free surface wave propagation also has to be accounted for; i.e. sloshing. This introduces extra non-linearity to the problem, since a free surface constitutes a boundary condition with an unknown location.

The main part of this report constitutes as a state-of-the-art summary where concepts important for FSI analyses are presented and important differences are discussed. Due to the different interests of the numerous disciplines engaged in this research area, a large number of methods have been developed, where each has different strengths and weaknesses suited for the problem in mind when developing the method. The focus of this report have been to describe the most important numerical techniques and the categories of methods that or of most interest for civil engineering problems, such as simplified analytical or mass-spring models, Acoustic Elements, Arbitrary Lagrangian-Eulerian (ALE) and coupled Eulerian-Lagrangian (CEL).

Thereafter two benchmark examples are presented, intended to highlight differences between the different methods. In the first study, sloshing of a liquid tank is studied where the numerical methods are compared to experimental results, regarding the movement of the free water surface. In addition, the hydrodynamic (fluid) pressures on the walls of the tanks are compared between the different numerical methods. It was shown that most analysis methods give accurate results for the sloshing wave height when compared with the experimental data. It should however be mentioned that the tank was only excited by a simple harmonic motion with a frequency that do not give rise to any resonance waves in the water body.

Also when it comes to fluid pressure good agreement between the different analysis methods was found, although no experimental data was available for this parameter. It was also noticed that for the sloshing tank, most of the change in pressure occurred close to the free surface of the water, which indicates that it mainly consists of a convective pressure, i.e. from the sloshing. Thereby, finite element programs that account the impulsive mass in civil engineering FSI problems should not be used for this type of analysis. In the second study, the numerical methods are compared based on different types of seismic input, such as a large earthquake with mainly low frequency content typically like an earthquake on the US west coast and one smaller earthquake with relatively higher degree of high frequency content typically like a Swedish type of earthquake. One important observation was that the

relative increase in induced stresses in the structure, with and without consideration of the water was significantly larger for the Swedish earthquake than for the US earthquake. One possible reason for this may be that the Swedish earthquake is not large enough to excite the relatively stiff structure without any water, but it will induce significant dynamic effects in the water which give rise to higher stresses in the concrete as well. However, this shows that it is very important to include water in seismic analyses.

Table of Contents

List of abbreviations

ALE	Arbitrary Lagrangian Eulerian
BWR	Boiling Water Reactor
CEL	Coupled Eulerian-Lagrangian
CFD	Computational Fluid Dynamics
CSM	Computational Solid Mechanics
DNS	Direct Numerical Simulation
FEM	Finite Element Method
FSI	Fluid-Structure Interaction
LES	Large Eddy Simulation
OBE	Operational Basis Earthquake
PDE	Partial Differential Equation
PFEM	Particle Finite Element Method
PWR	Pressure Water Reactor
RANS	Reynolds Averaged Navier-Stokes Equation
RSM	Reynolds Stress Models
SPH	Smooth Particle Hydrodynamics
SRSS	Square Root of the Sum of Squares
SSE	Safe Shutdown Earthquake
VOF	Volume of Fluid

1 Introduction

1.1 Background

Performing seismic evaluation of nuclear facilities requires detailed analyses of large and complex buildings. In addition, these buildings contain water filled pools of various sizes, for example the spent fuel and condensation pools. In Figure 1-1, sketches of a Swedish BWR reactor (Forsmark I) and a Swedish PWR reactor (Ringhals III) are shown and in Figure 1-2 another example of a nuclear facility with a large volume of water, the SKB interim storage facility (Clab), is illustrated.

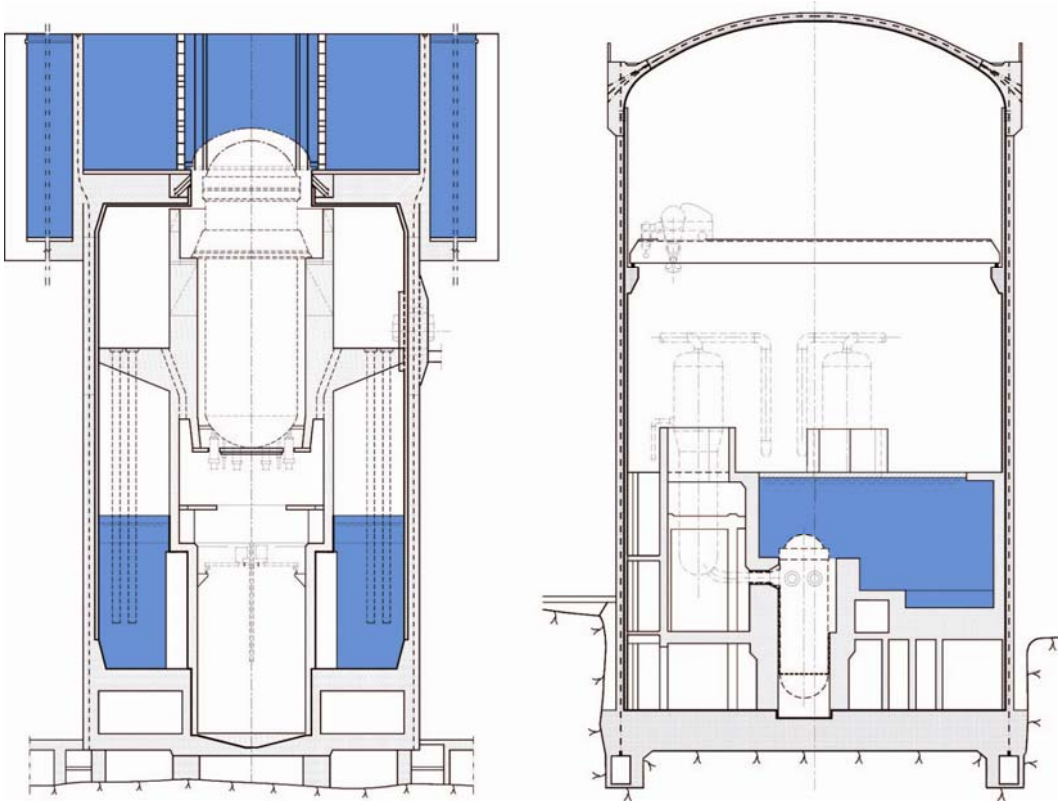

Figure 1-1: Sketch of a BWR (Forsmark I) and PWR (Ringhals III) reactor, from Roth et al (2002).

Figure 1-2: Illustration of SKB interim storage facility Clab.

These water filled pools will affect the dynamic behaviour of the structure in different ways during a seismic analysis. The first effect is that mass of the water will reduce the natural frequencies compared to the original concrete structure. The second effect is that the water will contribute with hydrostatic and hydrodynamic water pressure that will act on the walls of the pools, due to the wave propagation in the fluid. Furthermore, the pools also have a free surface towards the environment so the free surface wave propagation, i.e. sloshing, also influence the behaviour.

There are several different methods, in numerical analyses, to account for the fluid structure interaction (FSI) with varying level of detail. A fluid structure interaction (FSI) problem is generally defined as a problem where one or more deforming solids interact with an internal or surrounding fluid flow. FSI problems have been one of the biggest focus points for research within the field of computational engineering for the recent years.

The purpose of this project is to give a presentation of different methods that could be used for seismic analyses of nuclear facilities including fluid structure interaction. In this report the classification between the different FSI methods is based on which reference frame the fluid is described in; Eulerian, Lagrangian or Arbitrary Lagrangian-Eulerian. The aim is not to give the reader a complete theoretical and mathematical description of every method, but instead focuses on the concepts, ideas and assumptions of the method as well as its advantages and disadvantages. In addition, these methods will be compared with two different benchmark examples that are presented in chapter 6.

- Sloshing of a liquid tank
- Seismic analysis of a simplified BWR containment (elevated pool).

In the first study, the numerical methods are compared to experimental results, regarding the movement of the free water surface. In the second study, the different methods are compared based on different types of seismic input, such as a large earthquake with mainly low frequency content typically like an earthquake on the US west coast and one smaller earthquake with relatively higher degree of high frequency content typically like a Swedish type of earthquake.

The aim of this project was to develop a report that could be used as a guideline for performing structural seismic analyses on nuclear facilities that includes fluid structure interaction.

1.2 Project organisation

The project group consists of representatives from Vattenfall Research and Development / Vattenfall Engineering and KTH Royal Institute of Technology. The project is financially supported by Elforsk AB, the Swedish Power Companies R&D association.

The project is coordinated by Dr. Richard Malm from Vattenfall R&D and KTH, who also contributes with knowledge on advanced structural analyses. Dr. Luca Facciolo from Vattenfall R&D contributed with knowledge on fluid mechanics. The PhD candidate Ms. Cecilia Rydell from Vattenfall R&D and KTH contributed with knowledge on Seismic analyses. Mr. Daniel Eriksson and Mr. Tobias Gasch both from Vattenfall R&D contribute with knowledge on advanced finite element modelling and have also done a majority of the numerical simulations presented in this report.

The work presented in this report has been reviewed by Dr. Kristian Angele (Vattenfall R&D) and by Mr. Arshad Abosh (Vattenfall R&D).

2 Seismic analysis

The response of a damped linear elastic multi-degree-of-freedom system subjected to seismic excitation is governed by the following system of differential equations (see e.g. Chopra, 2001):

$$\mathbf{m\ddot{u}} + \mathbf{c\dot{u}} + \mathbf{ku} = -\mathbf{m}\{\mathbf{1}\}\ddot{x}_g(t)$$

$\mathbf{m}$	Mass matrix
$\mathbf{\ddot{u}}$	Relative acceleration
$\mathbf{c}$	Viscous damping matrix
$\mathbf{\dot{u}}$	Relative velocity
$\mathbf{k}$	Stiffness matrix
$\mathbf{u}$	Relative displacement
$\{\mathbf{1}\}$	Column vector of ones
$\ddot{x}_g(t)$	Ground acceleration

The first term is the *inertia forces*, the second the *damping forces*, the third the *spring forces* (or *restoring forces*) and the right hand side is *the equivalent seismic forces*. The solution to the differential equations governs the relative displacements $\mathbf{u}(\mathbf{t})$ (absolute displacement minus ground displacement) wherefrom the stresses can be calculated. The forces acting on the system due to seismic excitation depend on both the seismic excitation itself and the response of the system/structure.

The nature of the problem (damping, linear/nonlinear etc.) will decide what method to use in solving for the displacements. Three methods are briefly described below; two based on modal superposition and one using direct time integration.

2.1 Mode superposition methods

The equation of motions can be transformed into a set of uncoupled modal equations provided that the system is classically damped (damping matrix is diagonal) and its response is within its linear elastic range. The response can thus be computed for each mode and then the contributions from all the modes can be combined (superposed) to give the total response. Here two procedures are presented; the modal dynamic time history method and the response spectrum method. In the first method the seismic excitation is represented by a ground acceleration time history giving a time history response. The second method uses a response spectrum describing the seismic excitation, but with this method only the peak response is obtained.

2.1.1 Modal dynamic time history method

In the first step of the modal dynamic time history analysis the natural frequencies of free un-damped vibration are determined, whereby the damped natural frequencies of vibration can be calculated. In this same step the modes of vibration are determined, which describe the shape of the displacements. The dynamic response is then evaluated by taking the mode-shape vector times the modal coordinate and summing these modal displacements.

Free vibration

The natural frequencies of vibration, $\omega_n\,(n = 1, 2, \dots)$, and mode shapes, $\phi_n\,(n = 1, 2, \dots)$, for the un-damped linear elastic system are determined by studying the free vibration of the system (see e.g. Chopra, 2001). The equation of motion is thus:

$$\mathbf{m\ddot{u}} + \mathbf{ku} = 0$$

The free vibration of this system in one of its natural modes can be described by:

$$\mathbf{u}(t) = Y_n(t)\phi_n$$

where $Y_n(t)$ describes the time variation of the displacement (modal coordinates) and, assuming a simple harmonic motion, can be expressed as:

$$Y_n(t) = A_n \cos \omega_n t + B_n \sin \omega_n t$$

Substituting this in the equation of motion gives:

$$[\mathbf{k} - \omega_n^2 \mathbf{m}]\phi_n = \mathbf{0}$$

which has nontrivial solutions if:

$$\det[\mathbf{k} - \omega_n^2 \mathbf{m}] = 0$$

By calculation of the determinant the natural frequencies of vibration are obtained, whereby the corresponding modes can be determined. The natural frequency of damped vibration, $\omega_{\mathrm{d}n}$, is related to the natural frequency of un-damped vibration, ω_n, through the damping ratio for each mode, ξ_n:

$$\omega_{\mathrm{d}n} = \omega_n \sqrt{1 - {\xi_n}^2}$$

The relation between the damping ratio for each mode and the damping is given below.

Response to dynamic loading

The dynamic response $\mathbf{u}(t)$ of a damped linear elastic multi-degree-of-freedom system is obtained by the mode superposition technique and expressed as (see e.g. Chopra, 2001):

$$\mathbf{u}(t) = \sum_{n=1}^{N} \phi_n Y_n(t)$$

Substituting this equation in the equation of motion gives:

$$M_n \ddot{Y}_n(t) + C_n \dot{Y}_n(t) + K_n Y_n(t) = -\phi_n^T \mathbf{m}\{\mathbf{1}\}\ddot{x}_g(t)$$

where:

$$M_n = \phi_n^T \mathrm{m} \phi_n \qquad C_n = \phi_n^T \mathrm{c} \phi_n \qquad K_n = \phi_n^T \mathrm{k} \phi_n$$

The term $\phi_n^T \mathbf{m}\{\mathbf{1}\}$ is also referred to as the *modal earthquake excitation factor* L_n. M_n, C_n, K_n and $P_n(t)$ are called the generalized mass, generalized damping, generalized stiffness and generalized force for the *n*th mode. The generalized viscous damping, C_n, is related to the damping ratio for each mode, ξ_n, by:

$$\xi_n = \frac{C_n}{2M_n\omega_n}$$

where ω_n is the n^{th} natural frequency of vibration for the system without damping.

The modal coordinates $Y_n(t)$ are evaluated using a numerical method such as for example *Newmark's method*. The total displacement response is then the summation of the responses for every mode:

$$\mathbf{u}(t) = \sum_{n=1}^{N} \phi_n Y_n(t)$$

2.1.2 Response spectrum method

In the response spectrum analysis the seismic excitation is described by response spectra. The response spectra give the maximum response of a single-degree-of-freedom oscillator as a function of its natural frequency of vibration and of its damping ratio due to a certain ground motion. It should be noted that in the design of new structures it is not appropriate to use a response spectrum. Instead a *design* response spectrum should be used, which is either specified in codes or developed for a certain site based on several ground motions. In most codes the defined spectra give the spectral accelerations.

Just as for the modal dynamic time history analysis the natural frequencies of vibration and the corresponding mode shapes for the different natural modes of vibration have to be calculated in a first step. The maximum relative displacement in mode *n* is then given by:

$$\mathbf{u}_{n,max} = \phi_n \frac{L_n}{M_n \omega_n^2} S_a(\xi_n, \omega_n)$$

where $S_a(\xi_n, \omega_n)$ is the spectral acceleration given by the response spectrum. The maximum base shear is given by:

$$\mathbf{v}_{n,max} = \frac{L_n^2}{M_n} S_a(\xi_n, \omega_n)$$

where L_n^2/M_n is the *effective modal mass* Γ_r which summed over all modes gives the total mass. To obtain the overall maximum of derived quantities, such as base shear, the square root of the sum of squares (SRSS) of all modal maximum values can be used. The SRSS is however not always the best to use and there are other methods to combine the modal contributions. See for example Reg. Guide 1.92 (US NRC, 2006) for other methods.

2.2 Direct time integration method

The method of direct time integration can be used when the system responds into the non-linear range. This method uses a numerical time-stepping procedure to solve the coupled system of differential equations of motion. The response of the non-linear system, with $\mathbf{f}_s(\mathbf{u}, \dot{\mathbf{u}})$ being the restoring force, is governed by (see e.g. Chopra, 2001):

$$\mathbf{m}\ddot{\mathbf{u}} + \mathbf{c}\dot{\mathbf{u}} + \mathbf{f}_s(\mathbf{u}, \dot{\mathbf{u}}) = -\mathbf{m}\{\mathbf{1}\}\ddot{x}_g(t)$$

with initial conditions at $t = 0$:

$$\mathbf{u} = \mathbf{u}(0) \quad \text{and} \quad \dot{\mathbf{u}} = \dot{\mathbf{u}}(0)$$

The ground motion is given as discrete values $\ddot{x}_g(t_i)$ with time interval:

$$\Delta t_i = t_{i+1} - t_i$$

The procedure starts with the known responses $\mathbf{u}_i$, $\dot{\mathbf{u}}_i$ and $\ddot{\mathbf{u}}_{\boldsymbol{i}}$ at time i satisfying:

$$\mathbf{m}\ddot{\mathbf{u}}_i + \mathbf{c}\dot{\mathbf{u}}_i + (\mathbf{f}_s)_{\boldsymbol{i}} = -\mathbf{m}\{\mathbf{1}\}\ddot{x}_g(t_i)$$

By the use of a numerical time-stepping procedure the responses $\mathbf{u}_{i+1}$, $\dot{\mathbf{u}}_{i+1}$ and $\ddot{\mathbf{u}}_{\boldsymbol{i+1}}$ at time $i+1$ can be calculated, the responses satisfying:

$$\mathbf{m}\ddot{\mathbf{u}}_{i+1} + \mathbf{c}\dot{\mathbf{u}}_{i+1} + (\mathbf{f}_s)_{\boldsymbol{i+1}} = -\mathbf{m}\{\mathbf{1}\}\ddot{x}_g(t_{i+1})$$

With $i = 1, 2, 3, \ldots$ the responses at every time instant can then be calculated. To find the unknown responses $\mathbf{u}_{i+1}$, $\dot{\mathbf{u}}_{i+1}$ and $\ddot{\mathbf{u}}_{\boldsymbol{i+1}}$ three matrix equations are needed. Two of these are derived from either finite difference equations for the velocity and acceleration vectors or from an assumption on how the response varies during a time step. The third equation is the equation of motion given above for a selected time instant. For the time instant being the current time i the method is called explicit and for the time being at the end of the step $(i+1)$ the method is called implicit.

Examples of numerical methods that are used are Central difference method, Newmark's method, Average acceleration method and Wilson's method. The method to be chosen depend on if the system is non-classically damped or non-linear.

In this study the direct time integration method will be used since most of the studied methods require this to describe the hydrodynamic effect of water.

2.3 Damping

Damping values to be used are found in Reg. Guide 1.61 (US NRC, 2007). This regulatory guide has been employed in Sweden within the nuclear power industry and give damping values acceptable to the USNRC. The values are reproduced in Table 2.1 for the safe shutdown earthquake (SSE) and the operational basis earthquake (OBE) analysis respectively (corresponding to two different stress levels). In this study, the damping ratio for the pre-stressed concrete structures is assumed to be 3% for both the Swedish earthquake and the El Centro earthquake.

Table 2.1: Damping values from Regulatory Guide 1.61 (US NRC, 2007).

Material type	Damping ratios for OBE	Damping ratios for SSE
Welded steel and friction bolted steel	0.03	0.04
Bearing bolted steel	0.05	0.07
Reinforced concrete	0.04	0.07
Pre-stressed concrete	0.03	0.05

When using direct time integration analysis the damping has to be explicitly modelled using dashpots or defined at material level as Rayleigh, Composite or Structural damping. Here the Rayleigh damping is used and the coefficients α and β are chosen to give structural response corresponding approximately to modal damping of 3%, see Figure 2-1. The damping of water is assumed to be 0.5%, as given in ASCE 4-98 (1998), see Figure 2-2.

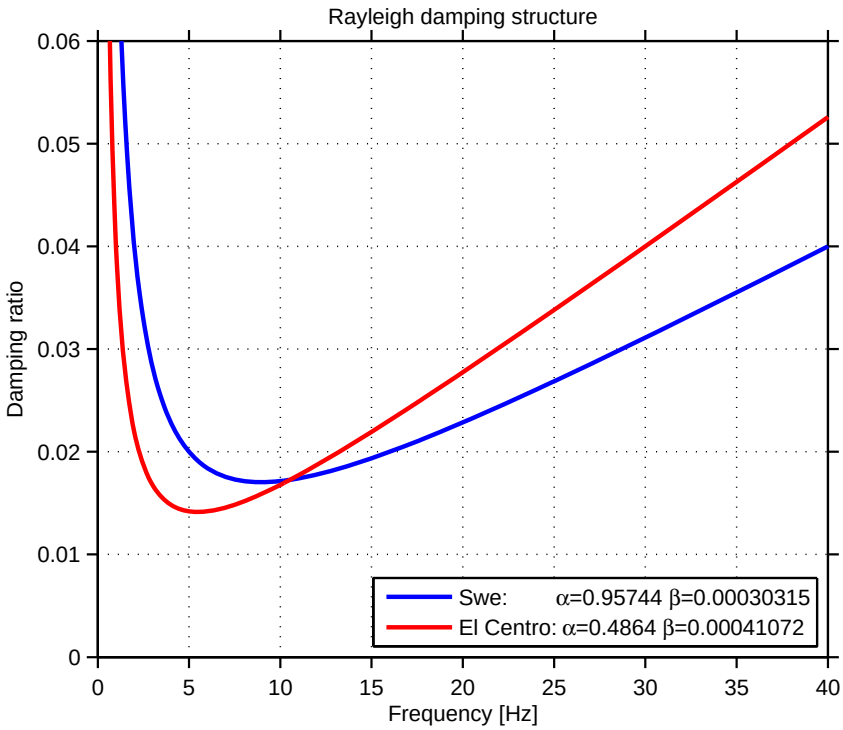

Figure 2-1 Rayleigh damping definition for the structural parts in the FE-model.

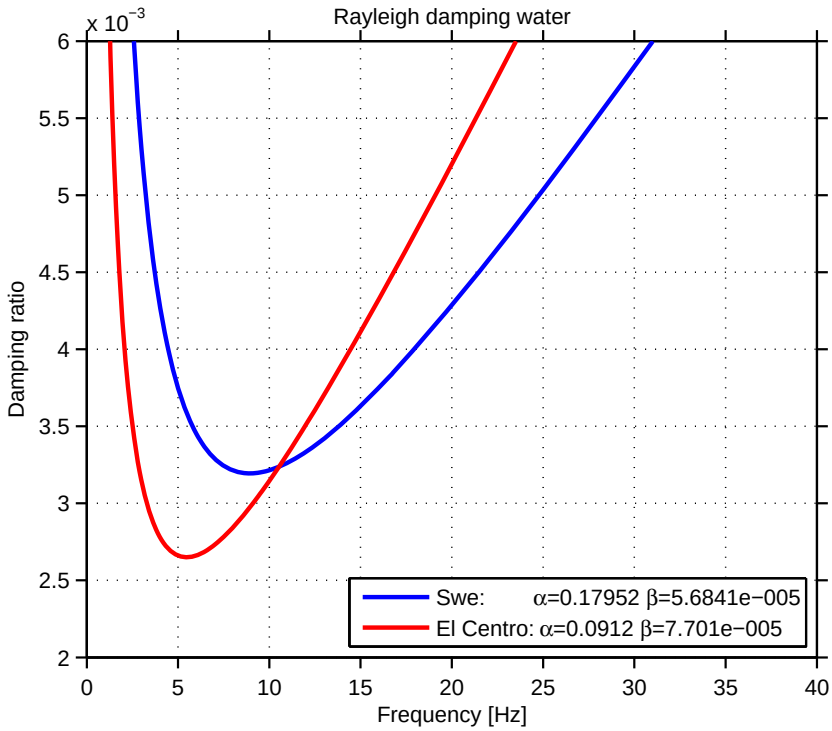

Figure 2-2 Rayleigh damping definition for the water in the FE-model.

Note that the damping definitions have been fitted to have a damping ratio less than 3 % and 0.5 %, respectively, in the frequency interval with the highest amplitudes in the two applied earthquakes, as shown in Figure 2-9.

2.4 Elements

Element size

The maximum element size is determined based on the shortest wavelength of the ground motion that is to be represented adequately by the mesh. For a sine wave at least five internodal points should fit into the shortest wavelength. The following equation is used (Dassault Systèmes, 2011):

$$L_{max} < \frac{c}{n_{min} \times f_{max}}$$

L_{max}	Maximum internodal interval of the element
c	Wave velocity (in concrete)
n_{min}	The number of internodal intervals per wavelength that is desired
f_{max}	Maximum frequency of excitation

For a frequency of excitation of maximum 100 Hz to be adequately represented by the model, wave velocity of 3000 m/s in concrete and five internodal intervals per wavelength, the maximum internodal interval of the element is 6 m. For a linear element this equals the element length, for a quadratic element this equals half the element length.

2.5 Seismic excitation

For the direct time integration analyses the seismic excitation is defined directly by the ground acceleration time history and applied to the model as a boundary condition at the base.

The seismic excitation would normally have to be considered in three directions (two horizontal and one vertical) but to facilitate comparisons to be made between the different types of analyses the ground acceleration is here only applied in the vertical direction and in one horizontal direction.

In this study, ground acceleration time histories representing a Swedish earthquake are used (CREA Consultants, 2007). In addition time histories recorded at a site in El Centro, California during the Imperial Valley, California earthquake of May 18, 1940 are also used. [obtained from http://www.vibrationdata.com/elcentro.htm].

The suite of ground acceleration time histories for the Swedish earthquake is composed of three sets, H1, H2 and V1, each consisting of five statistically independent time histories. The time histories are generated so that the averaged spectrum of each set is to match the 1E-5 Swedish response spectrum for 5% damping (SKI Technical Report 92:3), following the provisions in ASCE 4-98 (1998). Each time history is 10s long, consisting of 2001 time points, giving $\Delta t = 0.005$s. In this study the time histories denoted H1-06, H2-06 and V1-06 are used, see Figure 2-3, Figure 2-4 and Figure 2-5.

For the El Centro ground motion the two horizontal components in the north-south and east-west direction and the vertical component are used, see Figure 2-6, Figure 2-7 and Figure 2-8. The time histories are 53.78s long, with 2690 time points, giving $\Delta t = 0.02$s.

Figure 2-9 shows a combined plot of the horizontal response spectra generated from the used time histories.

To be noted is that the damping value considered for the structure, when subjected to both the Swedish and the El Centro earthquake, is 3% in this study. However, the time histories for the Swedish earthquake are generated as to match the Swedish response spectra for 5% damping. In this study this is not specifically addressed since this work is aimed at showing on the characteristics of fluid structure interaction for different levels of loading. For a design situation this would, however, have to be considered.

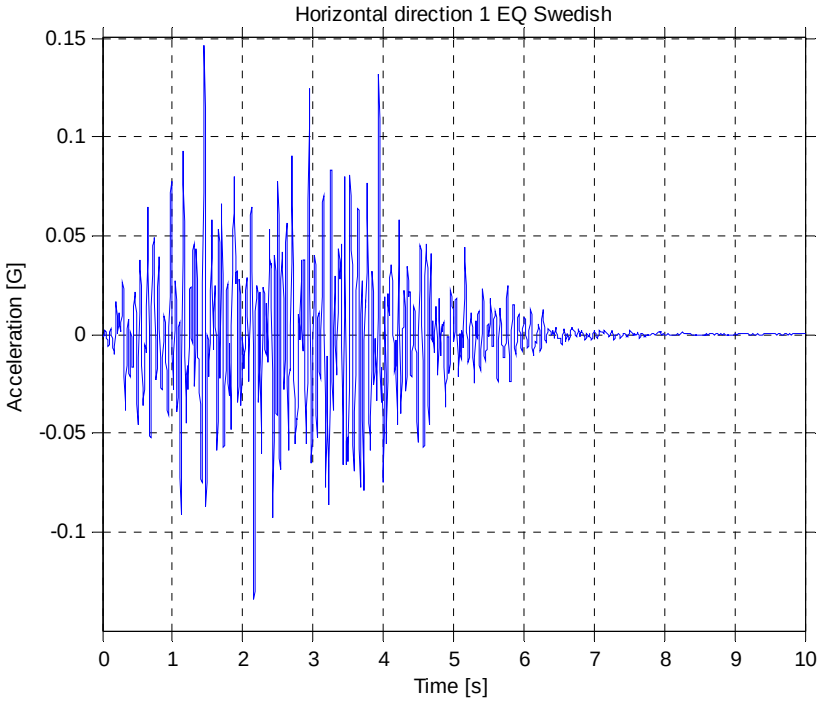

Figure 2-3: Time history of the horizontal component (H1-06) of the Swedish earthquake.

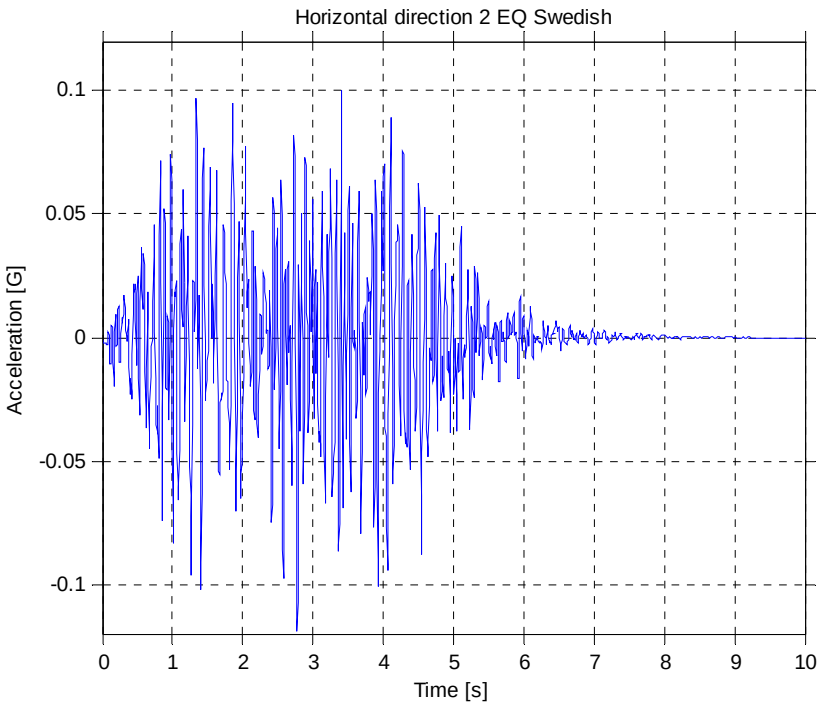

Figure 2-4: Time history of the horizontal component (H2-06) of the Swedish earthquake.

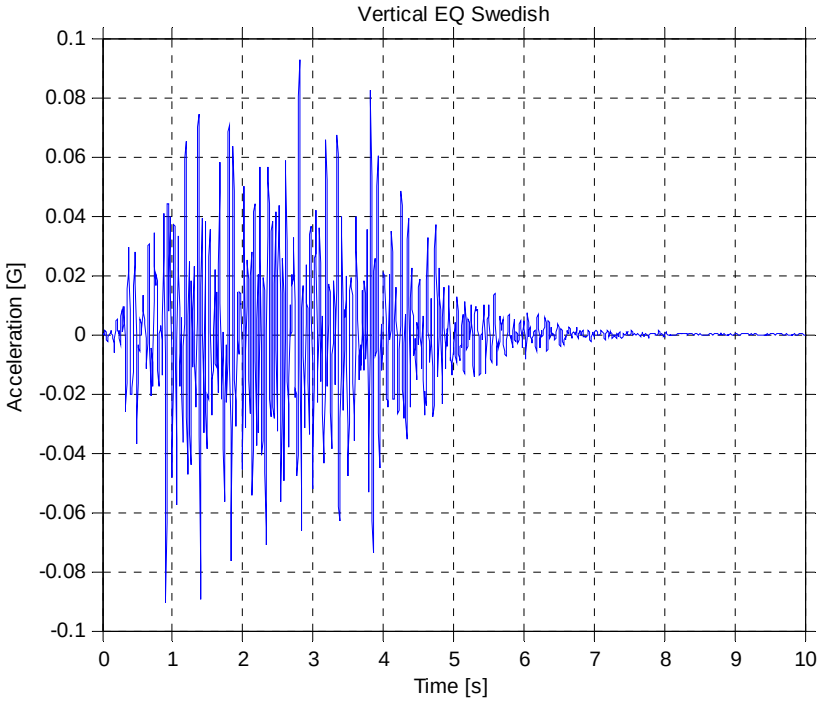

Figure 2-5: Time history of the vertical component (V1-06) of the Swedish earthquake.

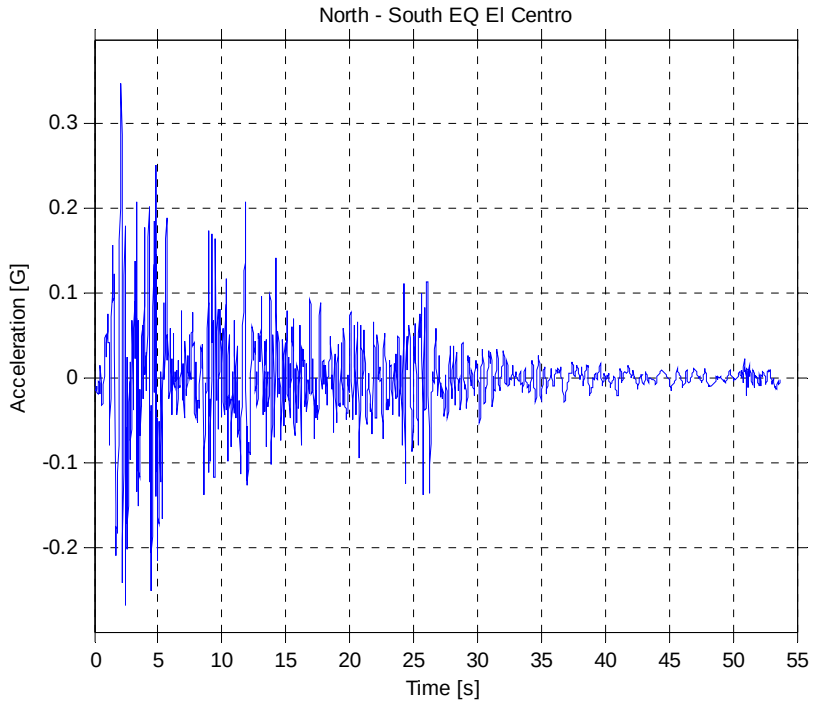

Figure 2-6: Time history of the horizontal component (NS) of the El Centro earthquake.

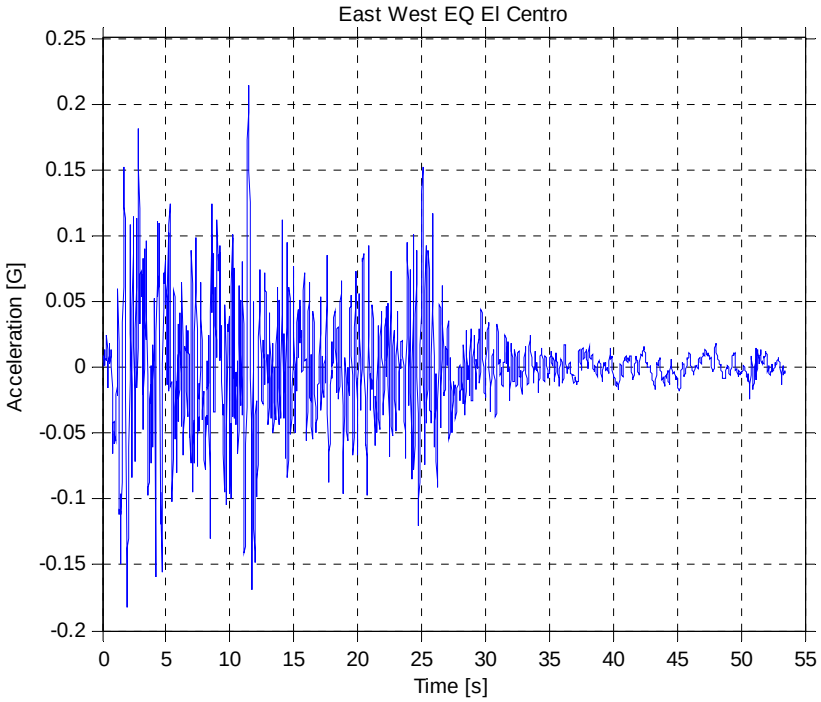

Figure 2-7: Time history of the horizontal component (NS) of the El Centro earthquake.

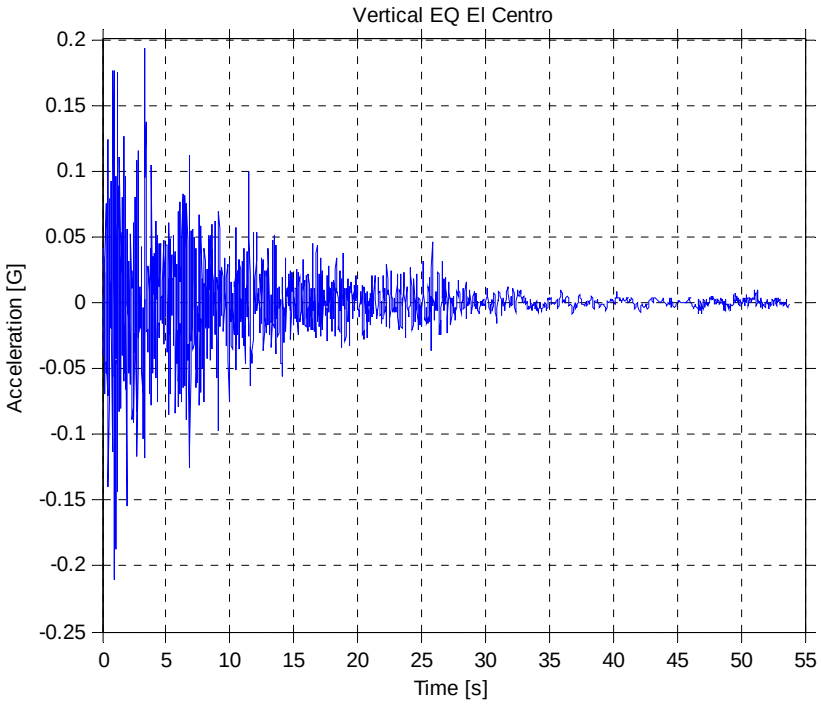

Figure 2-8: Time history of the vertical component (UP) of the El Centro earthquake.

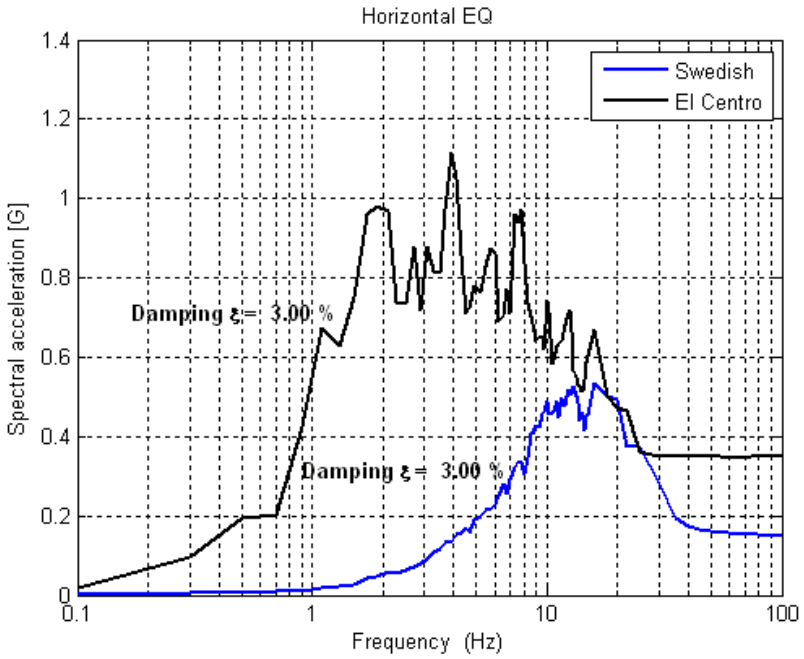

Figure 2-9: Response spectra for the horizontal components of the Swedish and the El Centro earthquake respectively.

3 Analytical methods

3.1 Codes and standards

3.1.1 ASCE 4-98

According to Section 3.1.6.3 in ASCE 4-98 (1998), fluids contained in basins within a structure shall be modelled to represent both impulsive and convective (sloshing) effects. In addition, both horizontal and vertical components of motion shall be considered.

For basins with walls that respond as a rigid body or for walls without local stress concerns, the entire horizontal impulsive mass may be located at a single height in the model. Similarly, the sloshing mass and associated horizontal spring constant may be located at a single height. The magnitudes and locations along the height of the structure for the masses and convective mode spring constants shall be determined on the basis of engineering mechanics principles.

When the basin walls do not respond as a rigid body or when local stresses are of interest, the masses and associated sloshing mode horizontal springs shall be distributed over part of the basin wall height as shown in Figure 3-1. The impulsive mass may be uniformly distributed over a height equal to twice the distance from the bottom of the basin to the center of mass (as determined for the case of a single impulsive mass as presented in Section 3.2.1). Similarly, the horizontal springs for the sloshing effect shall be distributed over a height from the top of the water surface to the center of mass (as determined for the case of a single sloshing mass as presented in Section 3.2.1). The sloshing mass M_c, shall be attached through a rigid link to the distributed springs.

The effects of water mass in the vertical direction shall be included in the building mode. For water depths less than 15 m (50 ft) the entire water mass may be lumped at the bottom of the basin. For greater depths of water, the effects due to compressibility of water shall be determined on the basis of engineering mechanics principles.

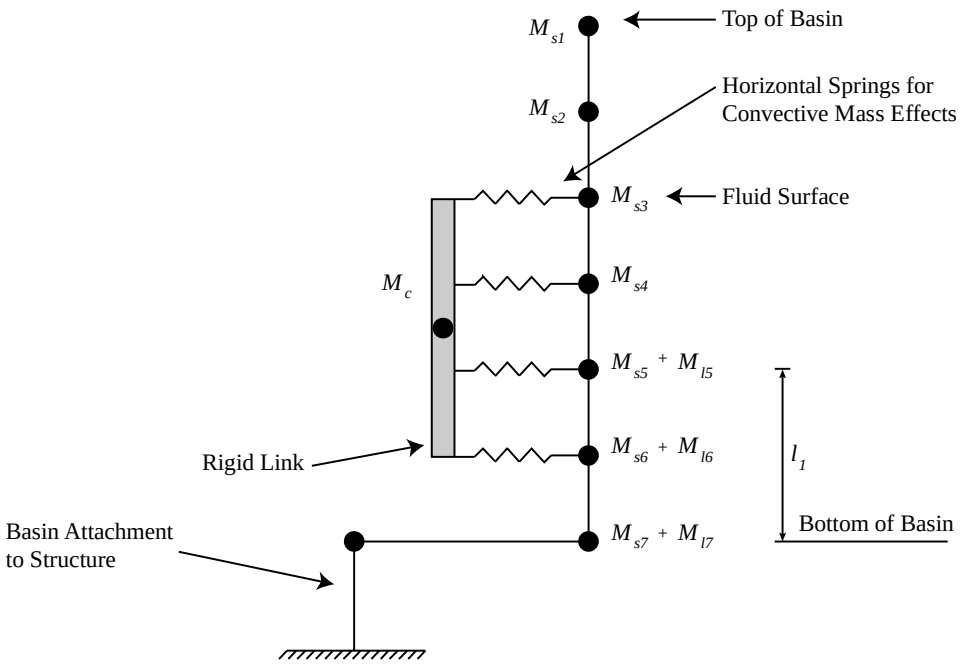

Figure 3-1: Distribution of Fluid Mass for Horizontal Seismic Response Analysis of Basins with Flexible Walls and/or Local Stress Problems. Reproduced from ASCE 4-98 (1998).

3.2 Analytical methods

Many different analytical and semi-analytical methods have been developed for liquid tank sloshing problems which can be used to verify and complement more advanced numerical methods. These methods are often limited to the analysis of tanks with simple geometries, such as rectangular or cylindrical tanks. Further, they often assume that the sloshing do not produce breaking waves or leads to waves hitting the tank ceiling or breaking over the tank walls. It is not the intention of this section to cover all methods available but it will introduce some simple methods. The methods that are presented here are the analytical methods by Westergaard (1931) and Faltinsen (1978) and the simplified approximate methods by Housner (1963) and Epstein (1972).

For a more extensive review of this research area, see for example Ibrahim (2005) or USACE 1110-6051 (2003).

3.2.1 Westergaard (1931)

Westergaard (1931) defined already in 1931 an analytical model to account for the water pressure on a dam (with a vertical upstream face) during an earthquake. In the analytical model, the water pressure of an infinite long reservoir caused by a horizontal harmonic excitation, due to the earthquake, could be considered. In this model it is assumed that the dam body is rigid.

The Westergaard hydrodynamic water pressure is shown in the following equation.

$$p = \frac{8a\rho H}{\pi^2}\cos(2\pi t/T)\sum_{n=1,3,5,\ldots}\frac{1}{n^2 c_n}\cdot e^{-q_n}\sin(n\pi(H-z)/(2H))$$

$$\text{with } c_n = \sqrt{1-\frac{16\rho H^2}{n^2 K T^2}} \text{ and } q_n = \frac{n\pi c_n Y}{2H}$$

where,

p is the hydrodynamic pressure (Pa)

ρ is the density of the fluid (kg/m^3)

t is the time (s)

T is the period of the harmonic excitation (s)

K is the bulk modulus of the fluid (Pa)

H is the depth of the reservoir (m)

Y is the horizontal distance from the dam upstream surface (m)

The boundary conditions for the Westergaard model is

- Zero velocity at the bottom of the basin (Z=0)
- The horizontal acceleration is equal to $a\cos(2\pi t/T)$ at the upstream face of the dam (Y=0)
- The water pressure is zero at the free surface (Z=H)
- The pressure converges to zero when Y becomes large.

3.2.2 Housner (1963)

Housner (1963) presented a simplified approximate method to account for the variations in water pressure during earthquakes of elevated water tanks. In this method, the fluid is replaced by an impulsive mass that is rigidly connected to the structure and a convective mass that is attached to the walls with a spring, as illustrated in Figure 3-2. In the paper by Housner (1963) equations are derived for both rectangular and cylindrical tanks, which are presented below.

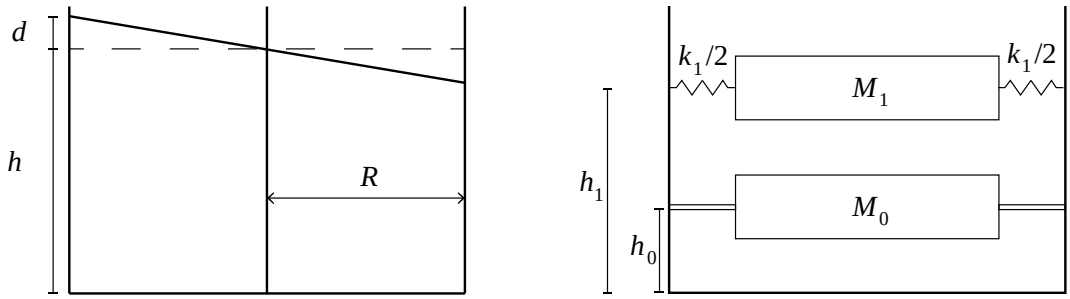

Figure 3-2: Equivalent dynamic system for a water tank, from Housner (1963).

The equations presented by Housner (1963) give good results for amplitudes of vibration $d < 0.2L$ and $d < 0.2h$, at larger vibration levels a certain amount of nonlinearity is observed in the observations.

The Housner method is based on the following assumptions, according to Seyoum (2005)

- The tanks are constant rectangular or circular sections
- Flat bottom of the tanks
- Purely horizontal seismic excitation
- Rigid tank walls

Cylindrical tank

For a cylindrical tank with a radius *R*, water depth *h* and the total mass of the water *M*, the impulsive mass M_0 and the convective mass M_1 are defined as

$$M_0 = M \frac{\tanh\left(1.7R/h\right)}{1.7R/h}$$

$$M_1 = 0.6M \frac{\tanh\left(1.8R/h\right)}{1.8R/h}$$

The convective spring stiffness is defined as $k_1 = 5.4\frac{M_1^2}{M}\frac{gh}{R^2}$

The height for the impulsive and convective masses are defined as

$$h_0 = \frac{3}{8}h\left[1+\alpha\left(\frac{M}{M1}\cdot\left(\frac{R}{h}\right)^2 - 1\right)\right]$$

$$h_1 = h\left[1 - 0.185\left(\frac{M}{M_1}\right)\cdot\left(\frac{R}{h}\right)^2 - 0.56\beta\frac{R}{h}\sqrt{\left(\frac{MR}{3M_1h}\right)^2 - 1}\right]$$

where $\alpha = 1.33$ and $\beta = 2.0$. However, if the heights h_0 and h_1 are determined on the basis of the dynamic fluid forces exerted on the walls of the tank only (not on the floor) then the following values should be used $\alpha = 0$ and $\beta = 1$.

The period of vibration of the fluid is determined as $T_w = 2\pi\sqrt{\frac{M_1}{k_1}}$

The maximum oscillation of the fluid is related to the oscillation of the convective mass M_1. If the convective mass M_1 is oscillating with displacement $x = a \cdot \sin(\omega t)$ at the crest of the wave at the wall of the tank will oscillate up and down with a displacement $y = d \cdot \sin(\omega t)$ and for a cylindrical tank the amplitude is defined as

$$d = \frac{0.63a\left(\frac{k_1 R}{M_1 g}\right)}{1 - 0.85\frac{a}{R}\left(\frac{k_1 R}{M_1 g}\right)^2}$$

Rectangular tank

For a rectangular tank with a length 2*L*, water depth *h* and the total mass of the water *M*, the impulsive mass M_0 and the convective mass M_1 are defined as

$$M_0 = M\,\frac{\tanh(1.7L/h)}{1.7L/h}$$

$$M_1 = 0.83M\,\frac{\tanh(1.6L/h)}{1.6L/h}$$

The convective spring stiffness is defined as $k_1 = 3\frac{M_1^2}{M}\frac{gh}{L^2}$

The height for the impulsive and convective masses are defined as

$$h_0 = \frac{3}{8}h\left[1 + \alpha\left(\frac{M}{M1}\cdot\left(\frac{L}{h}\right)^2 - 1\right)\right]$$

$$h_1 = h\left[1 - \frac{1}{3}\left(\frac{M}{M_1}\right)\cdot\left(\frac{L}{h}\right)^2 - 0.63\beta\frac{L}{h}\sqrt{0.28\cdot\left(\frac{ML}{M_1 h}\right)^2 - 1}\right]$$

where $\alpha = 1.33$ and $\beta = 2.0$. However, if the heights h_0 and h_1 are determined on the basis of the dynamic fluid forces exerted on the walls of the tank only (not on the floor) then the following values should be used $\alpha = 0$ and $\beta = 1$.

The period of vibration of the fluid is determined as $T_w = 2\pi\sqrt{\frac{M_1}{k_1}}$

The maximum oscillation of the fluid is related to the oscillation of the convective mass M_1. If the convective mass M_1 is oscillating with displacement $x = a \cdot \sin(\omega t)$ at the crest of the wave at the wall of the tank will oscillate up

and down with a displacement $y = d \cdot \sin(\omega t)$ and for a rectangular tank the amplitude is defined as

$$d = \frac{0.84a\left(\frac{k_1 L}{M_1 g}\right)}{1 - \frac{a}{L}\left(\frac{k_1 L}{M_1 g}\right)^2}$$

3.2.3 Epstein (1976)

The model presented by Housner (1963), as shown in 3.2.2, has a few shortcomings, such as the walls are assumed to be rigid. It has been shown in several investigations that this method is not always conservative and that the hydrodynamic forces may be underestimated Epstein (1976). To account for the flexibility of the structure, Epstein (1976) further developed Houser's method.

Epstein (1976) developed just as Housner (1963) simplified approximate solutions for rectangular and circular tanks. In addition, Epstein (1976) defined two sets of equations depending on the relation of the depth and height of the tanks. In Epstein (1976), shallow tanks (where h/L or h/R ≤ 1.5) are derived in the same manner as in Housner (1963), see section 3.2.2. For tall tanks that has a greater depth in relation to its length or radius, i.e. (h/L or h/R > 1.5) one additional impulsive mass is introduced into the system. Tall tanks are however not considered in this report, since it is considered outside of the scope of this work where the focus is on water filled pools that typically have a small depth to length ratio.

In the following only the equations for rectangular tanks are shown. The equations for a circular tank may be found in Epstein (1976). For a shallow rectangular tank with a length 2*L*, water depth *h* the relation between the depth and height is defined as

$$\alpha = \frac{h}{L} \leq 1.5$$

The total mass of the water is defined as *M*, the impulsive mass M_0 and the convective mass M_1 are defined as

$$M_0 = M\left[\frac{\alpha}{\sqrt{3}}\tanh\left(\frac{\sqrt{3}}{\alpha}\right)\right]$$

$$M_1 = M\left[\frac{0.527}{\alpha}\tanh\left(1.58\alpha\right)\right]$$

The heights for the impulsive and convective masses are derived on the basis of producing the correct moment about the base. The bending moment on a horizontal section just above the base is resisted by the tank shell. The equivalent height needed to give this moment are given by

$$h_0 = \frac{3}{8}h$$

$$h_1 = h\left[1 - \frac{\cosh(1.58\alpha) - 1}{1.58\alpha \sinh(1.58\alpha)}\right]$$

The dynamic pressure distribution on the bottom of the tank must be included in calculating the overturning moment that exists on a horizontal plane just below the base of the tank and is resisted by the foundation. If the same masses M_0 and M_1 are used to define the problem, new equivalent heights denoted by the superscript o) must be used to account for this bottom pressure. These heights are given by

$$h_0^o = \left[\frac{1}{8}\left(\frac{4}{\left[\frac{\alpha}{\sqrt{3}}\tanh\left(\frac{\sqrt{3}}{\alpha}\right)\right]} - 1\right)\right]h$$

$$h_1^o = h\left[1 - \frac{\cosh(1.58\alpha) - 2}{1.58\alpha \sinh(1.58\alpha)}\right]$$

The convective spring stiffness is according to Versluis (2010) defined as $k_1 = \left(\frac{5}{6} g \tanh^2(1.58\alpha)\right)$

The period of vibration of the fluid is determined as $T_w = 2\pi\sqrt{\frac{M_1}{k_1}}$ or

$$T_w = 2\pi\sqrt{\frac{L}{1.58g\tanh(1.58\alpha)}}$$

The maximum oscillation of the fluid is related to the oscillation of the convective mass M_1. If the convective mass M_1 is oscillating with displacement $x = a \cdot \sin(\omega t)$ at the crest of the wave at the wall of the tank will oscillate up and down with a displacement $y = d \cdot \sin(\omega t)$ and for a rectangular tank the amplitude is defined as

$$d_{\max} = \frac{0.833\left(\frac{a}{g}\right)L}{1 - 1.58\left(\frac{a}{g}\right)\tanh(1.58\alpha)}$$

The method developed by Epstein (1976) is suitable for using for instance in finite element methods when the fluid is described as a mass-spring system. In the report by USACE 1110-6051 (2003), a comparison of the maximum hydrodynamic pressure obtained from Epstein (1976) with the hydrodynamic

pressure obtained with Westergaard (1931) is presented. This comparison is shown here in Figure 3-3. The Westergaard model is as mentioned earlier based on an infinite length of the water. In the figure the results from the Epstein model are shown for an increasing length of the water (i.e. decreasing ratio of height to length). As seen in the figure the results from the Epstein model becomes similar to the Westergaard model for cases with a small height to length ratio.

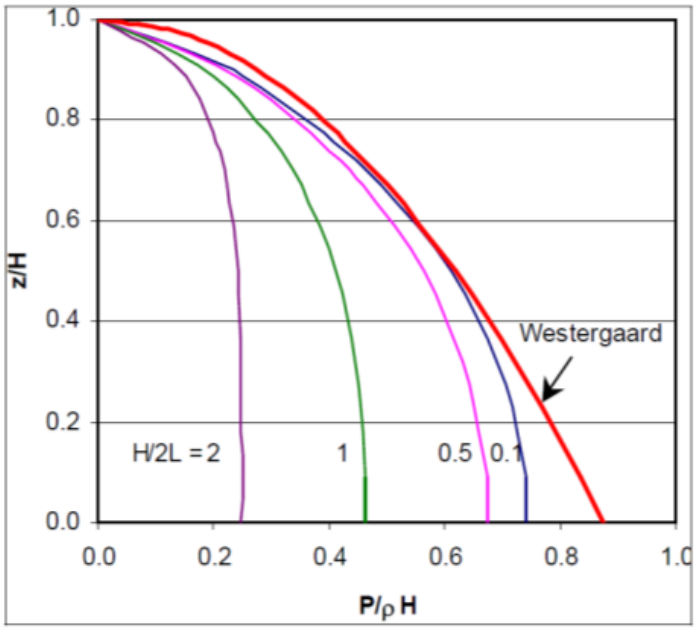

Figure 3-3: Maximum hydrodynamic pressure obtained with Epstein (1976) and Westergaard (1931) respectively.

3.2.4 Faltinsen (1978)

A simple analytical linear solution to a potential based wave theory for sloshing in a rectangular liquid storage tank can be found in Faltinsen (1978). The problem statement is for a two dimensional tank excited by a horizontal base motion described by $X(t) = A\sin(\omega t)$, where A is the excitation amplitude, t is the time and ω is the angular frequency. The liquid inside the tank is assumed to be inviscid and irrotational and the flow is two dimensional. A schematic model is depicted in Figure 3-4.

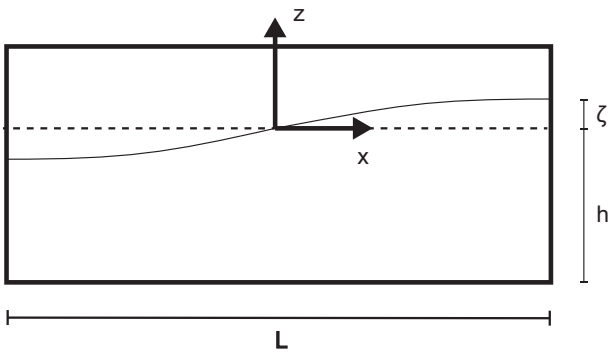

Figure 3-4: Schematic model of the considered tank.

The governing equation of the potential based theory is given by Eq. [3-1].

$$\nabla^2 \emptyset = 0 \qquad [3\text{-}1]$$

where $\emptyset$ is the velocity potential. The boundary conditions towards the fixed boundary of the tank is given by Eq. [3-2]

$$\begin{aligned} \frac{\partial \emptyset}{\partial x} &= 0, \qquad x = \pm L/2 \\ \frac{\partial \emptyset}{\partial z} &= 0, \qquad z = -h \end{aligned} \qquad [3\text{-}2]$$

where L is the width of the tank and h is the depth of the liquid. Further, the dynamic boundary condition of free surface located at $z = \xi$ can be described by Eq. [3-3].

$$\frac{\partial \emptyset}{\partial t} = \frac{\partial \emptyset}{\partial z}\frac{\partial \xi}{\partial t} - g\xi - \frac{1}{2}(\nabla\emptyset \times \nabla\emptyset) - x\ddot{X}(t) \qquad [3\text{-}3]$$

And the kinematic boundary condition of the free surface can be described by Eq. [3-4].

$$\frac{\partial \xi}{\partial t} = \frac{\partial \emptyset}{\partial z} - \frac{\partial \emptyset}{\partial x}\frac{\partial \xi}{\partial x} \qquad [3\text{-}4]$$

The above presented equations constitute a non-linear problem which is difficult to solve analytically. Apart from the equations being non-linear, the free surface conditions are imposed on the actual location of the free surface, $z = \xi$. Since the location is unknown it has to be included in the solution, which is one of the major sources of non-linearity.

Hence, in a linearized solution a couple of assumptions has to be made, first it has to be assumed that the boundary conditions of the free surface are imposed on the original location of the free surface, $z = 0$. Secondly, the second-order differential terms in Eq. [3-3] and Eq. [3-4] has to be neglected, since they are nonlinear terms. This leads to a solution with some limitations including:

- The liquid depth cannot be shallow
- The sloshing cannot include breaking waves
- The sloshing has to be moderate and the liquid must not hit any ceiling or break above the tank walls.
- The walls of the tank has to be vertical

The equations for the linearized solution from (Faltinsen, 1978) to the above system are presented in Eq. [3-5] to [3-13]. The velocity potential can be calculated according to Eq. [3-5] and the velocity potential can then be used to calculate the dynamic fluid pressure with Eq. [3-6].

$$\emptyset(x,z,t) = A\sum_{n=0}^{\infty}\left(C_n\cos(\omega t) - \left(C_n + \frac{H_n}{\omega^2}\right)\cos(\omega t)\right)\frac{\cosh\left(k_n(z+h)\right)}{\cosh(k_n h)}\sin(k_n x) \qquad [3\text{-}5]$$

$$p = -\rho\left(\frac{\partial\emptyset}{\partial t} + x\frac{d\dot{X}}{dt}\right) \qquad [3\text{-}6]$$

where $n = 0,1,2,\ldots$, is the number of eigenmodes of the fluid.

Further, the elevation of the free surface at any horizontal location can be calculated with Eq. [3-7], which contains to components. The first component, ξ_1, corresponds to the contribution from the excitation frequency ω and is calculated according to Eq. [3-8]. The second component, ξ_2, corresponds to the contribution from the natural frequencies ω_n and can be calculated according to Eq. [3-9].

$$\xi(x,t) = \xi_1(x,t) + \xi_2(x,t) \qquad [3\text{-}7]$$

$$\xi_1(x,t) = \frac{A}{g}\left(x\omega^2 + \sum_{n=0}^{\infty} C_n\omega\sin(k_n x)\right)\sin(\omega t) \qquad [3\text{-}8]$$

$$\xi_2(x,t) = \frac{A}{g}\sum_{n=0}^{\infty}\omega_n\left(C_n + \frac{H_n}{\omega^2}\right)\sin(k_n x)\sin(\omega_n t) \qquad [3\text{-}9]$$

The parameters in Eq. [3-5] to [3-9] are defined according to Eq. [3-10] to [3-13].

$$\omega_n^2 = g k_n \tanh(k_n h) \qquad [3\text{-}10]$$

$$k_n = \frac{2n+1}{L}\pi \qquad [3\text{-}11]$$

$$H_n = \omega^3 \left(\frac{4}{L}\right)\left(\frac{4(-1)^n}{k_n^2}\right) \quad [3\text{-}12]$$

$$C_n = \frac{H_n}{\omega_n^2 - \omega^2} \quad [3\text{-}13]$$

The coefficient k_n is the so called wave number. In the presented solution only uneven wave numbers are included, .i.e. $k_n = 1\pi, 3\pi, 5\pi \ldots$. To calculate the frequencies for all wave numbers $k_n = n\pi/L$ and the frequencies are calculated according to Eq. [3-11].

It should, however, be noted that the above presented solution only concern so called gravity waves which describe the movement of the free surface. Another type of waves, so called acoustic waves, might also be present which normally have a higher natural frequency then the gravity waves, normally above 100 Hz. Therefore they are normally not as dominating as the gravity waves when considering seismic loading, and are generally only of interest when looking at shock wave problems. The natural frequency for the acoustic waves for the same tank as presented above in Figure 3-4 can be calculated according to Eq. [3-14]

$$\omega_n^2 = c^2 \left(\frac{n\pi}{L} + \frac{2n+1}{2h}\pi\right) \quad [3\text{-}14]$$

where c is the wave speed of the liquid.

4 Fluid mechanics

This chapter pretends to be only a short introduction to basic fluid mechanics. For a more thorough description of the subject see for example (Tritton, 1988), (Tennekes and Lumley, 1972) or (Pope, 2000).

Fluids are present in our everyday life in physical or natural phenomena as well as in technological applications. Our life itself is strictly dependent on fluid dynamics, from the air we breathe to the blood circulating in our body to the water that constitutes the most of our body mass. The study of fluids cover many inter-disciplinal areas like biological sciences, atmospheric sciences, geophysics, oceanography, astrophysics and many industrial fields like, for example, aerospace systems, internal combustion engines, pipelines, fluid-structure interactions, heating, cooling and ventilation systems, waste disposal, pollution control systems.

The study of fluids has an old and long history. Since water is fundamental for our existence the basic practical understanding of fluid dynamics was already well clear thousands of years ago in order to supply the fields and the villages with the precious fluid.

A modern approach to fluid dynamics started with Leonardo da Vinci and continued with the studies of Euler and Bernoulli. The basic equations of fluid dynamics was derived and introduced by Navier in 1820's and completed by Stokes in 1840's. The complete set is known as Navier-Stokes equations and is of fundamental importance for all the studies and the development done in fluid dynamics.

The following section deals with the introduction and definition of fluid and its properties.

4.1 Continuum hypothesis

In order to have a proper definition of our media and matter of study, the fluid, it is necessary to make some assumptions. The fundamental idea that rules the fluid mechanics is the continuum hypothesis.

The structure of a fluid consists of billions of molecules or atoms moving more or less randomly and covering an average distance between consecutive collisions, the so-called *mean free path* indicated with λ. If L is the characteristic length of the problem under investigation the Knudsen number is defined as $Kn=\lambda/L$. The case $L>>\lambda$, or rather $Kn\rightarrow 0$, represents the condition of continuum. Under this hypothesis it is reasonable to disregard the local molecular nature of the fluid and to treat any fluid property as varying continuously within the fluid. Ultimately it is possible to associate with any volume of fluid (fluid element) the macroscopic properties (such as velocity, pressure, temperature etc.) that are associated with the bulk fluid.

4.2 Definition of fluid

A simple and effective definition of fluid is any substance that deforms continuously when subject to a shear stress (tangential force), no matter how small. In contrast, a solid can stand a deformation imposed by a shear stress until an extreme amount.

Shear stress

Shear stress is defined as a tangential force per unit area. The average shear stress acting on the fluid element is $\tau=F/S$, see Figure 4-1.

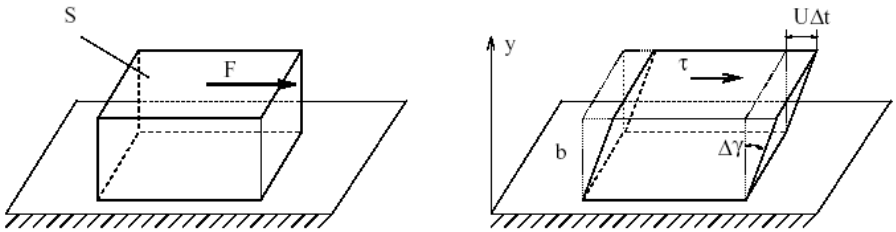

Figure 4-1: Behaviour of fluid element under shear stress.

The upper surface of the fluid element moves with velocity *U*. The lower surface at the stationary plate respects the no-slip condition: in the continuum hypothesis the fluid element is stuck to the surface.

4.3 Fluid properties

In this section we go through the transport and physical properties that distinguish the behaviour of different fluids.

4.3.1 Viscosity

The first transport property that we discuss is the viscosity. In our everyday experience viscosity corresponds to a sort of "internal resistance". As a definition we can say that viscosity is the fluid property through which the fluid offers friction to shear stress.

Newton's Law of viscosity

The definition of viscosity implies that the deformation rate is limited. Referring to Figure 4-1 by geometrical consideration:

$$tan(\Delta\gamma) = U\Delta t/b \cong \Delta\gamma, \qquad [4\text{-}1]$$

and the rate of angular deformation is:

$$\dot{\gamma} = \lim_{\Delta t \to 0} \Delta\gamma/\Delta t = U/b = dU/dy. \qquad [4\text{-}2]$$

Newton's law of viscosity states that for a given rate of angular deformation, the shear stress is proportional to the fluid viscosity:

$$\tau = \mu\dot{\gamma} = \mu\frac{dU}{dy} \qquad [4\text{-}3]$$

hence shear stress is proportional to angular deformation rate with viscosity being the constant of proportionality.

In the case the viscosity is only a function of the fluid and the temperature $\mu=\mu(fluid, T)$ then the fluid is referred as Newtonian. For the non-Newtonian fluid, the law of viscosity must be replaced with a more complicated description. The viscosity for different fluids is illustrated in Figure 4-2.

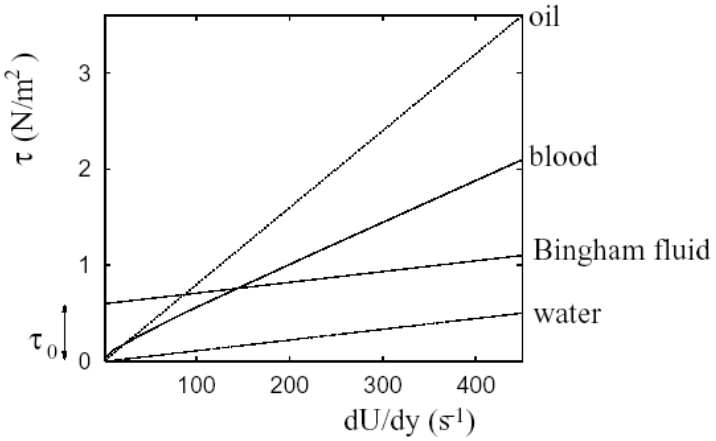

Figure 4-2: Newtonian and non-Newtonian fluids

Physical origins

Viscosity arises on molecular scales from to main mechanisms: intermolecular cohesion and transfer of molecular momentum. The first is dominant in most liquids where the molecules are relatively close to each other while the second mechanism is dominant in most gases where the molecules are more at a relative larger distance and move at higher velocity. As a consequence it is expected that the viscosity of fluids will decrease with increasing temperature, while viscosity of gases will increase.

Diffusion of Momentum

The diffusion of momentum is the mixing on molecular scales of a high momentum part of flow with a lower momentum part. In Figure 4-3 the high momentum, i.e. high speed, possessed by the top layer of the fluid attached to the upper plate is transferred to the lower layers. This can happens

because of the viscosity of the fluid, which diffuses the momentum between neighbouring layers.

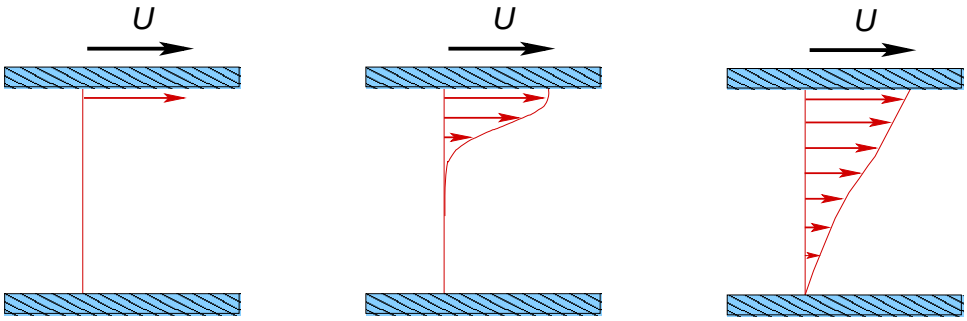

Figure 4-3: Diffusion of momentum, in early time, intermediate time, and steady state profile.

4.3.2 Thermal conductivity

Thermal conductivity is the transport property that indicates how quickly the thermal energy, heat, diffuses through a substance.

Fourier's Law of heat conductivity

Fourier´s law is the basic formulation of heat transfer:

$$q = -k\frac{dT}{dy} \qquad [4\text{-}4]$$

where q is the heat flux, the amount of heat per unit area and time, k is the thermal conductivity and dT/dy is the thermal gradient. The formula is analogous to Newton's law of viscosity. The minus sign is a convention. The dependency of k on temperature is very small at least compared with the dependency of μ.

4.3.3 Mass diffusivity

Mass diffusivity is the transport property that indicates how a certain substance can diffuse inside another substance.

Fick's Law of diffusion

Fick´s law is the basic formulation of diffusion:

$$j_1 = -\rho D_{12} \frac{dm_1}{dy} \qquad [4\text{-}5]$$

where j_1 is the mass flux of species 1 with mass fraction m_1, ρ is the density of the mixture of specie 1 and 2, while D_{12} is the mass diffusivity of specie 1 in specie 2.

4.3.4 Density

The density of a fluid is the amount of mass per unit volume. It is indicated with the Greek letter ρ, as seen in Fick´s law.

$$\rho = \frac{\Delta m}{\Delta V} \qquad [4\text{-}6]$$

In thermodynamics is common to use the *specific volume* v, that is the reciprocal of the density: $v=1/\rho$.

4.3.5 Pressure and surface tension

A fluid exerts a tangential and a normal force on the contact surface. The shear stress τ represents the tangential force per unit area as already seen. The pressure is the normal force per unit area:

$$p = \frac{\Delta F_n}{\Delta A} \qquad [4\text{-}7]$$

where ΔF_n is the normal component of the force $\Delta \boldsymbol{F}$, see Figure 4-4.

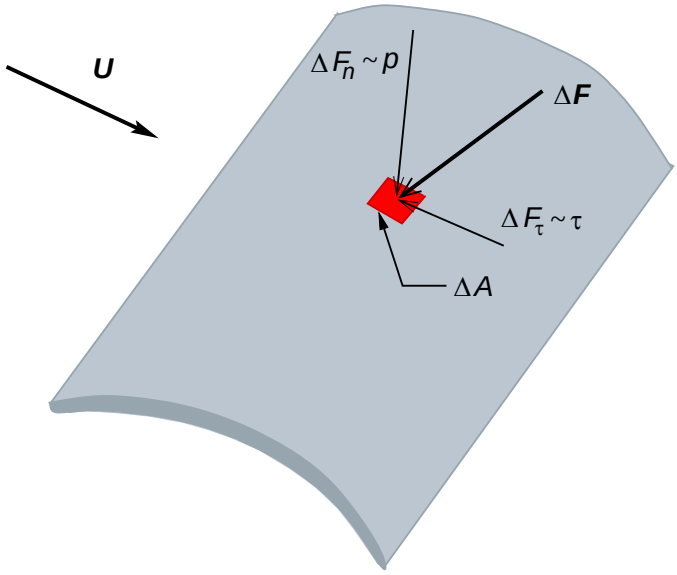

Figure 4-4: Forces on a surface, pressure and shear stress.

From the physical point of view the pressure is given by the collision of the molecules with each other and with the walls of the container. In static applications it is possible to think of the pressure as the force exerted by the weight of the fluid on a surface. If the fluid is in motion there is another pressure component to take into account.

In a gas the pressure is always a compressive force. A liquid can stand very high compressive force and also weak tensile forces which are associated to the surface tension.

For a bubble immersed in another fluid, like water in air the equilibrium equation is:

$$\Delta p = \frac{2\sigma}{r} \qquad [4\text{-}8]$$

where r is the radius of the bubble and σ is the surface tension, see Figure 4-5.

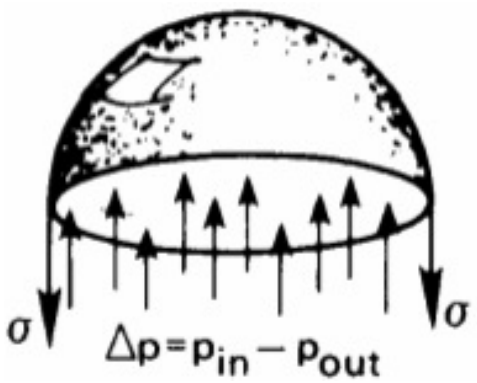

Figure 4-5: Half bubble balance.

Another surface tension effect is the capillarity: at the contact between the fluid and the surface the surface is distorted with the formation of a *meniscus* that shows a *contact angle*.

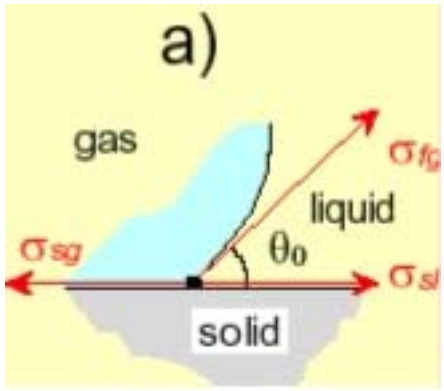

Figure 4-6: Contact angle.

On a flat surface the contact angle is ruled by Young´s equation:

$$\cos\Theta_0 = \frac{\sigma_{sg} - \sigma_{sf}}{\sigma_{fg}} \qquad [4\text{-}9]$$

The lower is Θ_o, the more the fluid is wetting.

4.3.6 Temperature

The temperature in gas is directly linked to the average translational energy of the molecules according to:

$$T = \frac{\frac{1}{2}m\overline{U^2}}{\frac{3}{2}k} \qquad [4\text{-}10]$$

where in the numerator there is the mean molecular kinetic energy and in the denominator *k* is Boltzmann´s constant.

4.3.7 Equation of state

The physical properties of a fluid can be related through various *equations of state.* For gases the equation of state of *ideal gas* is usually employed:

$$p = \rho RT \qquad [4\text{-}11]$$

where *R* is the specific gas constant. This equation is for a thermally perfect gas and it is a good approximation of real gases at moderate-high temperature and low-moderate pressure. Many other equations of state for gases and specific applications can be found in literature. For fluid the equation of state are far less general and much more complex.

4.4 Classification of flow phenomena

In this section we present a general and intuitive classification of fluid flow. This is done regarding the flow and not the fluid itself.

4.4.1 Steady and unsteady flow

A flow is characterised as *steady* if all properties of the flow are independent of time, otherwise it is *unsteady*. If the time dependency is weak such as it is reasonable the use of steady state treatment it is referred as *quasi-steady* analysis. The flow is classified as *transient* when it exhibits a short in time unsteady behaviour before reaching a proper steady state. If the flow is unsteady but shows a qualitative nature of the behaviour that can be considered fixed though the detailed motion varies in time it is referred as *stationary* flow.

4.4.2 Flow dimensionality

The dimensionality of the flow is given by the number of coordinate necessary to describe all properties of the flow. In general a flow can be described as 1-D, 2-D or 3-D.

4.4.3 Uniform and non-uniform flows

In a uniform flow all velocity vector are identical in all flow field at any time, otherwise it is non-uniform.

4.4.4 Rotational and irrotational flows

A flow is said *rotational* if it has *vorticity*, otherwise, if the vorticity is zero, the flow is *irrotational*. The vorticity is mathematically defined as in 3-D:

$$\omega = \nabla \times \boldsymbol{U} = \begin{vmatrix} i & j & k \\ \frac{\partial}{\partial x} & \frac{\partial}{\partial y} & \frac{\partial}{\partial z} \\ u & v & w \end{vmatrix} = \left(\frac{\partial w}{\partial y} - \frac{\partial v}{\partial x}\right) i + \left(\frac{\partial u}{\partial z} - \frac{\partial w}{\partial x}\right) j + \left(\frac{\partial v}{\partial x} - \frac{\partial u}{\partial y}\right) k \quad [4\text{-}12]$$

where $\boldsymbol{U}=(u,v,w)^T$ is the fluid velocity.

Shear flows

Shear flow are typical example of rotational flow. Noting the 1-D example shown in Figure 4-1 and Figure 4-3 there is no sign of swirl or vortex but there is rotation of fluid element.

4.4.5 Viscous and inviscid flows

All fluids have viscosity but if the forces generated by the viscosity on the fluid element are small compared with other forces then it is reasonable to treat the fluid as *inviscid* ignoring the viscous effects. On the other hand, if viscous effects are important and cannot be neglected, the flow is *viscous*.

4.4.6 Incompressible and compressible flows

If the density of the flow is constant then the flow is *incompressible*, otherwise it is *compressible*. In general gases are compressible flow but in many applications the variation of density is marginal and they can be considered incompressible.

4.4.7 Laminar and turbulent flows

Sir Reynolds performed a series of experiments in the 1880's and 1890's. His job is, still today, the best and easiest understanding of the nature and distinction between *laminar* and *turbulent* flow. The word *turbulence* has been introduced by Leonardo da Vinci who first described this type of flow behaviour with the help of sketches.

Sir Reynolds, in his famous experiment of flow running in a pipe, see Figure 4-7, noted that the behaviour of the flow changes with different velocity of

the flow. He injected dye at the centreline of a pipe where water was running at a given constant velocity.

He noticed that for a low velocity, the dye was following a smooth and very regular trajectory: this condition is denoted as laminar (top in Figure 4-7). Increasing the flow velocity the dye begins to show a wavy, basically periodic, motion that is time dependent: it is the transitional flow (in the middle of Figure 4-7). At a higher flow rate the dye shows a much more complicated three dimensional, time dependent paths that exhibit a high degree of mixing: this is the turbulent flow (bottom of Figure 4-7).

It is worth to note that the same flow behaviour with the passage from laminar to transient and finally turbulent regime can be detected in space: a flow that is at the beginning laminar undergoes instabilities that develop turbulence.

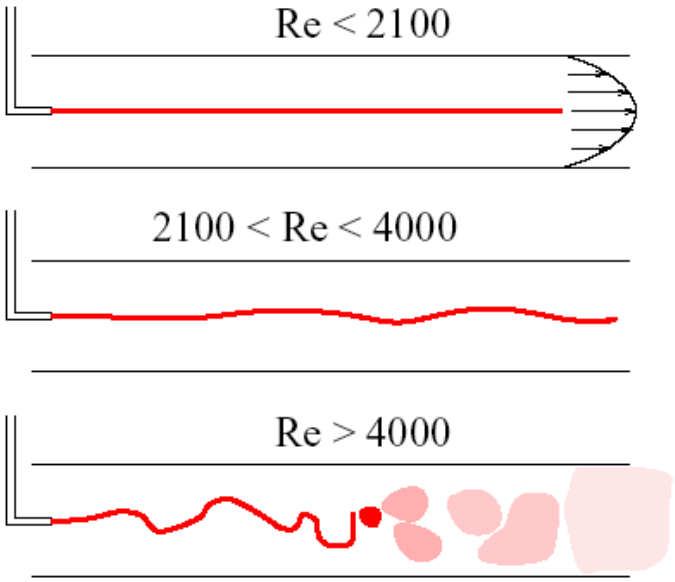

Figure 4-7: Reynolds experiment visualising laminar, transitional and turbulent flow.

The Reynolds´ number *Re*, ratio between inertial and viscous forces, is used to characterize the flow regime.

4.4.8 Separated and unseparated flows

If the flow stays "attached" following the surface in all domain at any time then it is denoted as *unseparated.* On the other end, if the flow cannot follow the surface and generates vortices and recirculation zones it is referred as *separated*, see Figure 4-8.

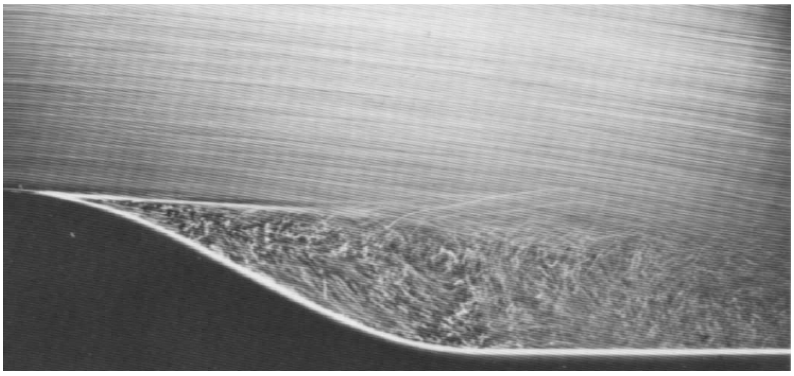

Figure 4-8: Visualization of flow separation.

4.5 Equation of fluid motion

This section will give a short overview of the fundamental equations of fluid mechanics and an introduction to Navier-Stokes equations that represent, even if only partially understood, the motion of the fluid in the continuum hypothesis.

Before getting into equations it is required to build up the frame of reference. In fluid dynamics there are two ways to view the flow motion: the *lagrangian* and the *eulerian* point of view.

4.5.1 Lagrangian coordinate

In the lagrangian coordinate system the motion of the flow is seen from the fluid element point of view: the observer follow the fluid element as it moves in space and time. As an example it looks like to follow the flow from a boat that drift down the river.

4.5.2 Eulerian coordinate

In the eulerian coordinate system the motion of the flow is seen from a fix point of view: the observer follows the flow as it change in time at a fix point of view. It is often referred as laboratory frame. As an example it looks like sitting on a bridge and watching the water in the river passing down.

4.5.3 The substantial derivative

The *substantial* or *material derivate* of a certain property is the eulerian representation of the lagrangian derivative of that property.

In a lagrangian coordinate system the spatial coordinate of fluid elements change in time. If we consider a general property $f(t,x,y,z) = f(t,x(t),y(t),z(t))$ and we differentiate it with respect to time t using the chain rule:

$$\frac{Df}{Dt} = \frac{\partial f}{\partial t}\frac{dt}{dt} + \frac{\partial f}{\partial x}\frac{dx}{dt} + \frac{\partial f}{\partial y}\frac{dy}{dt} + \frac{\partial f}{\partial z}\frac{dz}{dt} = \frac{\partial f}{\partial t} + u\frac{\partial f}{\partial x} + v\frac{\partial f}{\partial v} + w\frac{\partial f}{\partial z} = \frac{\partial f}{\partial t} + \boldsymbol{U}\cdot\nabla f \qquad [4\text{-}13]$$

where $\boldsymbol{U}=(u,\ v,\ w)^T$ is the velocity vector.

In the case of velocity components the substantial derivative is the *lagrangian acceleration.* Just considering the x component, $f=u$, the lagrangian or total acceleration a_x in the eulerian frame of reference is:

$$\frac{Df}{Dt} = \frac{\partial u}{\partial t} + u\frac{\partial u}{\partial x} + v\frac{\partial u}{\partial v} + w\frac{\partial u}{\partial z} \qquad [4\text{-}14]$$

The first term on RHS is the *local acceleration* that is the variation of velocity respect to time in a fix spatial location as seen from the eulerian point of view. The second term represents the *convective acceleration* $U\cdot\nabla u$ that depends on local velocity and local velocity gradient. It represents spatial changes of velocity due to motion of the fluid element convected by the flow field. It implies that the flow can spatially change, accelerate, being time independent i.e. steady flow.

4.5.4 Gauss´s theorem (divergence)

We now need to introduce some mathematical tool to derive later the equation of fluid motion.

We start with the *Gauss* or *divergence theorem*: if $\boldsymbol{F}$ is a continuously differentiable vector field defined on a neighbourhood volume *V* defined by a piecewise smooth boundary surface *S* then we have:

$$\iiint_V (\nabla\cdot\boldsymbol{F})\,dV = \oiint_S (\boldsymbol{F}\cdot\boldsymbol{n})\,dS \qquad [4\text{-}15]$$

where $\nabla\cdot\boldsymbol{F}$ is the divergence and n is the vector locally normal to the surface. The equation can be interpreted as the radiation of a quantity from a volume (LFH) equals the flux of the quantity coming through the surface of the volume (RHS).

4.5.5 Transport Theorems

Transport theorems come in deriving the equations of fluid dynamics and transport phenomena. The basic problem is moving the differentiation of an integral directly to the integrand.

General transport

If ***F*** is a continuously differentiable vector or scalar field defined on a neighbourhood volume *V* defined by a piecewise smooth boundary surface *S* and W is the velocity field of the time independent movement of *S* then we have:

$$\frac{d}{dt}\int_V \boldsymbol{F}(\boldsymbol{x},t)dV = \int_V \frac{\partial \boldsymbol{F}}{\partial t}\,dV + \int_S \boldsymbol{FW}\cdot\boldsymbol{n}\,dS \qquad [4\text{-}16]$$

Reynolds transport

A corollary of the *general transport theorem* is the *Reynolds transport theorem.*

Let ***F*** be any continuously differentiable vector or scalar field defined on a fluid element *V* with surface *S* traveling at the flow velocity ***U***, then:

$$\frac{D}{Dt}\int_V \boldsymbol{F}\,dV = \int_V \frac{\partial \boldsymbol{F}}{\partial t}\,dV + \int_S \boldsymbol{FU}\cdot\boldsymbol{n}\,dS \qquad [4\text{-}17]$$

The LHS is now differentiated with respect to the substantial derivative and in the second term of the RHS there is the fluid element velocity.

4.5.6 Conservation of mass

From a thermodynamical point of view a system can be *open* or *closed*. Considering a volume or a fluid element it is important to have a fix mass, independently weather it is the same mass all the time: only that the amount is the same.

Generally, we can define an extensive property *B* through an intensive property *b* in a volume *V*:

$$B = \int_V \rho b\,dV \qquad [4\text{-}18]$$

Considering b=1, *B* results to be the mass in the volume *V*:

$$m = \int_V \rho\,dV \qquad [4\text{-}19]$$

If we want to impose the mass conservation in the fluid element volume *V* that can change in time it is necessary to have a zero change of rate of the mass:

$$\frac{dm}{dt} = \frac{d}{dt}\int_V \rho \, dV = 0 \qquad [4\text{-}20]$$

4.5.7 Continuity equation

Now we can apply the mathematical tools we have just introduced. Using the general transport theorem it is possible to write the conservation of mass as:

$$\frac{dm}{dt} = \int_V \frac{\partial \rho}{\partial t} \, dV + \int_S \rho \boldsymbol{U} \cdot \boldsymbol{n} \, dS = 0 \qquad [4\text{-}21]$$

where $\boldsymbol{U}$ is the fluid element velocity. Now, with the help of Gauss´s theorem:

$$\int_V \left(\frac{\partial \rho}{\partial t} + \nabla \cdot (\rho \boldsymbol{U}) \right) dV = 0 \qquad [4\text{-}22]$$

that is the integral *continuity equation.* In a differential form the continuity equation is:

$$\frac{\partial \rho}{\partial t} + \nabla \cdot \rho \boldsymbol{U} = \frac{\partial \rho}{\partial t} + \boldsymbol{U} \cdot \nabla \rho + \rho \nabla \cdot \boldsymbol{U} = 0 \qquad [4\text{-}23]$$

For an incompressible flow the density ρ is a constant so that the continuity equation is reduced to:

$$\nabla \cdot \boldsymbol{U} = 0 \qquad [4\text{-}24]$$

Control-volume continuity equation

The continuity equation has to hold in any point of the fluid. Now, considering a control-volume instead of a fluid element volume, the continuity equation is:

$$\frac{d}{dt}\int_V \rho\, dV + \int_S \rho(\boldsymbol{U}-\boldsymbol{W})\cdot\boldsymbol{n}\, dS = 0 \qquad [4\text{-}25]$$

where $\boldsymbol{U}$ is the fluid velocity and $\boldsymbol{W}$ is the control-surface velocity. The products $\boldsymbol{U}\cdot\boldsymbol{n}$ and $\boldsymbol{W}\cdot\boldsymbol{n}$ are obviously zero on the fixed solid surfaces and identical on the moving surfaces. That means the surface integral needs to be calculated only on the surface where the flow can enter or exit through.

$$\frac{d}{dt}\int_V \rho\, dV = \int_S \rho(\boldsymbol{W}-\boldsymbol{U})\cdot\boldsymbol{n}\, dS \qquad [4\text{-}26]$$

is the *control-volume continuity equation* and expresses the balance between the time rate of increase of control volume mass, LHF, and the net mass flux into the control volume, RHS.

4.5.8 Momentum Balance

Following Newton´s second law of motion, in fluid dynamics we can say that the time rate change of momentum of a fluid volume must balance the sum of forces acting on the same fluid volume.

Newton´s second law of motion

The momentum is the product of mass times the velocity so, a general expression for Newton's second law in 1D is:

$$F = \frac{d(mu)}{dt} \qquad [4\text{-}27]$$

that is possible to express per unit volume:

$$\frac{F}{V} = \frac{d(\rho u)}{dt} \qquad [4\text{-}28]$$

Time-rate change of momentum

As already for the mass conservation, we can write the momentum conservation. The time rate of change of momentum for a fluid element using a eulerian coordinate system that requires the substantial derivative is:

$$\frac{D}{Dt}\int_V \rho\boldsymbol{U}\, dV \qquad [4\text{-}29]$$

This needs to be balanced by the forces acting on the fluid element.

Forces

The forces are the body forces $\boldsymbol{F}_B$, acting on the volume $\boldsymbol{V}$ and the surface forces $\boldsymbol{F}_S$, acting on the surface $\boldsymbol{S}$.

Momentum equation of fluid flow

So, the complete balance is:

$$\frac{D}{Dt}\int_V \rho \boldsymbol{U}\, dV = \int_V \boldsymbol{F}_B\, dV + \int_S \boldsymbol{F}_S\, dS \qquad [4\text{-}30]$$

The LFH, with the help of Reynolds transport theorem and Gauss´ s theorem, become, in the *x* component:

$$\frac{D}{Dt}\int_V \rho u\, dV = \int_V \frac{\partial \rho u}{\partial t}\, dV + \nabla \cdot (\rho u \boldsymbol{U})\, dV \qquad [4\text{-}31]$$

where $\nabla \cdot (\rho u \boldsymbol{U}) = \boldsymbol{U} \cdot \nabla(\rho u) + \rho u \nabla \cdot \boldsymbol{U}$ which under the divergence free and incompressible conditions become:

$$\nabla \cdot (\rho u \boldsymbol{U}) = \rho \boldsymbol{U} \nabla \cdot u \qquad [4\text{-}32]$$

Substituting in the previous expressions the result for the momentum equation is:

$$\frac{D}{Dt}\int_V \rho \boldsymbol{U}\, dV = \int_V \rho \frac{D\boldsymbol{U}}{Dt}\, dV = \int_V \boldsymbol{F}_B\, dV + \int_S \boldsymbol{F}_S\, dS \qquad [4\text{-}33]$$

Differential momentum equation

Clearly the surface forces $\mathbf{F}_S$ must be a vector that it is possible to express as the product of a matrix $\boldsymbol{T}$ and the normal vector $\mathbf{n}$:

$$\int_V \rho \frac{D\boldsymbol{U}}{Dt}\, dV = \int_V \boldsymbol{F}_B\, dV + \int_S \boldsymbol{T} \cdot \boldsymbol{n}\, dS \qquad [4\text{-}34]$$

and, using Gauss's theorem we can get a differential form of the momentum equation:

$$\rho \frac{D\boldsymbol{U}}{Dt} - \boldsymbol{F}_B - \nabla \cdot \boldsymbol{T} = 0 \qquad [4\text{-}35]$$

4.5.9 Treatment of surface forces

Now we can focus our attention on the surface forces. We can say that the surface forces can be normal or tangential to the surface as sown in Figure 4-9.

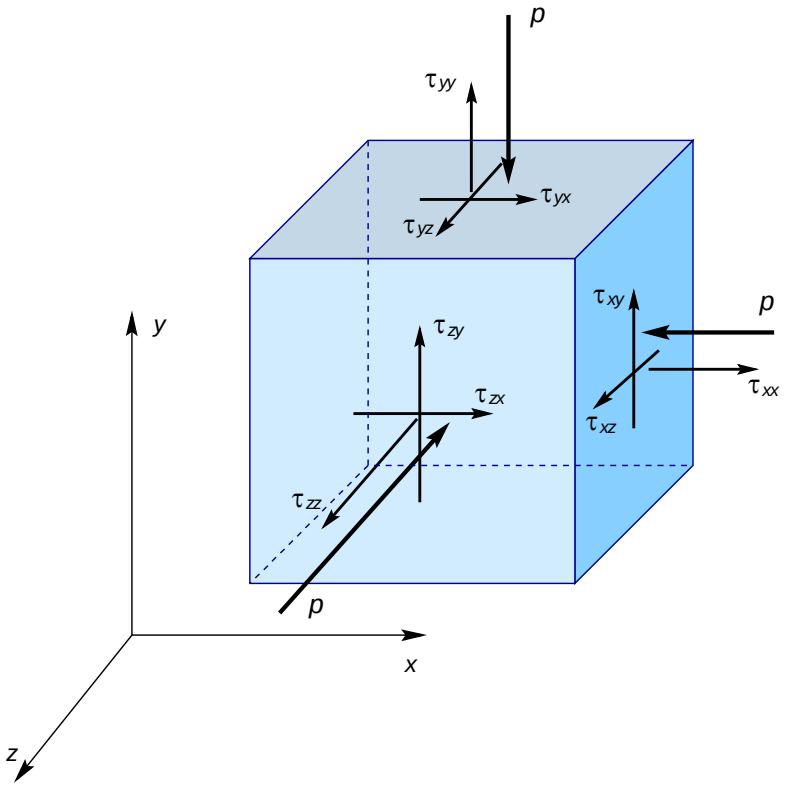

Figure 4-9: Pressure and viscous stresses acting on the fluid element.

From the balance of the volume comes:

$$\tau_{ij} = \tau_{ji} = \mu\left(\frac{\partial u_i}{\partial x_j} + \frac{\partial u_j}{\partial x_i}\right) \qquad [4\text{-}36]$$

and we can write the complete matrix $\boldsymbol{T}$ as:

$$\boldsymbol{T} = \begin{bmatrix} -p+\tau_{xx} & \tau_{xy} & \tau_{xz} \\ \tau_{yx} & -p+\tau_{yy} & \tau_{yz} \\ \tau_{zx} & \tau_{zy} & -p+\tau_{zz} \end{bmatrix} = -p\begin{bmatrix} 1 & 0 & 0 \\ 0 & 1 & 0 \\ 0 & 0 & 1 \end{bmatrix} + \begin{bmatrix} \tau_{xx} & \tau_{xy} & \tau_{xz} \\ \tau_{yx} & \tau_{yy} & \tau_{yz} \\ \tau_{zx} & \tau_{zy} & \tau_{zz} \end{bmatrix} = -p\boldsymbol{I} + \boldsymbol{\tau} \quad [4\text{-}37]$$

where $\boldsymbol{\tau}$ is the *viscous stress tensor*.

4.5.10 Navier-Stokes equations

Now we can replace the new expression of the matrix T inside the differential momentum equation. Considering only the *x* component we can write:

$$\rho\frac{Du}{Dt} = -\frac{\partial p}{\partial x} + \frac{\partial \tau_{xx}}{\partial x} + \frac{\partial \tau_{yx}}{\partial y} + \frac{\partial \tau_{zx}}{\partial z} + F_{Bx} \quad [4\text{-}38]$$

Using the above seen expression for τ and dividing all terms in the equation by the density ρ:

$$\frac{\partial u}{\partial t} + u\frac{\partial u}{\partial x} + v\frac{\partial u}{\partial y} + w\frac{\partial u}{\partial z} = -\frac{1}{\rho}\frac{\partial p}{\partial x} + \nu\nabla^2 u + \frac{1}{\rho}F_{Bx} \quad [4\text{-}39]$$

where $\nu = \mu/\rho$ is the *kinematic viscosity* and ∇^2 is the *Laplacian operator*. Similar expressions are derived in the *y* and *z* component. The set of equations derived in the three components represent the *Navier-Stokes equations* for incompressible flow.

4.6 Analysis of Navier-Stokes equations

It is worth to remember that the Navier-Stokes equations have been derived from Newton's second law applied to the fluid element under the continuum hypothesis and for constant density ρ which means for a divergence free field $\nabla \cdot U = 0$.

Further we used Newton's law of viscosity to describe the shear stresses and the normal shear stresses considering a constant viscosity.

Under the hypothesis of smooth velocity and pressure field, the above derived Navier-Stokes equations describe the motion of incompressible flow in time and space.

4.6.1 Mathematical structure

From the mathematical point of view the Navier-Stokes equations are a 3-D, time dependent system of nonlinear partial differential equations. The nonlinear term is $\boldsymbol{U} \cdot \nabla u$ in the dependent variable *u*. The set of the three equations, one for each dimensional component, introduce four unknowns: the pressure *p* and the three velocity components *u*, *v*, *w*. That means we need another linearly independent equation to solve the system. The continuity equation $\nabla \cdot \boldsymbol{U} = 0$ comes in our help. The mathematical difficulties rise from the fact that the pressure *p* does not explicitly appear in the continuity equation. Finally, in order to get a *particular solution* of the Navier-Stokes equations we need to supply appropriate *initial* and *boundary conditions*.

Navier-Stokes equations are one of the seven *Millennium Prize Problems* stated by the *Clay Mathematics Institute* in 2000. Even if these equations are widely used and are fundamentals for fluid mechanics they are not fully understood yet. There is no mathematical proof of the existence and smoothness of the solution for the three-dimensional problem with given initial conditions.

4.6.2 Physical interpretation

Now we focus the attention on the physical interpretation of the different terms in the Navier-Stokes equations.

Inertial terms

In the LHS of the equations there are the so called the *inertial terms*. They come from the substantial derivative of the velocity and represent the total acceleration divided in the local acceleration and the convective acceleration. This last term can be seen as the acceleration caused by spatial changes in the velocity. At the same time the LHS can be seen as the time-rate of change of momentum per unit mass.

Pressure forces

The first term on the RHS represent the normal surface forces due to pressure or rather, forces per unit mass since the dimension need to be compatible with the time-rate of change of momentum, i.e. acceleration as it can be easily proven.

Viscous Forces

The viscous forces appear in the second term of the RHS: $\nu \nabla^2 u$. This is a peculiar term that distinguishes fluids from the other state of matter and makes Navier-Stokes equations unique. The dimensions are consistent with the rest of terms in the equation, i.e. acceleration.

The second order derivative in a differential equation is usually associated with diffusion, smoothing or mixing. As we know, viscosity is related to the diffusion of momentum. The effects of the viscous forces on the solution of Navier-Stokes equations can be seen considering two different fluids with different viscosity, one with high- and one with low-viscosity, under the same initial and boundary conditions.

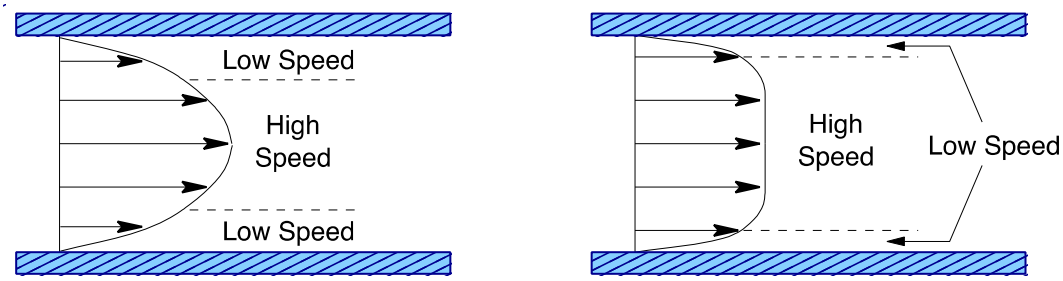

Figure 4-10: High- versus low-viscosity flow.

We consider now the flow in a duct with a fix constant mass flow rate. A fluid with high viscosity shows a velocity profile that varies smoothly from the wall, where the no-slip conditions are verified, to the centre of the channel, where the maximum velocity is reached (see Figure 4-10, picture on the left). We can notice that the low-speed regions close to the wall are relatively large compared with the high-speed region in the centre. This is because the high viscosity can diffuse the viscous forces from the near to wall region where high shear stress arises through the flow field involving the entire velocity profile.

On the other ends, the flow of a fluid with low viscosity shows relatively narrow region of low-speed compared with the large central high-speed region (see Figure 4-10, picture on the right). It is worth to note that the speed, in the central region is almost constant and, for the conservation of the mass, it shows a velocity that is smaller compared with the peak velocity of the high-viscosity fluid flow.

In both cases the viscosity acts with a diffusive action that means it dissipates the mechanical energy possessed by the fluid breaking the large fluid structures into smaller structure until, ultimately, converting the mechanical energy in thermal energy through friction. The action of the viscous terms results in a non-conservative behaviour of the momentum equations: in order to preserve the motion of the fluid it is necessary to continuously apply pressure, shearing or body forces.

4.6.3 Body Forces

The last term on LHF represents the body forces. These are all the external forces that can act on the fluid such as gravity, electromagnetic forces (Magneto-Hydro Dynamics), the forces introduced by non-inertial coordinate system like Coriolis or Euler forces. Generally these forces can be expressed

as the gradient of a scalar quantity so that their effect can be included in the pressure term using a modified pressure:

$$-\nabla p + \boldsymbol{F}_B = -\nabla p + \nabla f_{B=} - \nabla(p - f_B) = -\nabla \tilde{p} \qquad [4\text{-}40]$$

4.6.4 Validity of assumptions

The Navier-Stokes equations can be applied to flow that satisfy all the assumptions used to derive the set of equations. In general we can say that the incompressible Navier-Stokes equations are valid for relatively low-speed flow. That guarantees a small compression (change of density ρ) effect that we can neglect. As a good approximation we can say that their validity is extended in the range $0 \leq M \leq 0.3$ where *M* is the *Mach number*, defined as the ratio between the local fluid velocity and the local speed of sound.

The viscosity of a Newtonian fluid changes with the temperature so, for a constant temperature, it can be considered constant. That means that for gases the viscosity is constant until the compressible effects are dominant.

The mathematical smoothness assumption of the pressure and the velocity fields are the most likely to be violated. Anyway, this is not of relevant importance for practical engineering applications.

4.6.5 Euler equations

In the case the viscous forces can be neglected compared to the inertial forces the Navier-Stokes equations can be simplified. For the incompressible case, considering only the *x*-component without body forces:

$$\frac{\partial u}{\partial t} + u\frac{\partial u}{\partial x} + v\frac{\partial u}{\partial y} + w\frac{\partial u}{\partial z} = -\frac{1}{\rho}\frac{\partial p}{\partial x} \qquad [4\text{-}41]$$

This last equation, together with the continuity equation, has been introduced by Euler before the formulation of Navier-Stokes equations. It is known as *Euler equation* and represents the inviscid case of Navier-Stokes equations. A similar expression can be derived for the compressible case where the density ρ is not a constant.

4.7 Navier-Stokes equations in Computational Fluid Dynamics

Navier-stokes equations have been continuously investigated since their introduction in the XIX century. The turbulence makes the mathematical solution and the physical interpretation particularly difficult. Turbulence is still

an open question: it is not clear how turbulence is generated and what its nature is. Turbulence shows different effects and behaviour for different flow conditions and geometries. That is the reason why there has been, and still is, a large effort made in order to try to capture its nature and to model it in form of equations.

4.7.1 Reynolds Averaged Navier-Stokes equations

The *Reynolds Averaged Navier-Stokes equations* are deducted from Navier-Stokes equations using the Reynolds decomposition $u = U + u'$ where the velocity *u* is divided into two components, a mean *U* and a fluctuating *u'* one (see Figure 4-11), and averaging over time.

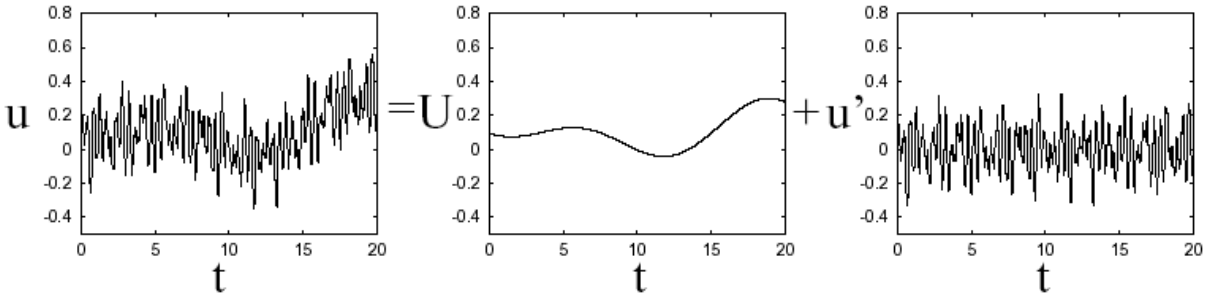

Figure 4-11: Reynolds decomposition for non-statistically stationary signal.

The average time operation is $U = \lim_{T\to\infty} \frac{1}{T}\int_0^T u\, dt$. The general Unsteady-RANS equation is:

$$\overline{U}_t + \overline{U} \cdot \nabla \overline{U} = -\frac{1}{\rho}\nabla \overline{p} + \nu \nabla^2 \overline{U} - \nabla \cdot (\overline{u'u'}) \qquad [4\text{-}42]$$

where $\overline{u'u'}$ are the Reynolds stresses that transfer the energy from the flow to the fluctuations. As can be easily noticed the number of unknowns passes from 4 (***u***, *p*, ***u'u'***) to 10 (***u***, *p*, ***u'u'***) in a 3-D problem. This is known as the *closure problem*: we need more equations in order to solve the fluid dynamic field. The extra equations come from the modelling of turbulence.

In the RANS equations all the turbulent scales need to be modelled.

4.7.2 Boussinesq hypothesis

One of the first models proposed is the *Boussinesq approximation* that is at the base of the RANS equations. The Boussinesq approximation is a milestone in turbulence modelling, introduced in the year 1877. It states that small-scale turbulent stresses should be proportional to the large-scale strain rates:

$$-\overline{u_i'u_j'} = \nu_T\left(\frac{\partial \overline{u_i}}{\partial x_j} + \frac{\partial \overline{u_j}}{\partial x_i}\right) \qquad [4\text{-}43]$$

where ν_T is the *turbulent eddy viscosity*.

Today we know that this hypothesis is inadequate for applications that show a sudden change in the mean strain rate, flow over curved surfaces, flow in ducts, flows with boundary layer separation, rotating or stratified fluids and, in general, 3-D flows. Unfortunately most of the flows involving engineering applications present such above-mentioned features.

Another difficulty in the Boussinesq hypothesis comes from the fact that the turbulent eddy viscosity is not a constant and *ad hoc* values needs to be used for different flows. Furthermore, this model for turbulence does not depend on its history.

There are different approaches to model the Reynolds stress and the RANS models are usually categorised by the number of transport equations associated with the model. Here we name some of the most used models

- 0-equation: Cebeci-Smith, Mixing Length
- 1-equation: Spalart-Allmaras
- 2-equations: *k*-ε, RNG *k*-ε, *k*-ω, SST *k*-ω

4.7.3 Reynolds Stress Model

A more elaborated modelling approach goes under the name *Reynolds Stress Models.* The strategy is to discard the eddy viscosity model and to compute directly the Reynolds stresses. This is a *Second Order Closure*. The new equations provided for each Reynolds stress include many unknowns terms which themselves must be modelled. For a 3-D problem typically 9 partial differential equations must be solved, compared with 4 with the only Navier-Stokes equations or the 6 with a 2-eqautions RANS. This means a higher computational effort. Anyway, the RSM models result almost independent from the Reynolds number and this make their use suitable for high Reynolds applications where other methods require an extremely high computational effort.

4.7.4 Large Eddy Simulation

LES is a widely used mathematical model for engineering applications. It requires a much higher computational cost compared with RANS. It consists in applying a low-pass filter to the Navier-Stokes equations. In practical terms it is possible to apply a spatial, a temporal or both filtering operations that results in the solution of a filtered velocity field. The filter removes the smallest scale of the flow so that LES resolves only the large scales. The unresolved scales need to be modelled. A sub-grid scale model which contains

all the scales that are smaller than the cut-off filter width, gives the extra equations for the modelling.

The filter operation can be implicit or explicit. In the implicit case the grid or the numerical discretisation scheme can be used as the low-pass filter. In this case the truncation error can be an important source of error. In the explicit case a well-defined filter shape is used over the discretised Navier-Stokes equations. This method minimises the truncation error. The disadvantage of the explicit filter is the need of a finer grid compared with the explicit filter.

4.7.5 Hybrid RANS-LES

It is possible to combine the two above-discussed techniques so that the turbulent scales near the walls are solved via RANS and the external regions of the flow field are treated via LES. In this way the computational cost is cut down because the grid resolution required is coarser than in the case of pure LES.

4.7.6 Direct Numerical Simulation

In DNS the Navier-Stokes equations are solved without any turbulence model or rather all the scales of turbulence need to be resolved. This requires a very fine computational mesh or rather an extremely high computational cost. For a 3-D study a DNS requires that the points $N^3 \geq Re^{9/4}$. However DNS is the only available computational tool for the study and understanding of turbulence.

5 Fluid-Structure Interaction

A fluid structure interaction (FSI) problem is defined as a problem where one or more deforming solids interact with an internal or surrounding fluid flow. FSI problems have been one of the biggest focus points for research within the field of computational engineering for the recent years. A reason for this is that the interaction between fluids and solids plays an important role in many different fields of engineering, for example (Souli and Benson 2010):

- Stability of aircraft wings in aerospace engineering
- Flow of blood through arteries in biomedical applications
- Response of bridges and tall buildings due to wind loads in civil engineering
- Oscillation of heat exchangers in nuclear engineering

A vast majority of these applications often include large and complex structures in combination with a strong nonlinearity due to the non-stationary coupling as well as the inherent nonlinearities from the respective domains, especially from the fluid domain. This makes it almost impossible to use analytical methods to obtain accurate solutions for these problems and the possibility to perform laboratory experiments is often limited and expensive. Hence, numerical methods have to be employed to investigate the often complex interaction between fluids and solids (Hou et. al. 2012).

As mentioned above, the research area of numerical methods for treating FSI problem is an area where a lot of work is currently being performed, which has resulted in a large number of different approaches to the problem, depending on the intended field of application. Hence, one typical method may be very accurate for its intended field of application, but it may neglect some effects that are important in another field of analysis, therefore, making it unsuitable for that field. Many of these methods are of course more or less related to each other and they can be classified with different aspects in mind. In Hou et. al. (2012) a distinction is for example made between methods which require conforming meshes between the fluid and the structural domain and methods that do not require conforming meshes. They also distinguish between methods where the governing equations of the two domains are treated by two solvers, partitioned approach, and where they are both treated within one solver, monolithic approach.

In this report the classification between the different FSI methods is based on which reference frame the fluid is described in; Eulerian, Lagrangian or Arbitrary Lagrangian-Eulerian. The concepts and differences between the three reference frames are discussed in section 5.1. In all three cases the structure is assumed to be deformable and described in a Lagrangian frame. The aim of this chapter is not to give the reader a complete theoretical and mathematical description of every method, but instead focuses on the concepts, ideas and assumptions of the method as well as its advantages and disadvantages.

5.1 Mesh description

Within the framework of the nonlinear finite element method a large variety of approaches are used for the formulation of the governing equations for solving the physical problem. These formulations can be classified with different parameters in mind, where one of great importance for fluid-structure interaction problems is how the finite element mesh is described. Another way of looking at the mesh description is that it defines the coordinate system in which the numerical simulation is performed and thus also the coordinate system of which the governing equations are formulated. The most common mesh descriptions are briefly covered in the following sections.

5.1.1 Lagrangian mesh formulation

The most common and popular mesh description within the field of computational solid mechanics (CSM) is the Lagrangian formulation. The Lagrangian mesh description is based on the concept of material coordinates, also called Lagrangian coordinates, where each material point is labelled by a unique Lagrangian coordinate. Usually the Lagrangian coordinate is taken as the Cartesian coordinates for the initial configuration of the continuum. When the continuum deforms the spatial location of each material point changes but its Lagrangian coordinates is unchanged. In other words, the spatial location of the Lagrangian coordinates changes as the continuum deforms with time, but it always tracks the same, and unique, material point. Thus, the Lagrangian coordinates of the nodes in a finite element mesh can be said to be time invariant, i.e. the nodes are coincident with material points (Belytschko et al. 2000).

As simple and illustrative way of looking at different mesh descriptions is by using an analogy with boats moving down a streaming river. If a Lagrangian mesh formulation is used, the position and velocity of a boat is determined by an observer that stands on that boat and follows it as it moves down the river. The observer is thus able to determine the position and velocity of that boat along the entire length of the river, i.e. the observer is attached to the moving object. But the observer cannot predict the movement of any of the other boats on the river.

In two dimensions, a Lagrangian finite element mesh can be compared with an etching on a material, and as the material deforms the etching deforms with it. This can for example be seen in Figure 5-1, which shows a pure shearing deformation of a two dimensional block. This concept can easily be generalised to three dimensions (Belytschko et al. 2000).

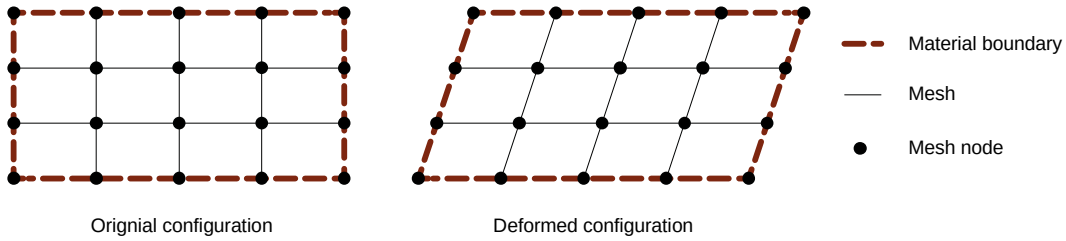

Figure 5-1: Two dimensional Lagrangian mesh in original and deformed configuration. Reproduction from (Belytschko et al. 2000).

As material points and finite element nodes are coincident in a Lagrangian mesh, boundary nodes will always remain on the boundary of the structure regardless of how much the structure deforms; this could be observed in the examples above. This makes it easy to handle boundary conditions and contact interfaces between different bodies, which is one of the major advantages of the Lagrangian description. Another advantage is, as the integration points of the finite elements remain coincident with the material points, it becomes relatively easy to treat materials in which the stress is history dependent; as for example concrete (Belytschko et al. 2000).

The major disadvantage of a Lagrangian mesh is that the finite elements can become severely distorted as the material deforms, since the material points and the mesh nodes remain coincident. As the accuracy of a Lagrangian element degrades as it distorts, the magnitude of deformation that can be simulated with a Lagrangian mesh is limited. This can for instance be a problem when simulating a fluid, which normally undergoes very large deformations (Belytschko et al. 2000).

5.1.2 Eulerian mesh formulation

The Eulerian mesh description is the most common and popular formulation of finite elements within the field of computational fluid dynamics (CFD). In an Eulerian formulation the mesh description is based on spatial coordinates; also called Eulerian coordinates. As the spatial coordinates do not deform with the material, neither does the location of the mesh nodes and thus a Eulerian mesh never deforms. Hence, a material particle of a body described by an Eulerian mesh can belong to different finite elements at different stages of the solution.

If the same analogy that was used in section 5.1.1 with boats moving down a streaming river is used for the Eulerian mesh formulation it goes as follows. The observer is located on a fixed location on the river bank and sees the boats moving through a typical section of the river. Thus the observer can predict the position and velocity of every boat that moves down the river, but only during the short time period that each boat passes through the section of the river that is observed by the observer, i.e. the observer is fixed in space.

In two dimensions an Eulerian mesh can be compared with an etching on a sheet of glass held in front of a body. As the body deforms, the etching is unchanged but the material passes through it. This is illustrated in Figure 5-2, which shows the pure shearing deformation of a body. From the figure it can be observed that the mesh has to be larger than the initial configuration of

the body to be able to observe the body in its deformed state. This concept can easily be generalised to three dimensions (Belytschko et al. 2000).

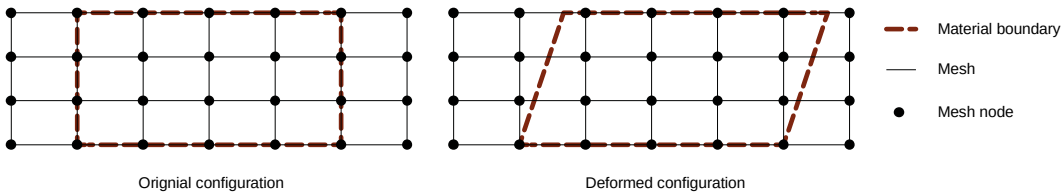

Figure 5-2: Two dimensional Eulerian mesh in original and deformed configuration. Reproduction from (Belytschko et al. 2000).

The major advantage of an Eulerian mesh is that the problem with distorting elements typically encountered in Lagrangian meshes is avoided, since the mesh is stationary in space. Hence, the main field of application for Eulerian meshes has been problems involving large deformations, such as fluid dynamics and other highly dynamical events (Brown et. al. 2002).

As the material points and mesh points does not coincide for an Eulerian mesh, it also means that the boundaries of the material cannot be described by the nodes of the mesh. Hence, the boundary conditions has to be imposed on points which are not mesh points, this has the consequence that specially developed tracking methods have to be used for treating these moving boundaries. The same problem also applies when dealing with interfaces between two materials. A further disadvantage with the moving material with respect to the finite elements is that the material particles associated with a specific integration point changes with time, this leads to difficulties in dealing with materials where the stress is history dependent (Belytschko et al. 2000).

5.1.3 Arbitrary Lagrangian-Eulerian mesh formulation (ALE)

To be able to exploit the advantages of both the Lagrangian and the Eulerian mesh formulations a family of methods called arbitrary Lagrangian-Eulerian (ALE) methods was proposed by Noh (1964) and Hirt et. al. (1974) among others for the simulation of fluid flows using the finite difference method. In the ALE version of the finite difference method the mesh consisted of vertices, which were not bound to either their initial spatial location (Eulerian) or to the movement of the material particles (Lagrangian). Instead, the vertices could move in an arbitrary prescribed manner; including the two limiting cases reducing to the Lagrangian and the Eulerian formulations. Later the framework of the ALE methods was extended and generalised to the finite element method in for instance Hughes et. al. (1981) and Donea et. al (1982) for the analysis of fluid flows.

The basic idea of the ALE formulation is to introduce the coordinates of the finite element mesh as a third and separate solution domain; separate from the previously defined material domain (Lagrangian) and spatial domain (Eulerian). This third domain is often referred to as the referential domain and the movements of its points can be described in an arbitrary way, in

accordance with the ALE formulation. The solution and state variables can then be mapped between the three domains to describe the actual physical problem.

To return to the same analogy with boats on a streaming river as used for the two previous mesh descriptions, the ALE formulation can be explained as follows. An observer based within the framework of the ALE formulation can basically choose which boat or boats to observe and how long each boat is observed. As an example, the observer can start to stand on one boat and observe its location and velocity, as in a Lagrangian formulation. After a given period of time the observer can then choose to relocate to an adjacent boat and instead observe the location and velocity of that boat. The new boat is then observed for a period of time after which the observer again moves to an adjacent boat. This pattern of observations can continue in an arbitrary and prescribed manner, independently of the actual movements of each individual boat; as defined by the ALE formulation.

In a two-dimensional ALE finite element mesh, the initial grid always coincides with the Lagrangian grid. But as the material deforms the grid does not need to follow the deformation of the material, instead it can be moved in an arbitrary fashion; se for example Figure 5-3. A normal approach is to prescribe the grid motion so that the boundary nodes follow the deformation of the material and so that the internal nodes are moved to minimise mesh distortion.

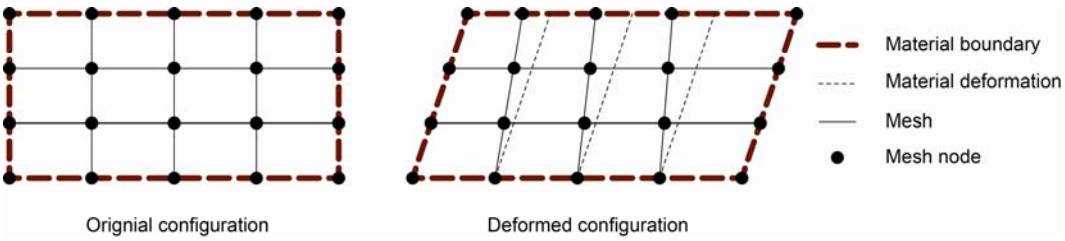

Figure 5-3: Two dimensional ALE mesh in original and deformed configuration.

The freedom in arbitrarily moving the mesh introduced through the ALE technique is often very attractive, however, it also introduces some new numerical difficulties and extra modelling tasks. For instance, the numerical formulation of the governing equations and kinematics has to be altered to include the arbitrary movement of the mesh and the convective movement of the material through the elements. Further, as the movement of the mesh is arbitrary it either has to be prescribed to fit the particular problem or an algorithm has to be included in the numerical model to automatically determine the mesh velocity, see for instance (Donea et. al. 1982). However, according to Souli and Benson (2010) these remeshing algorithms often fails when dealing with complex structures which undergo large deformations, therefore the ALE mesh often needs to be combined with a rezoning method. The rezoning method creates a new smoothened mesh and maps the solution from the old distorted mesh to the new mesh through a numerical algorithm.

5.2 Analysis of coupled systems

One of the major research areas within the field of numerical analysis has for the recent years been the simulation of coupled systems. A system can be viewed as a computational domain where an arbitrary physical field problem is to be solved. But the same physical field problem can also be viewed upon as different systems depending on the numerical description of the problem, for example; if the coordinates are given in Lagrangian or Eulerian form, if an implicit or explicit integration scheme used and so on. Thus, many different ways of coupling systems are possible and in theory no limitation on how many systems that can be coupled exists, however, this is in reality limited by the available computer resources and numerical stability. Some examples of coupled systems are given below.

- Structure (implicit) - Structure (explicit)
- Fluid - Structure
- Thermal - Structure
- Soil - Structure
- Fluid - Thermal - Structure
- Fluid - Porous fluid - Thermal - Structure

There are many different approaches for numerically handling the interaction between the systems, which approach that is suited for a typical problem often depends on how strong the coupling is between the systems. According to Felippa et. al. (2001), the approaches on how to handle coupled systems can be divided in the following three categories:

Field elimination - One of the computational fields are eliminated and accounted for outside the numerical simulation.

Monolithic treatment - The whole problem, including all physical systems, are treated as one entity and are solved simultaneously in time.

Partitioned treatment - The different systems are treated as isolated entities and are solved separately in time. Interactions between the systems are then viewed as forcing effects that are communicated between the different entities during the solution.

The basic ideas of some of the approaches important for fluid-structure interaction are given in the following sections. More about different numerical methods for handling the analysis of coupled system can be read in for example (Farhat and Lesoinne 2000), (Felippa et. al. 1980), (Felippa et. al. 2001), (Giannopapa 2004), (Hübner et. al. 2004), (Matthies et. al 2006), (Rugonyi and Bathe 2001), (Ryzhakov et. al. 2010) and (Zhang et. al. 2003).

5.2.1 Monolithic solution

In the monolithic or direct approach the entire physical system is viewed upon as a single computational entity. This means that a single set of equations is written, which takes all different field problems into consideration, including their different nonlinearities and the coupling of the systems. According to Hübner et. al. (2004) and Ryzhakov et. al. (2010), the major advantage of using a monolithic approach is that it ensures unconditional stability and

accelerates convergence of the numerical solution. Hence, the monolithic approach is recommended for coupling problems where the physical coupling of the systems is strong. The disadvantage of the monolithic approach is that it leads to very large and ill-conditioned system matrices, which are very time consuming to solve and often requires the use of an iterative or explicit solver instead of the normally used direct sparse solvers, see Ryzhakov et. al. (2010).

The typical solution scheme of a monolithic approach is illustrated in Figure 5-4a) for a fluid-structure interaction problem. From the figure it can be seen that both systems are solved within the same iteration loop and are thus solved with a consistent time integration scheme. The figure also shows a mesh updating procedure which can be included in the iteration scheme. In the monolithic scheme a single system matrix has to be formulated for the entire coupled system, an example of such a matrix is shown in Figure 5-4b) for a fluid-structure interaction problem. The matrix is basically assembled from the system matrices of the decoupled systems, K_F and K_S , but also includes the contributions from the coupling of the systems, matrices B_F and B_S. It can be noted from Figure 5-4b), that the coupled system matrix may have zeros in its diagonal due to the inclusion of the coupling matrices, which also hinders the sparseness of the matrix according to Felippa et. al. (2001). The assemblage of the coupled system matrix and load vectors is described in more detail in for example (Hübner et. al. 2004) and (Zhang et. al. 2003).

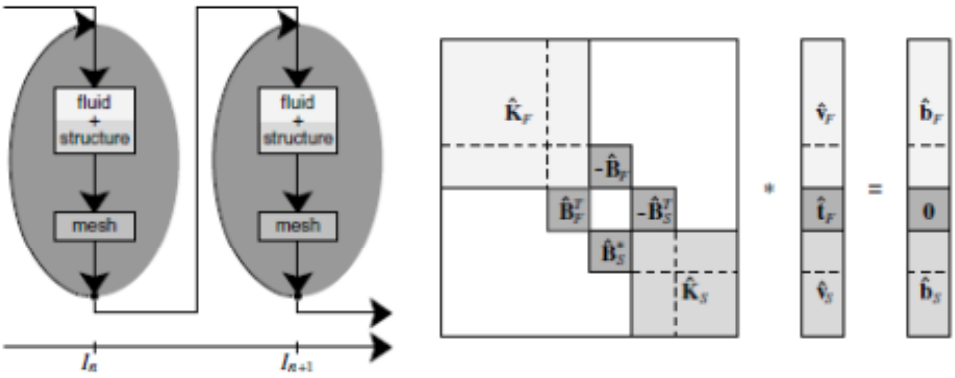

Figure 5-4: Monolithic approach (Hübner et. al. 2004).

5.2.2 One way coupling

The simplest version of the partitioned approach is the so called one way coupling. In this approach, two or more systems are solved separately and the boundary condition of the leading system is transferred to one or more surrounding systems, but no data is transferred in the opposite direction. This one-way approach is only recommended for systems with a very weak physical coupling, as for example a thermal - structure interaction. Data can be transferred from the leading system at predefined time points of the solution, ranging from every time step to only the final time step.

The advantage of the one way coupling is that it is very simple to treat numerically, where the leading solution can be solved in advance and the

results are then applied as loads in the next system to be solved. But as mentioned above, the one-way coupling is a large simplification of the actual behaviour of many physical problems and the solution may therefore lack in accuracy.

5.2.3 Sequential coupling scheme

The sequential coupling approach, also referred to as the staggered approach, is one of the first developed schemes for partitioned analysis of coupled systems with a two-way interaction. It is often based on a so called Gauss-Seidel method of solving partitioned mathematical systems. The basic idea of a sequential analysis is that one system is chosen as the leading solution while the other system lags, hence, the solution is sequential. A simple sequential simulation scheme considering the interaction between two systems X and Y is illustrated in Figure 5-5. The first step of the solution is to predict the solution of system Y at time *t+1* based on its solution at time *t*. Next, the predicted value at *t+1* of Y is given as a boundary condition to system X which is then solved for time *t+1*. The third step is to update the boundary conditions to be given to system Y from system X at time *t+1*. The fourth and final step of the scheme is then to update the solution of system Y at time *t+1* with the new boundary conditions. In this example system X is the leading system and system Y lags (Felippa et. al. 2001).

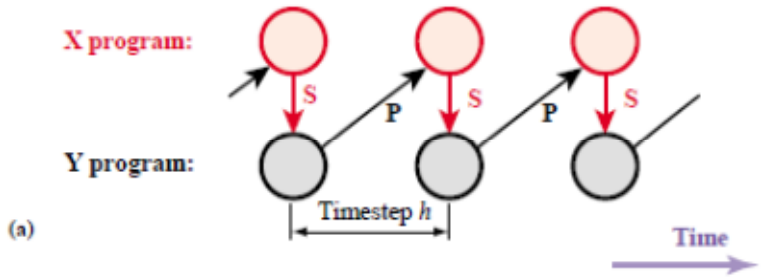

Figure 5-5: Staggered approach (Felippa et. al. 2001).

According to both Felippa et. al. (2001) and Matthies et. al (2006) the main concern with a sequential coupling scheme is that it often fails to converge due to instability of the numerical procedure. The numerical coupling is not guaranteed to converge even for very small time steps. One big issue with the stability is to make an accurate prediction of the lagging solution to be able to advance the leading solution, where an inappropriate prediction may lead to a fast diverging solution.

Compared to the monolithic solution, a sequential coupling solution has lower accuracy, which in some sense is inherent to the problems with numerical stability; especially for non-linear problems. However, according to Felippa et. al. (2001), the accuracy is improved if an iterative procedure between the coupled systems is included for every time step of the solution. Due to the numerical stability and accuracy problems the sequential coupling scheme is normally only recommended for problems where the physical coupling between the solved systems is weak. A further issue reported in Felippa et. al.

(2001) with the sequential coupling is that the coupling scheme cannot be parallelised due the serial manner in which the algorithm is defined.

Despite its disadvantages the sequential scheme is an effective and simple scheme for solving coupled problems and the actual coupling requires very little computational effort, when compared to the separate systems. Hence, in a large problem the computational time of a coupled problem can be approximated by adding the time it takes to solve the decoupled systems separately (Felippa et. al. 2001).

5.2.4 Parallel coupling scheme

Another approach for solving partitioned systems is to use a parallel coupling scheme, often based on a so called Jacobi method. The idea of a parallel algorithm is that all systems are advanced in time simultaneously and by doing so no system is leading nor lagging in the solution of the whole coupled system. Looking at an example of two systems X and Y, a simple parallel coupling scheme between the two systems is illustrated in Figure 5-6. The first step of the parallel scheme is to predict the boundary conditions that are to be imposed on system X by system Y and vice versa at time $t+1$, based on the solution of the respective system at time t. The second step is an iteration process between the two systems which continues until the convergence criteria of the coupling is fulfilled or the solution diverges. Following this scheme allows the two systems to be solved simultaneously (Felippa et. al. 2001).

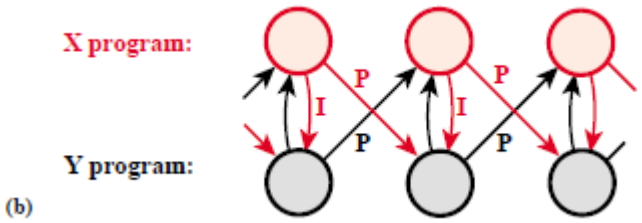

Figure 5-6: Parallel approach (Felippa et. al. 2001).

Many of the concerns of the sequential scheme also applies for the parallel scheme. For example prediction of the result based on the solution from a previous time step may lead to numerical instability and accuracy problems. The parallel coupling scheme is, however, generally more numerically expensive to solve than the sequential scheme, but on the other hand it is in its nature very simple to parallelise which increases the computational speed (Matthies et. al. 2006). Due to these concerns the parallel scheme is mostly recommended for problems with a weak physical coupling between the partitioned systems.

5.2.5 Advanced coupling schemes

To avoid the many drawbacks of the three basic coupling schemes for solving partitioned systems (one-way, sequential and parallel) the on-going research is and has been to develop more advanced coupling algorithms. The first step

in doing this is to append various numerical techniques to the basic algorithms such as:

- **Extra iterations** for predicting or correcting the variables transferred between the coupled systems.
- **Subcycling** of solutions. This means that the solutions uses different time steps and only communicates with each other at predefined time points.
- **Correction** of the predicted values. The predicted value is improved through looking at previous time steps.

With these kinds of modifications the basic algorithm of the sequential or parallel schemes is not altered, but the accuracy and stability of the solution is improved. The next in finding even better coupling scheme is to develop new algorithms, often based on the aforementioned schemes. In Farhat and Lesoinne (2000), two examples of such improved algorithms are given. In the modified sequential algorithm presented in Figure 5-7, the points in time of the solutions for the two systems are shifted, where the structure is solved for time *t+1* and the fluid for time *t+1/2*. This shift in points in time allows the algorithm to use the so called midpoint rule when evaluating, in this case, the structural equations. No iterations are needed between the coupled systems to achieve the desired accuracy and stability, which makes the algorithm very computationally economical. It is shown in Farhat and Lesoinne (2000) that this coupling scheme has almost the same accuracy as the normally more accurate monolithic methods when applied to an aero-elastic problem. For the same problem it is shown that the traditional sequential scheme needs to use a five times smaller time step than the improved scheme to reach the same numerical stability and accuracy.

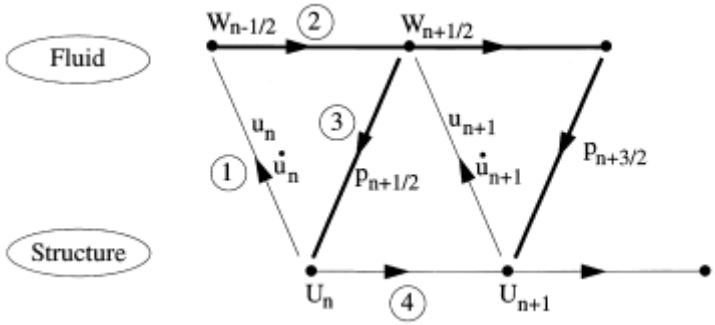

Figure 5-7: Improved staggered approach (Farhat and Lesoinne 2000)

The other presented example in Farhat and Lesoinne (2000) is an improved parallel coupling scheme, shown in Figure 5-8. This algorithm also uses a concept of half time steps for the fluid solution. Information is exchanged between the two systems at time t, after which the fluid solution is advanced to time *t+1/2* and the structural solution is advanced to time *t+1*. At this point the information is again exchanged between the two systems. The fluid state at time *t+1/2* is given as a boundary condition to the structure at time *t*, while the first prediction of the structural solution at time *t+1* is given as a boundary condition to the fluid at time *t+1/2*. Next, the fluid solution is advanced from time *t+1/2* to time *t+1* with the updated structural boundaries. For the structural solution a new solution is performed from time *t* to time *t+1* with the updated fluid boundaries from time *t+1/2*. Since an extra fluid step is introduced in the improved parallel scheme it is more

computationally heavy but more accurate than the traditional parallel scheme. When compared to the improved sequential scheme, Farhat and Lesoinne (2000) showed that it was not as numerically stable and required a smaller time step.

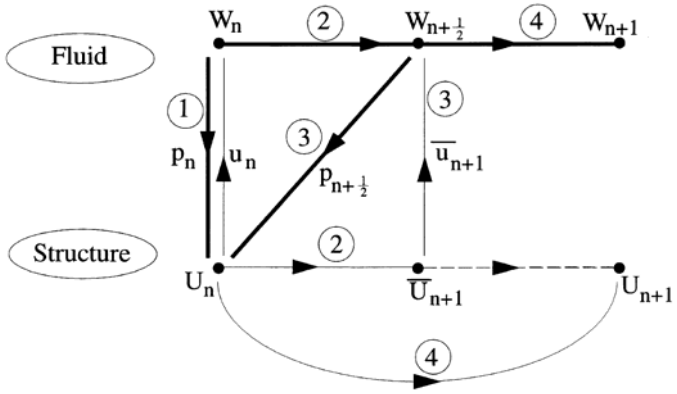

Figure 5-8: Improved parallel approach (Farhat and Lesoinne 2000).

Although these two examples are developed for aero-elastic problems with a much weaker physical coupling than that of the interaction between solids and water, they highlight the complex nature of performing a partitioned analysis. It is always important to observe the numerical stability of the solution when performing a partitioned analysis, especially for problems with a strong physical coupling, otherwise the simulation results can be very inaccurate and unrealistic. The risk when performing a partitioned analysis is therefore that the time step of both solutions is limited by the coupling due to this numerical instability, which can lead to very time consuming simulations.

5.3 Interaction between a fluid and a solid domain

A FSI problem is basically an interaction problem between two computational domains, the solid and the fluid. Looking at how the problem is formulated, the physics within each domain is solved independently with equations and numerical procedures appropriate for each domain, as previously mentioned. The actual FSI comes in when describing the interface between the domains, which in its most simple point of view can be regarded as a contact problem. This means that the boundary conditions of one domain is applied as a load in the other domain and vice versa. A schematic view of a typical FSI problem is shown in Figure 5-9, where the interface is also included. This section will focus on how this interface is described when simulating FSI problems. (Hou et. al. 2010)

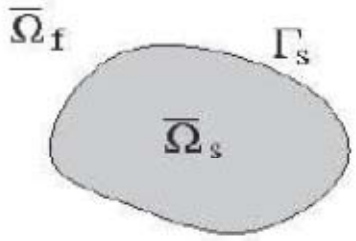

Figure 5-9: Schematic view of a FSI problem (Hou et. al. 2010).

To maintain the no-slip condition of fluid flow close to a surface, which implies that the fluid is stuck to the surface, the following conditions has to be imposed on the interface according to Hou et. al. (2010). Eq. [5-1] states that the velocities on the interface have to be equal in both domains, which gives the Dirichlet boundary condition when solving the governing equations. As an alternative Eq. [5-3] can be used as the Dirichlet boundary condition which states that the location of the nodes along the interface coincides. The other boundary condition that has to be imposed on the interface is given by Eq. [5-2], which states that the normal stress, or normal force, has to be equal on both sides of the interface. This is called the Neumann boundary condition when applied to the governing equations. These boundary conditions ensure the continuity of the solution over the interface.

$$v_i^s = v_i^f \qquad [5\text{-}1]$$

$$\sigma_{ij}^s n_i = \sigma_{ij}^f n_i \qquad [5\text{-}2]$$

$$x_i^s = x_i^f \qquad [5\text{-}3]$$

Although, the no-slip condition is almost universally used for all viscous flows, it can sometimes be simplified. This is typically made for simple analyses of inviscid flow where the boundary layer effects are of little interest. In that case the fluid velocity parallel to the surface is assumed to be unrestricted, but the normal velocities of the interface are still equal for both domains, according to Eq. [5-1] and [5-3], at the interface; this is the so called no-penetration condition.

As previously mentioned, these interface conditions are often treated and interpreted in the same manner as contact between two solids in a structural finite element simulation. The most common way of treating contact problems is by either using the so called penalty method, by introducing Lagrange multipliers to the equation system or by a combination of these two methods. As pointed out in Cook et. al. (2002), the simulation of contact is in its nature a very non-linear problem, since it introduces both geometrical nonlinearities and sudden stiffness changes. Thus, the treatment of contact problems is a very extensive area and a detailed description of different contact algorithms will not be covered in this report.

But, to give a basic understanding of how contact algorithms work, since it is of such significance to FSI, a simple example of a penalty contact is given in Figure 5-10. The penalty contact method enforces contact by introducing a force proportional to the penetration distance that would occur if no contact was present. Hence the contact force can be looked upon as a spring force, where the spring stiffness is very large when two surfaces are in contact and zero otherwise (Cook et. al. 2002).

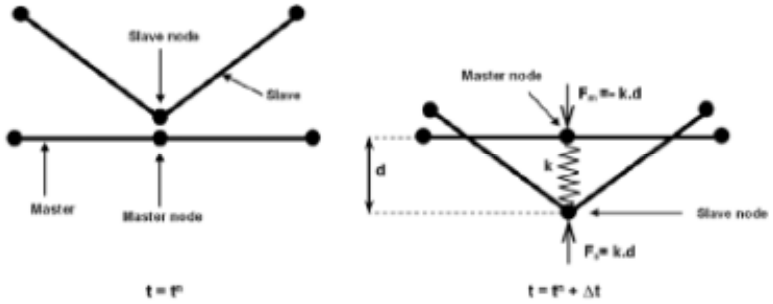

Figure 5-10: Schematic illustration of a penalty contact algorithm (Souli and Benson, 2010).

According to Souli and Benson (2010) it can be difficult to treat contact between fluid and structures, especially for transient dynamic analyses, since the mesh of the fluid often gets highly distorted. This is one of the major difficulties to overcome when analysing a problem which includes FSI. Many different approaches have been proposed for dealing with this problem, e.g. different contact algorithms which eliminate the loss of accuracy due to mesh distortion and remeshing algorithms (ALE) which eliminates mesh distortion. Some of these approaches will be covered in the following sections which deal with different methods to account for FSI.

Since the structure is of most interest for the problem formulation of this report it will always be formulated from a Lagrangian point of view, which has been shown to give the most accurate results for solid mechanics. The fluid on the other hand can be described in many different ways:

- Different kinematical description (Lagrangian, Eulerian or ALE)
- Level of detail when solving the Navier-Stokes equation
  - Acoustic equations
  - Euler equations
  - Full Navier-Stokes equations
  - Turbulence models
- Choice of independent variable in the governing equations
  - Displacements
  - Velocities
  - Pressure
  - Scalar functions (e.g. velocity potential)

In the following, different methods to account for FSI will be reviewed, the methods are roughly categorised based on the kinematic description of the fluid domain. Further, categorisation is made with the governing equations of the fluid in mind.

5.4 Simplified FSI

The most extensively used approach when FSI effects needs to be accounted for is to include the fluid as added mass on the structure, thus changing the dynamic properties of the structure. This technique can be described in some sense as field elimination, see section 5.2, where the actual equations of the fluid flow is eliminated from the system. However, it should be observed that this approach only give viable results when the problem involves small displacements and small deformations of the structure. Further, it is assumed that no movement occurs in the fluid, except for the small movement induced by the deforming structure. (Souli and Benson, 2010)

When performing this kind of analysis for concrete structures subjected to seismic loading it is good practice to follow the recommendations in ASCE 4-98 (1998) presented in section 3.1 of this report. Depending on the type of structure that is to be analysed, the most appropriate of the presented methods in chapter 3 should be used when calculating the amount and location of the mass that is to be added to the structure.

5.4.1 Added fluid mass

The simplest way of including the influence of the fluid is to only add the impulsive mass of the fluid, as defined in chapter 3. The addition of the extra mass will alter the dynamic properties of the structure and lower its natural frequency.

5.4.2 Added fluid mass with springs

If the hydrodynamic effects of the fluid are desired in a simplified FSI analysis, it is possible to also add the convective mass, apart from the impulsive mass, as defined in chapter 3. By adding the system of convective masses and springs, the basic sloshing modes of the fluid will be included in the analysis. This further alters the dynamic response of the structure by introducing the mass inertia of the fluid to the system.

It is also possible to account for the damping in the fluid by the use of discrete dashpots. Usually, the damping in the sloshing modes is very low (around 0.5%) as mentioned in Section 2.3, and damping is thereby generally not considered in the added fluid mass with springs method, HSE (2007).

5.5 ALE fluid methods

The basic idea of the arbitrary Lagrangian Eulerian kinematical description for the fluid is to combine the advantages of both the pure Lagrangian and pure Eulerian kinematical descriptions, see section 5.1. Looking at how the governing equations are formulated for the fluid, the ALE methods introduces a new computational domain, the referential domain, in which the motion of the computational grid is solved. As described in section 5.1 a mapping

function is typically used to transfer results between the three domains. This new domain alters the formulation of both the finite element equations and also the equations that governs the physics of the domain, in this case the fluid. For a more thorough description on how the finite element equations are implemented for an ALE method see for instance (Belytschko et al. 2000), (Donea et. al., 1982), (Donea et. al., 2004) and (Souli and Benson, 2010).

One of the main implications of the ALE method is that a new velocity *W* component is introduced, this velocity is actually the velocity of the computational grid; the mesh. With the introduction of this new velocity component the governing equations needs to be modified to take the moving grid into account, in the case of the fluid this means that the Navier-Stokes equations presented in section 4.5 needs to be rewritten. In Souli and Benson (2010) the new formulation of the N-S equations is given for the ALE kinematic description. The most important equations are also given below in Eq. [5-4] to [5-6] with the same notation as in chapter 4.

$$\frac{Df}{Dt} = \frac{\partial \hat{f}}{\partial t} + (U - W) \cdot \nabla f \qquad [5\text{-}4]$$

$$\frac{\partial \rho}{\partial t} + (U - W) \cdot \nabla \rho + \rho \nabla \cdot U = 0 \qquad [5\text{-}5]$$

$$\rho \frac{\partial U}{\partial t} + \rho (U - W) \cdot \nabla \mathrm{U} - \nabla \cdot \mathrm{T} - \mathrm{F_B} = 0 \qquad [5\text{-}6]$$

where $\hat{f}$ is a function described in the ALE coordinate system. Eq. [5-4] gives the substantial derivative, Eq. [5-5] is the equation of mass conservation and Eq. [5-6] is the equation of momentum conservation. Note that the time derivates in Eq. [5-5] and [5-6] are with respect to the location of the particle in the ALE coordinate system.

The use of ALE for the fluid domain can be implemented in many different ways in numerical schemes for solving fluid flow and FSI, depending on the desired level of detail in the solution etc. A few methods for describing the fluid flow which can be formulated within the ALE framework is given below, with different levels of detail in the N-S equations.

5.5.1 Acoustic fluid

Acoustics is the field of physics that studies the propagation of pressure waves in gases, liquids, and solids. Waves can originate from many different sources such as vibration, sound, ultrasound and infrasound; thus the field of acoustics is not limited to a single engineering discipline. The mathematical description of acoustics is derived from the theory of fluid dynamics, see chapter 4. To derive the equations for acoustic wave propagation a number of assumptions has to be made, which simplifies the equations of fluid dynamics. The following assumptions are generally made for the conservation of momentum according to Reynolds (1981):

- The fluid is Newtonian
- The flow is irrotational
- Body forces are negligible

- No viscous forces
- Small disturbances
- The medium is homogeneous
- The medium is at rest, i.e. no actual flow occurs and pressure waves are assumed to propagate rapidly through the medium.

With these assumptions the momentum conservation for an acoustic medium is given by Eq. [5-7], compare with Eq. [4-35] form section 4.5.

$$\rho_0 \frac{\partial u}{\partial t} + \nabla p = 0 \qquad [5\text{-}7]$$

For the mass conservation the following assumptions is generally made according to Reynolds (1981):

- Small disturbances
- The medium is homogeneous
- The medium is at rest
- The medium is an ideal gas, in which the waves compress the medium in and adiabatic and reversible manner.

With these assumptions the mass conservation of an acoustic medium is given by Eq. [5-8], compare with Eq. [4-23] from section 4.5.

$$\frac{\partial p}{\partial t} + \rho_0 c_0^2 \nabla \cdot u = 0 \qquad [5\text{-}8]$$

Combining Eq. [5-7] and Eq. [5-8] gives the acoustic wave equation which governing equation to be solved. The acoustic wave equation is given in Eq. [5-9] with the acoustic pressure *p* as the independent variable.

$$\frac{\partial^2 p}{\partial t^2} - c_0^2 \nabla^2 p = 0 \qquad [5\text{-}9]$$

The choice of independent variable in Eq. [5-9] is not limited to the acoustic pressure, it can also be chosen as the wave speed *u* in which case the acoustic wave equation is given in Eq. [5-10].

$$\frac{\partial^2 u}{\partial t^2} - c_0^2 \nabla^2 u = 0 \qquad [5\text{-}10]$$

Another often used assumption is to choose the independent variable as a scalar potential function, for example a velocity potential $u = \nabla \emptyset$. In this case the acoustic wave equation is given in Eq. [5-11].

$$\frac{\partial^2 \emptyset}{\partial t^2} - c_0^2 \nabla^2 \emptyset = 0 \qquad [5\text{-}11]$$

Since the above equations for acoustic waves have no degrees of freedom for displacement of material points no actual flow occurs in an acoustic simulation. Apart from being a simplification of the bulk behaviour of the fluid, this also effects how the boundaries of a fluid domain can be described. For boundaries adjacent to a structural domain, the nodes of the acoustic medium can be prescribed to follow the node of the structural domain, giving a pressure change in the acoustic medium. However, when it comes to describing the motion of a free fluid surface, special measures have to be used due to the lack of displacement degrees of freedom. The most basic approach is to use a pressure boundary which prescribes zero acoustic pressure on the free surface; however, this still gives no actual displacement of the free surface but is correct in the sense of wave propagation in the medium. Neglecting the actual surface waves in a dynamic analysis with a free surface induces undesirable zero energy modes in the system according to Ross (2006).

Another method often used is to introduce a free surface interface element which gives the free surface additional translation degrees of freedom, see (Sussaman and Sundqvist, 2003) and (Ross, 2006). The translation degrees of freedom parallel to the free surface are either removed or given a very low stiffness so that they do not contribute to the solution. The translation degree of freedom normal to the free surface is given a stiffness which corresponds to the hydrostatic pressure of the motion of the free surface. This means that the pressure of the free surface p_s varies according to Eq. [5-12]

$$p_{surface} = p_{atm} - \rho g z(x,t) \qquad [5\text{-}12]$$

where $z(x,t)$ is the normal displacement from the original acoustic surface, p_{atm} is the atmospheric pressure. In Eq. [5-12], the term ρg can be considered as the normal stiffness of the surface. A typical surface wave is shown in Figure 5-11.

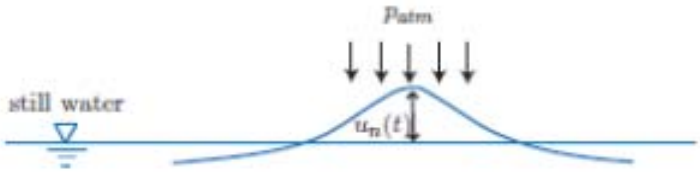

Figure 5-11: Free surface wave (Ross, 2006).

As for the interface with a structural domain, the acoustic node on the free surface can be prescribed to follow the motion of the interface element, which

makes it possible to visualise the free surface motion. It should however be noted that this approach assumes that the motion of the free surface has a small amplitude and is inaccurate for problems involving large sloshing effects.

Another limitation of the found when looking at the governing equations of acoustic waves, Eq. [5-7] to [5-11], is that they do not include any terms for body forces; this means that forces such as gravity are not included in the equations. Hence, hydrostatic pressure is assumed to be negligible when looking at acoustic wave propagation, as in the basic assumption above. However, if FSI is to be accounted for, the hydrostatic pressure has to be included as it has a significant influence on the displacement of the structure, this can for example be made through applying pressure load on the fluid structure interface. Another possibility is to include body forces when deriving the momentum conservation equation, Eq. [5-7].

The advantages of the acoustic formulation is that it is very simple and effective to treat numerically, as it assumes no material flow and thus no mesh distorting. Further, it only has one degree of freedom per node in the computational grid, if the pressure of scalar potential is used as the independent variable, compared to three of a normal Lagrangian element, which significantly reduces the size of the problem.

If an acoustic formulation is to be used in a FSI problem where the structure is subjected to large deformation, as in a seismic analysis, the acoustic mesh has to be able to follow the structural deformation. In such an application the ALE framework can be used to prescribe the movement of the acoustic mesh, including interior nodes, to follow and adapt to the movement of the structure.

The use of acoustic elements can, apart from wave propagation and free surface movement mentioned above, also be coupled with other effects associated with seismic excitation of water bodies. One such effect mentioned in Ross (2006) is phenomenon called cavitation. Cavitation occurs when the absolute pressure of the fluid falls below the vapour pressure, which results in that micro bubbles are created in the fluid. This has the effect that the bulk modulus of the cavitating zone is reduced to zero which can affect the response of the fluid. Ross (2006) among others, have studied the effects of cavitation on the Koyna dam excited by the El Centro earthquake. From the studies it has been concluded that for high intensity accelerations events ($>1.2g$) the inclusion of cavitation can have some effects on the results. In the study of the Koyna dam, cavitation reduced the displacement of the dam crest with up to 50 %. However, it is also concluded that the effect of cavitation can be neglected for low intensity acceleration events. If cavitation is to be included in the FE-simulations, it is often necessary to use an explicit time integration scheme; which can significantly increase the solution time.

There are more advanced methods available which are derived from the acoustic formulation. One example is given in (Sussaman and Sundqvist, 2003), where a nonlinear term is added to the acoustic equations; thus introducing actual fluid flow to the equations. Another example is the so called spectral element method, e.g. (Spraque and Geers, 2004), where the basic functions of the finite elements are changed to better describe wave propagation problems, i.e. a higher order.

5.5.2 Simultaneous solution of solid and fluid domain

This category of FSI methods can contain a wide variety of methods which in some way include the actual fluid flow in a simultaneous approach using the methods as described in section 5.2.1, and using the ALE as the framework kinematical description for the fluid. This can be compared to the acoustic methods, which normally only consider the wave propagation in the fluid. Since actual fluid flow is to be analysed, the governing equation of the fluid domain must correspond to the Navier-Stokes equations, see section 4.5.10. In some cases, depending on assumptions made, the Euler equations, section 4.6.5, might also be used.

When deriving the NS-equations with an ALE kinematical description, the most important equations needed are the conservation equations given in Eq. [5-4]-[5-6]. Comparing these equations with the equations from chapter 4, given in an Eulerian frame, it can be concluded that it is only the material velocity in the convective terms that has changed to a convective velocity, which is the difference between the velocities of the material and the computational grid.

The two main numerical aspects that needs to be considered when using this FSI approach is how to describe the boundary conditions between the fluid and the structure and how to define the movement of the computational grid, i.e. the mesh. Other important aspects are of course associated with each computational domain depending on the method used to solve the governing equations of each domain.

First looking at how to treat the material boundaries of the fluid domain, a distinction can first be made between boundaries that constitute a free surface and those in contact with a structure. When defining a free surface boundary, the main condition that has to be fulfilled is that no fluid particles are allowed to cross the boundary surface. This means that detached drops of the fluid due to sloshing is not possible to capture. The location of a free surface can then be computed using two different approaches, (Donea et. al., 2004). In the first method the velocity normal to the free surface $z = z(x, y, t)$ is given by the hyperbolic function given in Eq. [5-13], used by for example (Souli and Zolesio, 2001).

$$\frac{\partial z}{\partial t} + U \cdot \nabla z = 0 \qquad [5\text{-}13]$$

The other alternative is perhaps a more straight forward approach when using the ALE framework. Since, in an ALE grid the velocities of each grid point can be arbitrarily defined, it is easy to set the grid velocity W equal to the fluid velocity U on the free surface. This means that a Lagrangian description is employed on the free surface. However, it is also possible to only describe that the normal velocities of the grid and fluid are equal, giving a more relaxed and numerically efficient boundary condition, see Eq. [5-14], (Donea et. al., 2004).

$$n \cdot W = n \cdot U \qquad [5\text{-}14]$$

From the weak formulation of the governing equation of the fluid domain and the natural boundary condition, Eq. [5-2], it is also given that the normal stress equal to the free surface is zero.

The fluid structure material boundary basically uses the same boundary conditions given by Eq. [5-1]-[5-3]. Then, depending on whether the flow is viscous or inviscid, either the no-slip or the no-penetration condition can be used, i.e. whether or not the fluid particles are free to move tangentially to the structure. But since in the ALE formulation the movement of the grid points can be chosen independently of the movement of the fluid, boundary conditions has to be specified for the grid points on the fluid structure boundary as well as for the free surface two alternatives are possible. The first is to constrain the fluid grid points to the nodes of the structure, .i.e. a Lagrangian boundary. The advantage with this approach is that all nodes in the sliding interface remains permanently aligned which makes the treatment of the contact equations very efficient. It can however lead to loss of accuracy and mesh distortion in other parts of the fluid domain, especially in the transition zone to a free surface. Hence, the other alternative is to let the grid points move freely tangentially to the boundary surface, thus making it possible to relocate grid points to for example a free surface. This method can however, make it more difficult to numerically treat the contact equations and flow of information across the boundary. (Donea et. al., 2004)

Concerning the transition zone between a fluid-structure boundary and a free surface, special considerations have to be taken. The above description of the fluid-structure boundary only applies to surfaces, or part of surfaces, where the structure nodes are submerged throughout the entire simulation. In areas where structure nodes can be either submerged or above the free surface, the fluid nodes have to be able to move along the interface. Special treatment is also necessary for the actual material boundary of this zone, where the no penetration condition is usually used instead of the no slip condition.

The other numerically important aspect of the ALE methods is how to define the movement of the computational grid in the entire fluid domain. For these methods to be both numerically efficient and user friendly, it is necessary that this movement is rendered automatically as a part of the FE solution. There are different strategies for defining these automatic algorithms, where the one of most interest to fluid problems is the so called mesh regularization. This means that the movement of the computational grid is used to avoid mesh entanglement and distortion during the solution. Another strategy is the so called mesh adaption, where the movement of the grid points is used to concentrate elements in areas which are highly non-linear. This technique is often employed in solid mechanics. However, only the mesh regularization will be explained further in this report, due to its interest to FSI problems.

It should, however, first be discussed how the governing equations, Eq. [5-5] and [5-6], are numerically treated. According to Souli and Benson (2010), there are mainly two alternatives on how to treat the equations. The first is to solve them directly with the convective terms as stated in Eq. [5-5] and [5-6]. The disadvantage with solving the equations directly is that the equations are unsymmetrical, which is computationally ineffective. The second method is to use a mathematical procedure called operator split, which works by dividing each increment into two steps. In each increment the material motion is decoupled from the motion of the computational grid. In this way a pure Lagrangian phase is first performed to determine the new state of the material, fluid or solid. This step is then followed by an Eulerian phase in which the computational grid is moved and material convected between the

old and the new grid. Each increment in the operator split method is very computational effective, compared to the direct method, and is therefore especially convenient to use in explicit integration schemes. It is, however, also frequently used in implicit schemes; see for instance (Dassault Systèmes, 2012). The direct method is more or less restricted to implicit integration schemes due to the computational cost of each increment.

Since the operator split method is most frequently used, the basic procedures for mesh regularization in the Eulerian phase of each increment is described in the following.

As stated above, the objective of the mesh regularization is to keep the computational grid as regular as possible throughout the whole simulation. Doing so successfully can significantly increase the convergence rate and the accuracy of the solution. It should first be mentioned that the motion of the boundary nodes of the ALE domain is determined by the conditions stated above, and that the mesh regularization is used to move the interior nodes of the domain with respect to the boundaries so that a good mesh quality is preserved. Several different techniques are available for achieving this, most based on some kind of interpolation function.

A common kind of smoothing method is to use some kind of geometrical interpolation or averaging. One such method is called volume weighted smoothing, see Figure 5-12, which relocates a node M by calculating a volume weighted average position of the centre points of each element surrounding the node, C1-C4. In Figure 5-12, node M will be moved towards element centre C3, thus reducing the element distortion.

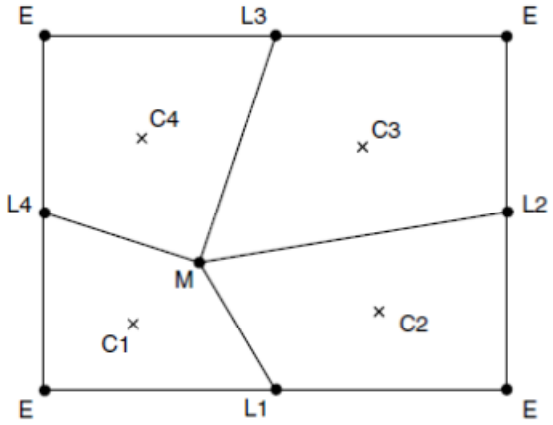

Figure 5-12: Mesh of four finite elements (Dassault Systèmes, 2012).

Another commonly used method is Laplacian smoothing. In this technique the movement of nodes consists of solving a Laplace equation, $\nabla^2\emptyset$, a second order PDE, for each component of the node velocity or position, in order to obtain a mesh that form lines of equal potential. Applying Laplacian smoothing to Figure 5-12, node M is relocated by calculating a second order weighted average of the surrounding nodes L and E, i.e. eight nodes. In three dimensions the weighted average is computed from the 18 neighbouring nodes.

When performing the smoothing of the computational grid, a consequence is that the field and state quantities has to be transferred to the new grid; so called convection or advection. Here a difference is made between element variables such as stress and density, which are typically located in the element center, or in the integration points for higher order elements, and nodal quantities such as displacement and velocity. For the element quantities the most popular method is the method proposed by van Leer (1977), which uses quadratic interpolation between elements and is second-order accurate. Other methods are also available, e.g. first-order methods. Such methods are commonly used due to their computational efficiency, but are generally not recommended for transient dynamic analyses due to lower accuracy.

When advecting nodal quantities, some method has to be used which projects the nodal quantity to the element centre so that the above mentioned advection methods can be used to advect the quantities to the new mesh. This process is often referred to as momentum advection, since it is normally the momentum of the element centre that is shifted, not the actual displacement/velocity quantities. Further, it can also be related to the convective terms of the mass and momentum conservation equations given in Eq. [5-5] and [5-6]. Using the momentum to transfer nodal quantities ensures that the equation of mass and momentum conservation is valid for the adaptive mesh. The process of momentum advection can roughly be described as follows; first the momentum of each element is calculated and transferred to the centre, i.e. integration point. Secondly, the element momentum of each element is transferred to the new mesh and finally the mass distribution of the new mesh is used to calculate the nodal velocities of the new elements from the element momentum. Many different methods have been proposed for the projection of nodal quantities to the element centre point or integration point and the following advection of the momentum. A summary of different methods is given in (Benson, 1992a), which are more or less accurate and computationally effective.

It should further also be noticed that the above described mesh smoothing and advection methods can be performed continuously at each increment of the solution or periodically at predefined intervals. Which approach to use depends on the expected severity of the mesh distortion and so on. Of course using a more frequent smoothing and advection requires more equations to be solved and if not necessary, due to e.g. mesh distortion, consequently reduces the computational efficiency of the solution.

Time stepping

When performing a transient dynamic analysis, a very important aspect is how to choose an appropriate time step for the given simulation. How to choose the time step can depend on different aspects. One limit for the time step often used in dynamic analysis is the desired resolution of the solution, in seismic analyses this is often related to the highest frequency of interest in the given time signal or response of the structure. However, in an FSI analysis special considerations need to be taken into account, partly due to the inclusion of the fluid but also depending on the choice of numerical treatment; this is of course very important when the fluid is described with an ALE grid.

As mentioned above, an explicit integration scheme is often used when performing a simultaneous analysis of fluids and structures. In such a case, the time step is often limited by the conditional stability of the integration scheme. This is often referred to as the stable time increment and can be related to the wave speed c of the material and the smallest length L_{min} associated with the finite elements. An estimation of the stable time increment is given by Eq. [5-15].

$$t_{stable} = \frac{L_{min}}{c} \qquad [5\text{-}15]$$

Further, when a fluid entity is included in the simulation the fluid domain often governs the size of the time increments. In the fluid domain the size of the time increment is limited by the physical phenomenon that needs to be included, e.g. waves. A condition normally used in CFD is the so called Courant-Friedrichs-Lewy condition; see (Courant et. al. 1967). The CFL condition states that if the amplitude is to be calculated for a wave moving across a spatial grid at discrete time points; then the length between the grid points must be smaller than the time it takes for the wave to travel between the adjacent grid points. In the general case, the CFL condition can be expressed as

$$C = \Delta t \sum_{i=1}^{n} \frac{u_{x_i}}{\Delta x_i} \leq C_{max}, \qquad [5\text{-}16]$$

where u is the wave velocity, $\Delta \mathrm{x}$ is the spatial interval, $\Delta \mathrm{t}$ is the time increment. The value $\mathrm{C_{max}}$ gives the limit for numerical convergence and n is the number of dimensions, typically $\mathrm{n} = 1,2,3$.

Depending on the numerical procedure, the value of $\mathrm{C_{max}}$ changes, for explicit methods $\mathrm{C_{max}} = 1$ typically applies, while for the more stable implicit methods a higher value can be used. It can observed that for an explicit method with $\mathrm{C_{max}} = 1$ and a wave velocity equal to the speed of sound in the material or fluid, the CFL conditions in Eq. [5-16] becomes the estimation of the stable time increment given by Eq. [5-15].

5.5.3 Partitioned solution of solid and fluid domain

The basic ideas and concepts of a partitioned solution of a multi-domain system are described in section 5.2. When applied to an FSI problem, the idea is that a solver specialised on CSM (Computational solid mechanics) and CFD can be used for the respective domains. Often when implementing this, a special interface algorithm needs to be included to transfer results between the two solvers, this algorithm can be based on some of the procedures described in section 5.2.

If the problem includes a deforming solid, as in FSI problems, consideration also has to be taken to the moving boundary of the two domains. An often used method to accomplish this is to include the ALE formulation within the CFD solver so that the fluid is able to follow the boundary motions from the

structural solver. Doing so means that the same considerations as described above in section 5.5.2 applies. Further, it is often recommended to use coincident meshes at the interface of the two domains as it can improve the accuracy, although it is not necessary.

When performing a partitioned solution the time increment size and stability of the solution is not only governed by the two solution domains as in a monolithic solution, but also on the stability of the interface algorithm. As previously mentioned, these interface algorithms can become unstable if the physical coupling is strong which can lead to very small time increments or a diverging solution. Therefore, it is only recommended to use this type of method for problems with a weak physical coupling.

5.6 Eulerian fluid methods

5.6.1 Coupled Eulerian-Lagrangian methods

The coupled Eulerian-Lagrangian (CEL) method attempts to capture the strengths of the Lagrangian and Eulerian formulations. In general, a Lagrangian reference frame is used to discretize the structure while an Eulerian frame is used to discretize the fluid. The boundary of the Lagrangian domain is typically taken to represent the actual interface between the solid and the fluid. Typical interface models use the velocity of the Lagrangian boundary as a kinematic constraint in the Eulerian calculation and the stress within the Eulerian cell to calculate the resulting surface force on the Lagrangian domain (Benson, 1992b). Different CEL algorithms may be characterized by the details of how this interface condition is treated. CEL algorithms generally provide good capability to solve simulations where the structure undergoes large deformations.

The CEL method was introduced by Noh (1964) in the sixties for a 2D problem. Successively it has been extended to a 3D problem. The solution of the equations in time is divided in three steps. In the first step the pressure in the Eulerian frame is used to calculate the force on the surface of the Lagrangian domain and, as a consequence, its motion. This operation could be done using many sub-cycles for each Eularian calculation. In the second step the modified Eulerian domain is calculated from the assumed position of the Lagrangian frame building up the new interface between fluid and structure. In the last step the discretised equations are solved in the Eulerian frame in order to calculate the new pressure that will act on the Lagrangian domain in the next time step.

The disadvantage of this method is that the acceleration of the fluid caused by the solid is not reflected in the fluid pressure causing an increased effective force acting of the structure.

A way to overcome this problem has been proposed by Olovsson (2000) with the introduction of a penalty force to be applied on both the Lagrangian and Eulerian nodes at the interface, see Figure 5-13. The penalty force is proportional to the relative displacement between the Lagrangian and the

Eulerian domains. In this case, all the Eulerian cells that contain a Lagrangian node will receive a restoring force. This can create a problem of mass leakage for the fluid cells that do not contain a Lagrangian node.

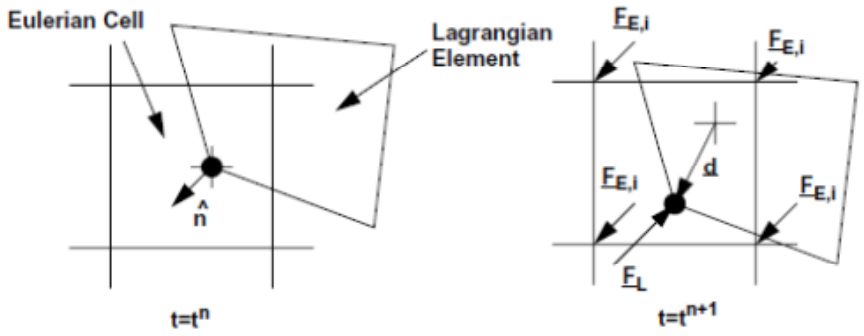

Figure 5-13: Introduction of a penalty force to the CEL contact, (Olovsson, 2000).

Another method consists in implicitly including the effect of the Lagrangian motion into the Eulerian materials. This is done by mapping the Lagrangian domain with its properties on the Eulerian domain before taking the next Eulerian time step. Anyway it is still necessary to calculate the forces acting on the Lagrangian cells due to the Eulerian material motion. The ZAPOTEC method, (Bessete et. al., 2003), couples an Eulerian code with a Lagrangian code through mapping the Lagrangian body over the Eulerian mesh, see Figure 5-14. All the Lagrangian properties are weighted by their volume overlap with the exception of the deviatoric stress that is instead weighted by the mass. All the mapped data are used for the Eulerian mesh update. The Lagrangian material surface is then determined by the stress state in the Eulerian mesh and the surface forces are calculated on it.

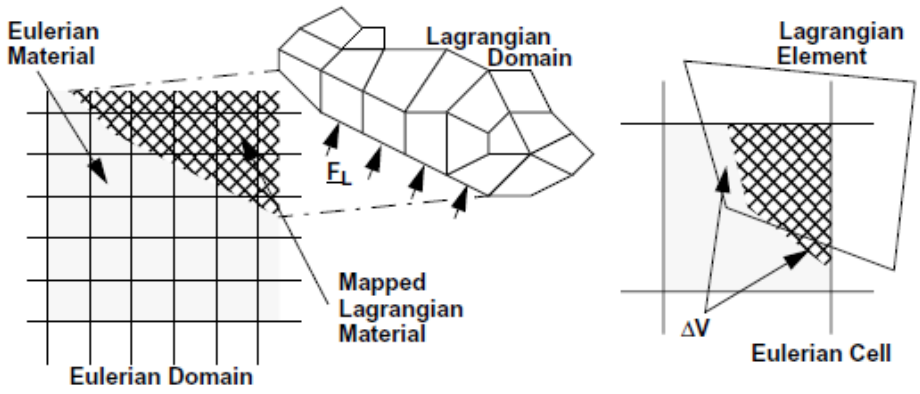

Figure 5-14: The Zapotec CEL method, (Brown et. al., 2002)

A summary of different CEL methods is given in (Brown et. al., 2002) when

applied to simulation of earth penetrating weapons. As previously stated, CEL methods are mainly used in applications where severe deformations are expected such as FSI with large structural and fluid displacements and various penetration applications. In extreme cases of structural displacement, or for interaction between two fluids, the same contact algorithms as used in CEL can be applied between two Eulerian materials.

5.6.2 Immersed boundary methods

The immersed boundary method was first introduced by Peskin in the 70s (Peskin, 1977) to study the interaction between viscoelastic bodies and viscous incompressible fluids. It is both a mathematical formulation, which uses a combination of Eulerian and Lagrangian variables and a numerical scheme. Typically the fluid is treated like an Eulerian variable that is defined over a Cartesian mesh while the solid is treated like a Lagrangian variable that is defined over a curvilinear mesh that moves independently through the Cartesian grid. The interaction between the Eulerian and the Lagrangian variables are treated by the numerical scheme with a smoothed approximation to the Dirac delta function.

The general idea is to have a method that easily can handle the fluid and structure dynamics equations. In fact, the Cartesian grid for the Eulerian variables facilitates the integration of the Navier-Stokes equations while the curvilinear grid for the Lagrangian variables facilitates the model of anisotropic viscoelastic materials.

Parallel to Peskin's method other methods using Cartesian grids have been developed with the same philosophical approach. It is common to refer to immersed boundary methods to include all such methods that treat viscous flow with immersed boundary on grids that are not tailored to the shape of these boundaries.

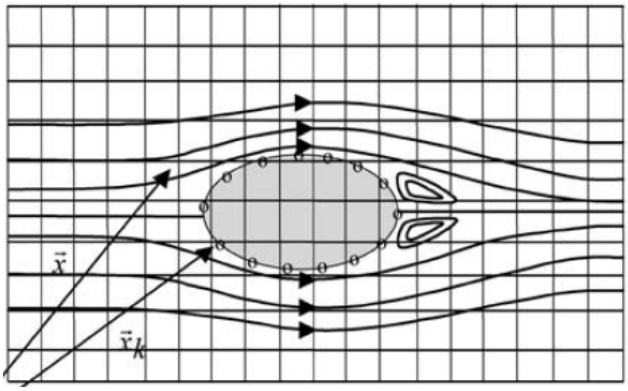

Figure 5-15: Eulerian $\vec{x}$ and Lagrangian $\vec{x}_k$ mesh

Immersed boundary methods strategy consists into discretize the Navier-Stokes equations on a non-body conformal Cartesian grid. The boundary conditions are imposed by a modification through a forcing function that

represents the body forces. There are two strategy to implement the forcing function: the first one, called continuous forcing, consists in including it directly in the Navier-Stokes equations that are then discretized on the whole domain, included the solid body; the second one, called discrete forcing, consists in firstly discretize the Navier-Stokes equations on the Cartesian grid and then modify them only in the cells near the immersed boundary.

The first strategy to implement the body forces gives very good results for immersed body with elastic boundaries. In presence of rigid body the solution is not so accurate and requires adjustments to improve the accuracy and the stability especially for high Reynolds number where the smoothing of the forcing function (Dirac function or other expressions) introduces blurring effects at the interface between the solid and the fluid. A general negative aspect of this first strategy is the necessary to solve the equations also inside the solid adding an additional computational effort.

The second strategy implements the forcing directly into the discrete equations. This introduces and higher order of difficulty to put it in place but it guarantees a sharp representation of the immersed boundary compared to the first strategy. In addition it is not required the solution of the equations inside the solid body saving computational power especially at high Reynolds number simulations. The drawback of this strategy is the difficulty of representing moving boundary and the necessity to introduce a pressure boundary condition at the immersed boundary.

Other immersed boundary methods do not use a forcing function. The cut-cell approach requires instead truncating the cells at the immersed boundary in order to create a mesh conforming the body shape. This method of course demands a higher computational effort in order to reshape the surface. In this case the shape of the cut cell can affect the stability. The ghost-cell method attempts to achieve a higher-order representation of the boundary using a ghost zone inside the body. Ghost cells are defined as cells in the solid that have at least one neighbour in the fluid. Then, for each ghost cell, an interpolation scheme includes implicitly the boundary conditions at the immersed boundary. (Tseng and Ferziger, 2003)

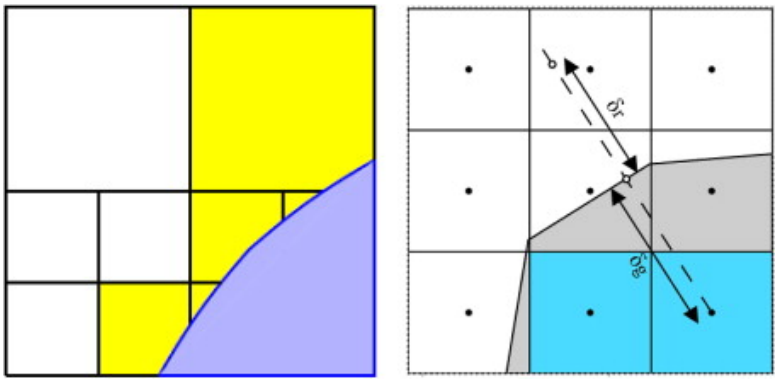

Figure 5-16: Cut-cell approach (left) and Immersed boundary methods with ghost cell.

Further there are methods that include a body conforming mesh into a Cartesian mesh.

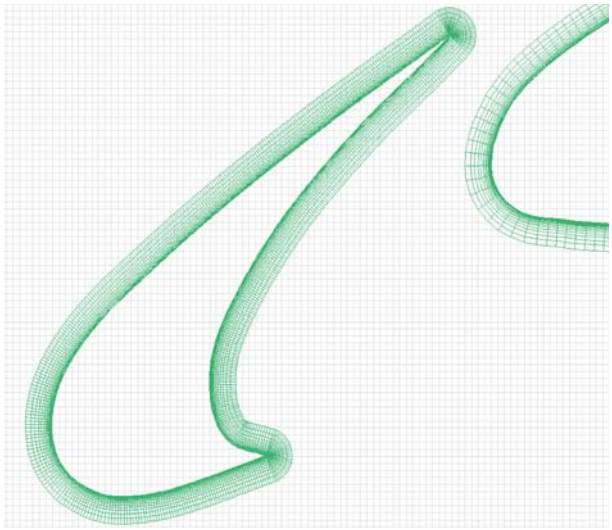

Figure 5-17: Body fitting mesh into Cartesian mesh.

For more information about the immersed boundary method see among others (Iaccarino and Verzicco, 2003), (Tseng and Ferziger, 2003), (Peskin, 2002) and (Mittal and Iaccarino, 2005).

5.6.3 Partitioned solution of solid and fluid domain

As for the partitioned methods described in section 5.6.3, it is possible to perform a multi-domain simulation with a separate structural solver and a separate CFD solver. In this case the CFD solver uses an Eulerian formulation which means that some method of tracking the location of the solid within the fluid domain has to be implemented in the interface procedure. Some variant of the above described CEL and immersed boundary method can for example be applied. Or for example in the case of an analysis which includes a free surface or a fluid-fluid boundary, the so called volume of fluid (VOF) method can be used (Hirt and Nichols, 1981).

Otherwise, the same consideration as previously described for partitioned solutions applies and special care needs to be taken when the physical coupling of the problem is strong.

5.7 Lagrangian fluid methods

The first developed finite element methods for analysing fluid dynamic problems were based on ordinary displacement based elements, so called

Lagrangian elements. But, due to the large deformation associated with fluid flow these proved to only have limited applicability to the problems. However, in recent years new Lagrangian methods has been developed, which uses the material formulation but are not constrained to the topology of the mesh that ordinary displacement based finite elements are, so called meshless Lagrangian methods. Although, many of these are in early stages of development they seem to show good promise, especially when dealing with problems that involve free surfaces. A couple of methods in this class are described in this section, but it should be noticed that many other exists.

5.7.1 Displacement based Lagrangian finite elements

In the early development of FSI methods with finite elements, the governing equations of fluid flow were discretised with ordinary Lagrangian displacement finite elements. These elements were chosen since they were well know and made the coupling between the solid and fluid domain easy. One example of such an FSI method using displacement based fluid elements is presented in Belytschko and Kennedy (1976).

When using a Lagrangian element, each node of an element is associated with a specific material or fluid particle, and follows that particle throughout the solution. In the case of fluid dynamics which often includes large flows, this assumption will inevitably lead the severe mesh distortion which will abort the simulation. Thus the use of Lagrangian based fluid elements is restricted to only certain kind of fluid problems. These can for example include static analyses, frequency analyses or transient dynamic analyses with very small flow or a very short time period. This is also noted in Belytschko and Kennedy (1976), where the presented simulation has a time period in the order of 10 milliseconds.

Due to these limitations the displacement based Lagrangian finite elements is seldom used for fluid flow and should only be used in special occasions.

5.7.2 Particle finite element method

The particle finite element method (PFEM) uses a complete Lagrangian description to model the motion of the nodes in both the fluid and the solid domain. The nodes represent particles that transport their momentum and physical properties. The method is suited for simulations that include free surface, fluid-structure interaction with large deformation of the physical domain.

The use of a Lagrangian mesh allows a unified formulation for solid and fluid domain with the suppression of the convective terms in the fluid equations. This simplification entails the necessity of frequent and efficient remeshing due to the large mesh motion. A finite element method is used to solve the continuum equations in both domains.

The method consists in using a finite element mesh to discretize the clouds of points in the solid and in the fluid domain. An Alpha Shape method is applied to identify the external boundary like free surfaces (Figure 5-18): all the

nodes on an empty sphere with a radius greater than an agreed value are considered as boundary nodes.

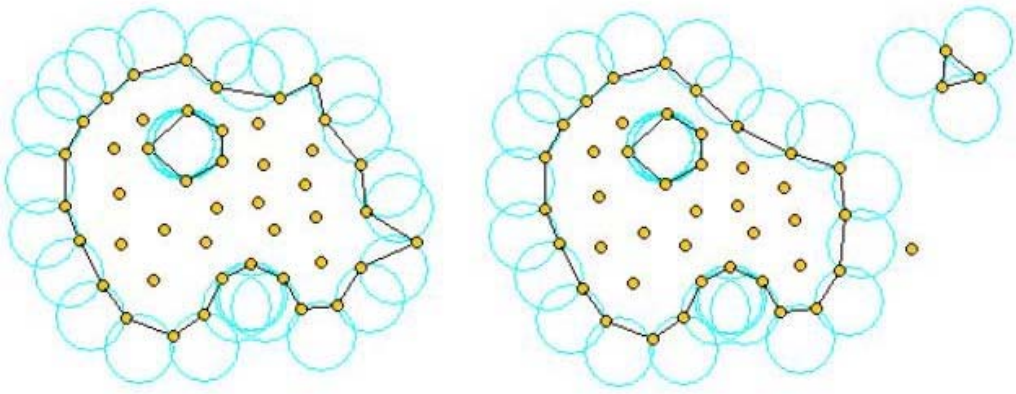

Figure 5-18: Schematic view of the Alpha Shape methods to identify external boundaries.

The equations of motions in the fluid and the solid domain are solved at the same time in a unified formulation. In this passage all the relevant variables of state are computed in both domains. Then the mesh is moved according to the solution. This passage can require the generation of a new mesh that is based on an extended Delaunay tessellation. The same process is then repeated in the next time step.

The generation of a new mesh is essential if the problem presents large deformation. Therefore, in order to improve this passage, special algorithms based on meshless finite element interpolation (MFEM) are used.

A finite calculus procedure (FIC) is used for the stabilization of the equations aiming to alleviate the volumetric locking effect caused by the incompressibility constrains imposed to the discretize solution of the finite element method: the fluid cannot penetrate the solid.

PFEM has been successfully used to solve strong coupling in fluid-structure interaction problems, see among others (Oñate et al., 2004), (Idelshon et. al, 2006) and (Oñate et. al 2011).

5.7.3 Smoothed particle hydrodynamics

The SPH methods simulate the continuum by means of discrete particles: the continuum is divided into pseudo-particles of constant mass. It has been developed by Gingold and Monaghan (1977) and Lucy (1977) for astrophysical application and successively applied to fluid and solid mechanics problems.

The fluid dynamics equations have the form

$$\frac{dA}{dt} = f(A, \nabla A, \boldsymbol{r}) \qquad [5\text{-}17]$$

where

$$\frac{d}{dt} = \frac{\partial}{\partial t} + \boldsymbol{v} \cdot \nabla \qquad [5\text{-}18]$$

is the derivative following the particle motion (Lagrangian). In the SPH method the approximation of the derivatives is computed by interpolating over the particles, which moves with the flow. The integral interpolation of any quantity A is based on the kernel function W:

$$A(\boldsymbol{r}) = \int A(\boldsymbol{r}')W(\boldsymbol{r} - \boldsymbol{r}', h)d\boldsymbol{r}' \qquad [5\text{-}19]$$

where ***r'*** is a differential volume element and *h* is a spatial distance known as smoothing length. This interpolation reproduces exactly A if the kernel is a delta function or rather if *h* tends to zero.

Dividing the fluid into a set of small mass, the integral can be approximated by a summation over the mass elements:

$$A_S(\boldsymbol{r}) = \sum_b m_b \frac{A_b}{\rho_b} W(\boldsymbol{r} - \boldsymbol{r}_b, h) \qquad [5\text{-}20]$$

Theoretically the summation is performed over all the mass particles but, in practice, it is limited to the neighbouring particle in the range 2*h* via the choice of a kernel function that vanish at a finite distance like a kernel based on cubic spline function (see Figure 5-19).

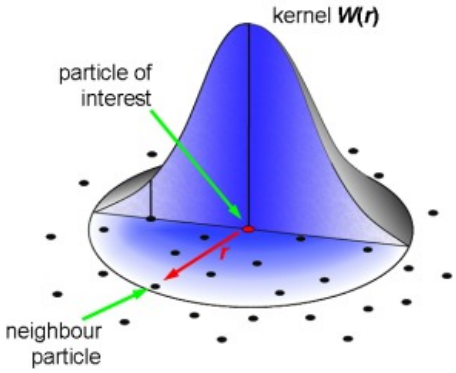

Figure 5-19: The principle of the SPH kernel function.

The SPH formulation allows a continuum description of FSI problems. Each particle can be characterised as fluid or solid preserving its properties along the simulation. Solving FSI applications need the addition of an artificial viscosity and an artificial stress into the momentum equation. The first is due in order to smooth out velocity oscillations which arise owing to non-uniform particle distribution in space where particles get too close to each other. The second one tends to eliminate the tensile instability caused by particles that tend to clump together causing non-physical fractures in the material.

A possible way to avoid the artificial viscosity in SPH methods is to apply time and space dependent smoothing length *h* in order to adapt it to the local conditions or to split the particles where needed.

SPH methods have the advantage to guarantee the mass conservation since the particles represent the mass. The pressure is directly calculated by the interaction with the neighbouring particles without solving linear system equations. The free surface is easily tracked by each particle properties (density).

The drawback is the need of a large number of particles in order to reach the same resolution of numerical methods based on mesh. Today SPH is mainly used for real time application where the accuracy is not a critical parameter.

More about SPH and its application in FSI and fluid mechanics analyses can be read in (Monaghan, 2005), (Anatoci et. al., 2007) and (Bøckman et. al., 2012).

6 Benchmark studies

The typical FSI problem encountered in a nuclear containment structure that is of interest during seismic loading consists of water filled pools of various size, for example the spent fuel and condensation pool. These water filled pools contributes with added mass to the structure which lowers the natural frequency of the structure as well as hydrostatic and hydrodynamic pressure that acts on the walls of the pool due to wave propagation in the fluid. Further, as the pools also have a free water surface towards the environment of the structure, free surface wave propagation also has to be accounted for; i.e. sloshing. This introduces extra non-linearity to the problem, since a free surface constitutes a boundary condition with an unknown location. The analyses presented in this section will focus on how different FSI methods can account for these effects.

The different FSI methods used in this section are available and implemented in general and commercial finite element analysis software. None of the methods used will be described in detail, but they will be referred to its general class of method described in section 5. Methods have been chosen so that as many of the different classes from section 5 as possible are represented. Two different benchmark examples will be analysed in this section to compare and evaluate the different FSI methods.

6.1 Tank sloshing

To be able to evaluate the accuracy of the different FSI methods the first benchmark example is chosen as a simple tank sloshing problem, for which both experimental results and a simplified analytical solutions according to section 3.2.4 are available. The main purpose of this example is to evaluate how different methods are able to describe the sloshing of the fluid as this is considered as the most difficult aspect to describe properly. The hydro-dynamic pressure on the tank walls and the deformation of the tank will be evaluated as well.

6.1.1 Experimental setup

The tank of the example is chosen from a series of experiments performed at the Hydraulic Institute of Stuttgart and presented in (Goudarzi and Sabbagh-Yazdi, 2012) among others. The experiments consisted of a series of shaking table tests of a partially water filled rectangular tank that was excited by a shaking table. The experimental setup is shown in Figure 6-1.

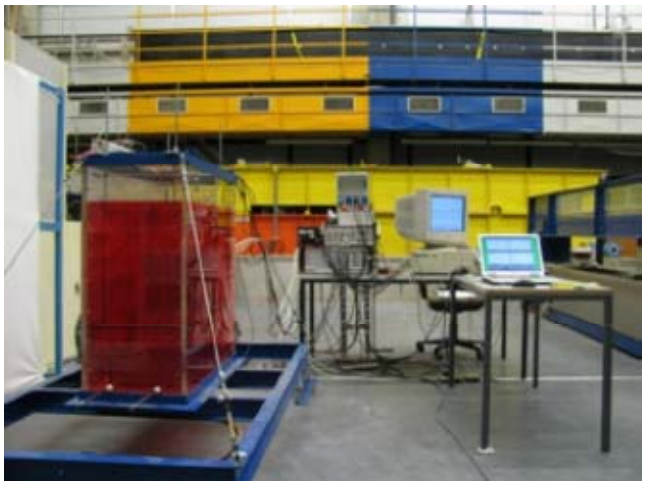

Figure 6-1: Experimental setup with tank model and shaking table, from (Goudarzi and Sabbagh-Yazdi, 2012).

The rectangular tank is made of 0.02 m thick reinforced acrylic glass (Plexiglas) and is 1 m high, 0.96 m long and 0.4 m wide. During the test series it was subjected to a periodic excitation in the length direction of the tank, with amplitude of 0.005 m and different frequencies. Further, test was also made for four different water levels; 0.192 m, 0.336 m, 0.48 m and 0.624 m.

For this benchmark example a test with a water level of 0.624 m has been chosen. Further, the excitation frequency is chosen as 79.1 % of the first natural frequency of the water body, this corresponds to approximately 4.409 rad/s.

6.1.2 Finite element model of the tank

Since the structure is assumed to be deformable a 3D model is used to be able to properly define the stiffness of the different tank walls. The finite element model of the tank is shown in Figure 6-2, which shows the mesh and also the areas at which boundary conditions are applied. It can be seen in the figure that symmetry conditions (green line) have been utilised. Normally this is not recommended in transient analyses, but since the excitation and thus the fluid flow occurs mainly in the x-direction it is deemed possible so that the size of the model can be reduced. Thus, a symmetry condition is placed in the middle of the tank in the yz-plane. Further, the initial water level is indicated by the blue line and the location of the shaking table by the red area. The shaking motion is applied as a translation in the x-direction while all other degrees of freedom at the bottom of the tank are constrained.

The fluid is not included in the figure since the mesh of the fluid is different for different FSI methods.

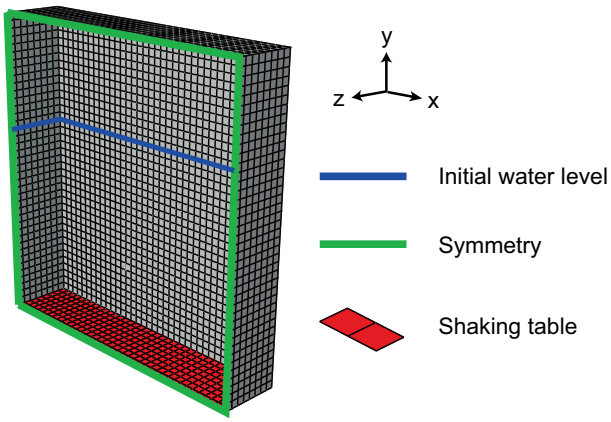

Figure 6-2: Finite element model of the tank including boundary conditions.

For all analyses, unless otherwise specified, the tank is modelled with 4-noded shell elements with full gauss integration in the in-plane directions and 2 point gauss integration in the thickness direction. The elements are given a thickness of 0.02 m and material properties according to Table 6-1 with a linear elastic material model.

Table 6-1: Material properties of the tank.

Acrylic glass	
Young's modulus	3.2 GPa
Poisson's ratio	0.3
Density	1200 kg/m^3

The water is given properties according to Table 6-2. However, for some FSI methods the bulk modulus is reduced with a factor 1000 to increase the maximum time increment, thus reducing the computational time of the simulation. Even with this assumption the bulk modulus is high enough to keep the flow incompressible and this assumption is widely used in the literature.

Table 6-2: Material properties of the water.

Water	
Bulk modulus	2.25 GPa
Dynamic viscosity	0.0013 Pa/s
Density	1000 kg/m^3

It should also be noticed that all analyses are performed with direct time integration methods, either implicit or explicit integration, and that no

damping is applied to the tank. In some of the FSI methods, however, damping occurs naturally in the governing equations of the fluid domain, due to their nonlinearity.

6.1.3 FSI methods

A number of different FSI methods are used in this example, ranging from purely analytical methods to advanced numerical methods. All numerical methods are available in commercial FE-software and in this study methods from the flowing software's have been used:

- ABAQUS, (Dassault Systèmes, 2012).
- ADINA, (Adina, 2011).
- SOLVIA, (Solvia, 2011).

All methods are summarised in Table 6-3, in which their main characteristics are given as well.

Table 6-3: Summary of FSI methods used.

Number	Method	Integration scheme	Analysis type	Software
1	Structure only	Implicit	Linear transient, Frequency	Abaqus, Solvia
2	Analytical	-	Linear transient, Frequency	Matlab
3	Housner	Implicit	Linear transient	Abaqus
4	Epstein	Implicit	Linear transient	Abaqus
5	Acoustic, potential based	Implicit	Linear transient, Frequency	Solvia, Adina
6	Acoustic, subsonic potential based	Implicit	Non-linear transient	Adina
7	Acoustic, velocity	Implicit	Linear transient, Frequency	Abaqus
8	ALE, monolithic	Explicit	Non-linear transient	Abaqus
9	ALE, monolithic	Implicit	Non-linear transient	Adina
10	ALE, partitioned	Implicit	Non-linear transient	Adina

To analyse the behaviour of the tank a frequency analysis is performed in which only the tank is included. This analysis is defined as method number 1. A reference transient analysis is also performed to study the response in the tank wall when water is only included as a hydrostatic pressure.

Analysis method number 2 is based on the simplified linear analytical solution to tank sloshing presented in section 3.2.4. The solution assumes a two dimensional flow and assumes the tank is rigid. It also neglects all non-linear terms of fluid flow. The solution is easy to use to verify more advanced numerical schemes.

Two versions of simplified FSI methods in which water is included as a mass and spring system, as described in 5.4, are also used. These two are labelled analysis method number 3 and 4 and are based on the theories of Housner (1963), section 3.2.2, and Epstein (1976), section 3.2.3, respectively. Both analyses are used to compare the response in the tank wall in a transient analysis.

Analysis methods number 5 to number 7 are all based on acoustic theory as presented in section 5.5.1. In method number 5 the unknown nodal quantity of the fluid is the scalar velocity potential and only linear terms are included in the governing equations, i.e. no actual flow in the equations. It should also be noted that this method is available in both ADINA and SOLVIA. Method number 6 is also based on the velocity potential as the unknown variable, but also includes the nonlinear terms in the wave equation. Thus actual flow can be described by the wave equations. In both method number 5 and number 6 body forces are included in the equations which make it possible to include the hydrostatic pressure implicitly in the simulation. This is not included in analysis method number 7, which is based on an acoustic formulation with the fluid velocity as the independent variable. In this method the hydrostatic pressure needs to be included as a pressure load on the structure. Common for all three methods is that the finite element mesh is stationary at all nodes except at the boundaries of the fluid domain, i.e. the fluid-structure interface and the free surface. Furthermore, since none of the acoustic nodes has a translational degree of freedom a boundary element has to be added to the free-surface boundary to describe the sloshing motion. It should also be noted that all the acoustic methods are solved with an implicit time integration scheme using either the Newmark method or the Hilber-Hughes method.

Analysis method number 8 is a non-linear method in which the fluid flow and the structure are solved simultaneously with an explicit time integration scheme. Since an explicit solver is used, this analysis uses the assumption with a lower bulk modulus of the fluid (2.25 MPa) to increase the stable time increment. The fluid is assumed as an incompressible fluid with small viscous forces that stabilises the fluid flow; i.e. basically inviscid flow. The fluid domain is spatially discretized with an ALE formulation, based on the operator split method as described in section 5.5.2, with 8-noded brick elements with reduced gauss integration. The fluid-structure interaction is included through contact equations with the no penetration criterion.

Both methods number 9 and number 10 are based on the same procedures for the structure and fluid respectively. But for method number 9 the equations of the fluid and the structure are solved simultaneously as described in section 5.2.1, while the equations in method number 10 are

solved in an iterative fashion as described in section 5.2.3. In both methods the fluid domain is described with an ALE-formulation based on an operator split and all equations are solved with an implicit time integrations scheme. The elements of the fluid domain are 3-dimensional so called flow-condition-based-interpolation (FCBI) elements, which incorporate some aspects of finite volume elements into the finite element formulation, see for example (Bathe and Zhang, 2002). Due to extensive computational time, method number 9 and number 10 will only be analysed in two dimensions. Since the side walls of the tank that are not included in a 2D analysis makes a significant contribution to the stiffness of the tank, the elastic modulus of the tank is increased to simulate an almost rigid tank. Hence, only the response of the fluid domain will be compared to the other analysis methods. To reduce the computational time as much as possible the bulk modulus of the fluid is reduced to 2.25 MPa to increase the maximum time increment that gives an accurate solution. With the used bulk modulus the maximum recommended time step is 2 ms, compared to 0.064 ms with the original bulk modulus.

6.1.4 Frequency analysis

To increase the understanding of the behaviour of the tank and the water body, frequency analyses are performed for the methods where it is possible; i.e. the linear methods. The first five natural frequencies are presented in Table 6-4 for analysis method number 1, 2, 5 and 7. It should also be noted that the frequency of the driving motion is 0.7 Hz in the longitudinal direction of the tank.

Table 6-4: Natural frequencies from different analysis method, first five modes.

Mode number [Hz]	1st	2nd	3rd	4th	5th
1. Tank only	46.69	48.28	83.07	93.75	99.08
2. Analytical, water	0.89	-	1.56	-	2.02
5. Acoustic, water longitudinal modes	0.89	1.28	1.57	1.81	2.03
7. Acoustic, water longitudinal modes	0.88	1.27	1.55	1.79	1.99

From the table it can be seen that the five lowest natural frequencies of the tank without any water lies in the interval 46.69 to 99.08 Hz, this is approximately a factor 100 times the driving frequency, which therefore should not excite the eigen modes of the tank. The eigen modes that correspond to the first five natural frequencies are shown in Figure 6-3. From the figure it can be observed that the sidewall of the tank is most keen to deform due to periodic excitement, which also corresponds to the deformation of the tank due to the hydrostatic pressure of the water body.

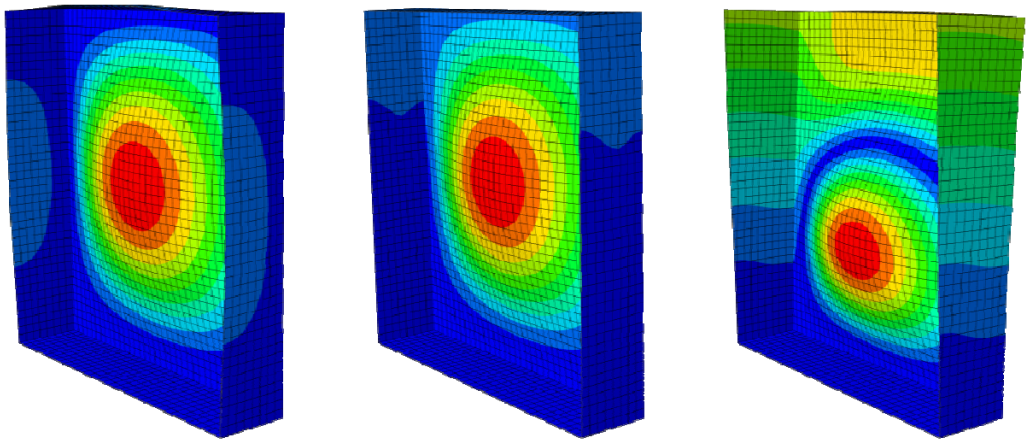

a) 46.69 Hz b) 48.28 Hz c) 83.07 Hz

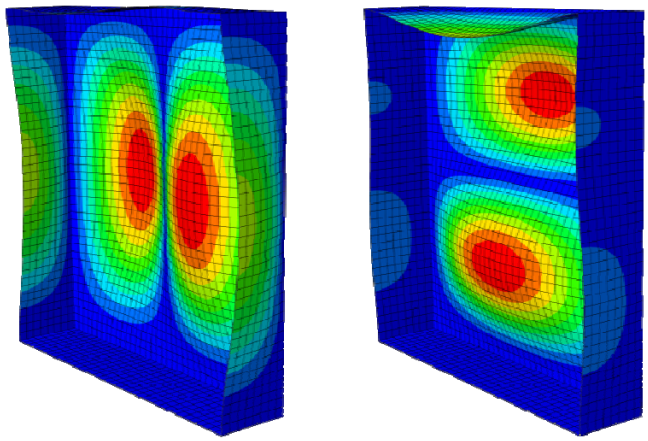

d) 93.75 Hz e) 99.08 Hz

Figure 6-3: First five eigen modes of the tank.

When looking at the natural frequencies of the water body it can be observed that the first five natural frequencies lie in the interval 0.88 to 2.03 Hz. These eigen modes correspond to gravity waves of the free surface of the water body which are shown in Figure 6-4 for both analytical and numerical methods. From the figure and table above it can be noted that both methods give equal results in both mode shape and frequency, and that the two numerical methods used also corresponds well with each other. It should however also be observed that the analytical method only gives results for uneven wave numbers as mentioned in section 3.2.4.

In addition, when the responses from different mode shapes are compared it can be observed that mode number 1 gives the largest response. Consequently mode number 1 will dominate the response of the water body, which is also noticed in the literature, e.g. (Goudarzi and Sabbagh-Yazdi, 2012). When comparing the frequency response with the experimental setup

it should be remembered that the driving frequency of the experiment was chosen to be close to the first natural frequency so that the first mode would dominate the response.

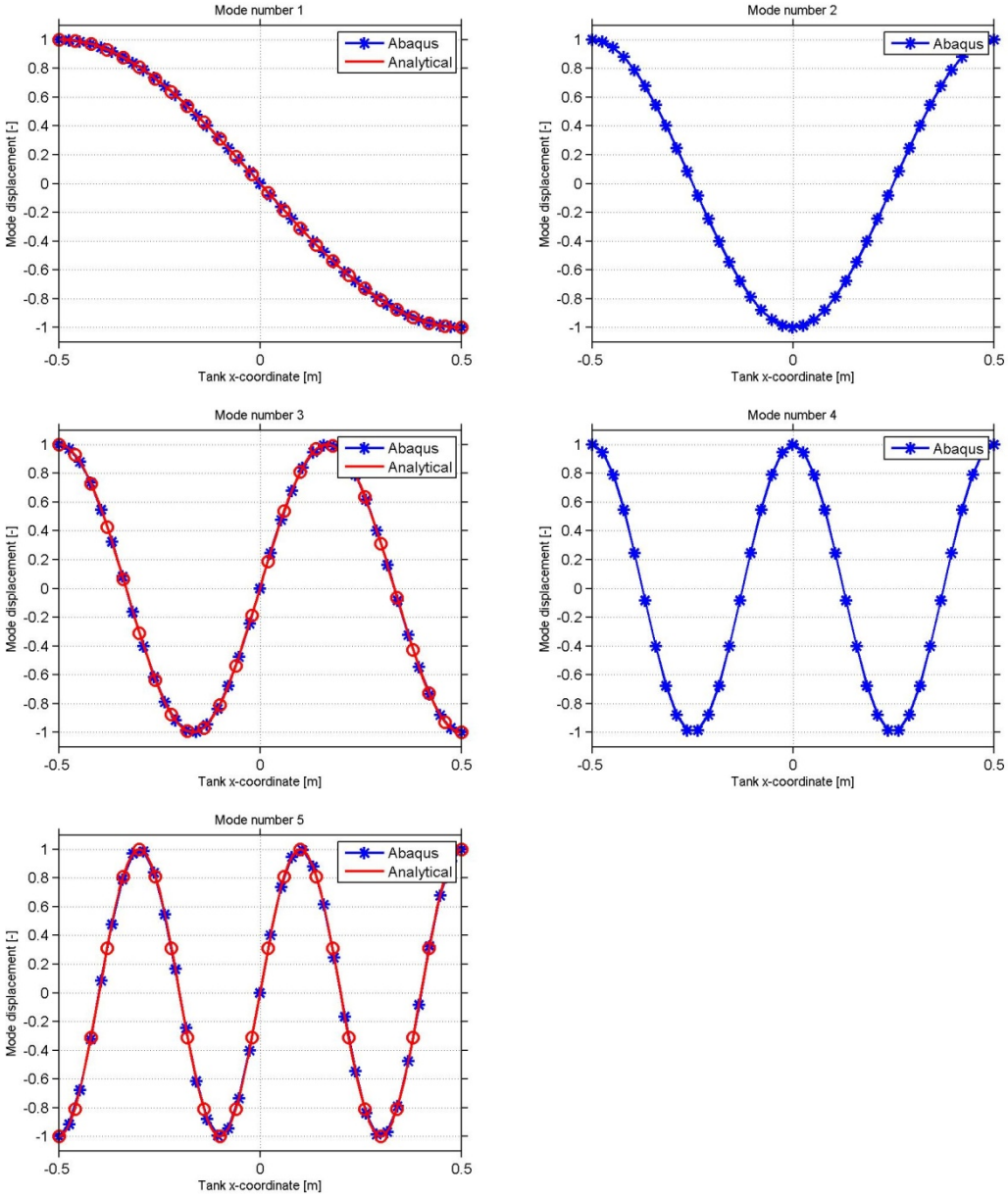

Figure 6-4: First five eigen modes of the water body.

The above presented mode shapes only considers waves in the longitudinal direction of the tank since these are of most interest since the harmonic excitation of the experimental setup is in this direction. It should, however, be noted that since the numerical methods are three dimensional there also exists eigen modes in other directions and two dimensional modes. An example of such a two dimensional mode is shown in Figure 6-5, which has a natural frequency of 2.11 Hz.

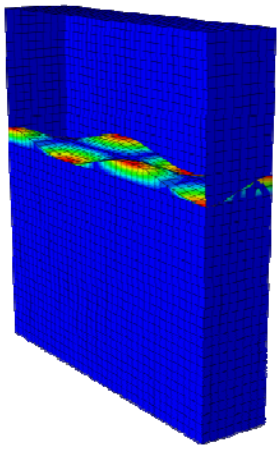

Figure 6-5: Two-dimensional eigen mode of the water body with a natural frequency of 2.11 Hz.

6.1.5 Water Free Surface

From (Goudarzi and Sabbagh-Yazdi, 2012), measurements of the free surface movement close to the left wall of the tank can be found. Therefore, this parameter is very important when comparing and validating the different analysis methods. In the following section, results from the different analysis methods are compared with the results from experimental measurements.

The time history of the free surface movement obtained from the analytical solution, method number 2, is presented in Figure 6-6. The result of the analytical solution corresponds very well with the experimental data, although the wave height is slightly overestimated. However, the analytical solution seems to deviate more from the experimental data in the three beating phases, where the peak of the second wave of each beating phase is largely overestimated. For the third beating phase the measurement only shows one peak, whereas the analytical solution shows the highest second peak in a beating phase.

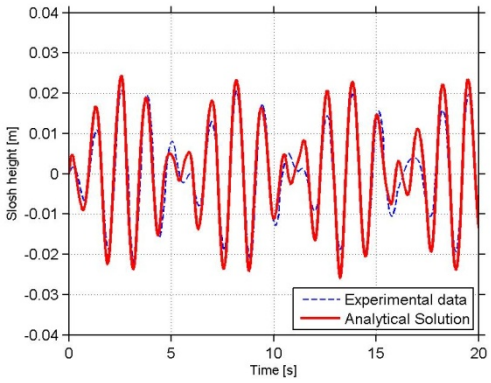

Figure 6-6: Wave height from the analytical solution, method number 2, and the experimental results.

The results of the free surface movement from the four different acoustic formulations, method number 5 to 7, are shown in Figure 6-7. It can be observed that all four analysis methods show consistency with the experimental results. The two linear potential formulations Figure 6-7a) and b), from Adina and Solvia respectively, overestimates the wave height slightly and misses the number of peaks in the beating phase. When switching to a non-linear potential formulation, Figure 6-7c), a slightly better agreement is reached concerning both the wave height and the beating phases, where the peaks have lower magnitude than the linear solution. The wave height is, however, still larger than in the experimental measurements. Results from non-linear velocity formulation shown in Figure 6-7d) also shows good agreement with the experimental results, for both the overall sloshing height and in the beating phases.

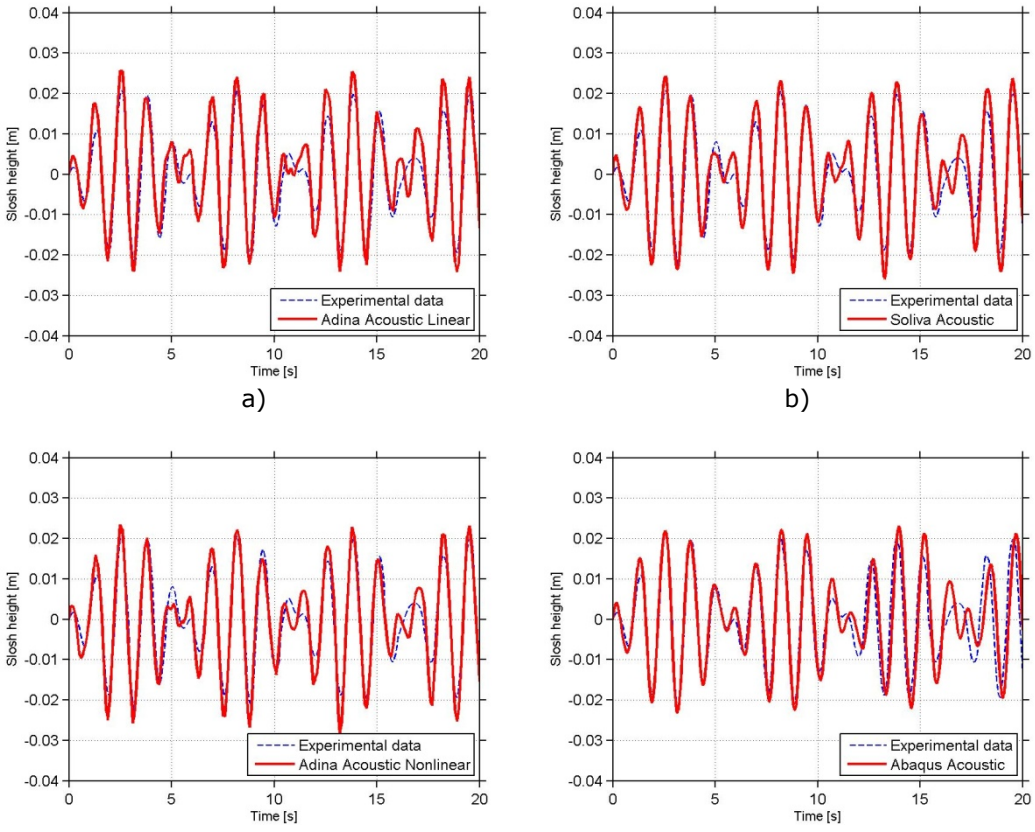

Figure 6-7: Wave height from the acoustic simulations, a) and b) method number 5, c) method number 6 and d) method number 7. Experimental results are included for comparison.

Regarding all the non-linear methods which describe actual fluid flow, it should be noticed that little effort has been put on adjusting numerical parameters of the analysis to obtain a more accurate solution. The purpose of this choice is to show that even though these non-linear methods have the

potential to describe the flow more accurately than the acoustic, they also demand a lot more from the user to obtain good results; especially when coupled with a structural analysis. With this in mind, the time history results of the sloshing height for the non-linear simulations is presented in the following.

In Figure 6-8 the time history results of the sloshing height is shown for analysis method number 6, a non-linear monolithic solution with explicit time integration, where the fluid domain is described with an ALE formulation. The sloshing height agrees well with the experimental results during the majority of the solution, but at the third beating phase, around 15 seconds, the solution starts to deviate from the measurements. For the last part of the solution the sloshing height deviates from the measurements but the periodicity of the wave is still preserved.

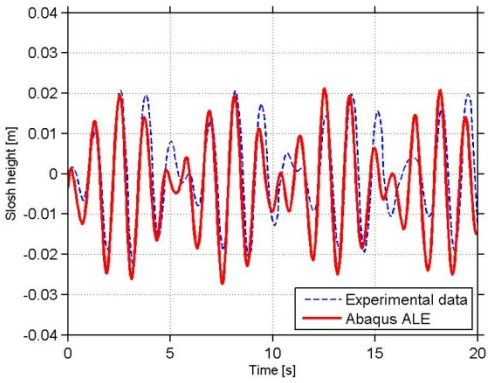

Figure 6-8: Wave height from the analysis method number 8 with experimental results.

The reason for the deviating solution after 15 seconds is probably due to significant amounts of hourglass energy, i.e. zero strain deformation modes of the elements, in the system, see Figure 6-9. In the final time increment of the simulation the hourglass energy in the whole model amounts to 20 % of the strain energy in the whole model.

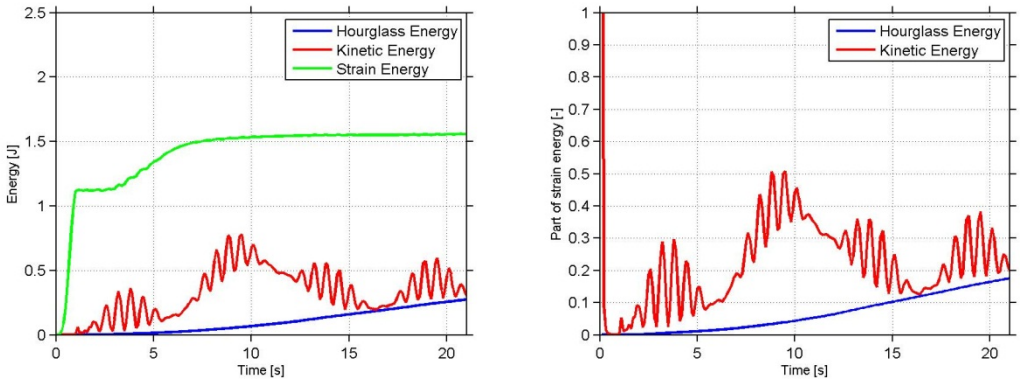

a) b)

Figure 6-9: a) Different energy measures of the whole model and b) energies compared with the strain energy.

Figure 6-10 shows how the hourglass energy is distributed in the fluid domain in the last time increment of the solution. The figure shows that most of the energy is concentrated at the side wall contact surface, red areas, but also towards the free surface and the bottom. It can also be observed that the introduction of hourglass energy creates spurious deformation modes in the elements that constitute the free surface. This deformation can be seen in Figure 6-10. This spurious deformation at the free surface can help to explain why the sloshing height is underestimated in some parts of the time history in Figure 6-8. It should, however, be noted that the vertical deformation is magnified with at factor 5 in Figure 6-10.

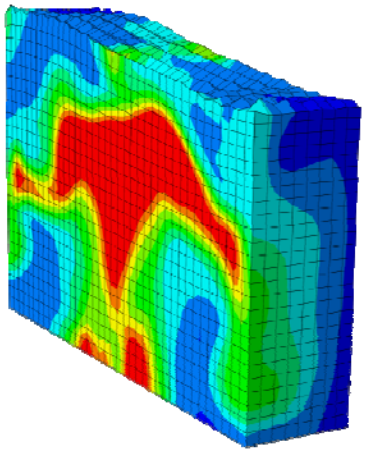

Figure 6-10: Hourglass energy and deformation of in the fluid domain at the last time increment of the solution.

Results from analysis method number 9 and 10 are shown in Figure 6-11. Both analyses basically use the same procedures except for how the fluid and solid domains are coupled, where monolithic coupling is used Figure 6-11a) and partitioned coupling is used Figure 6-11b). The results, however, show that both simulations give almost identical results and agree very well with the experimental results.

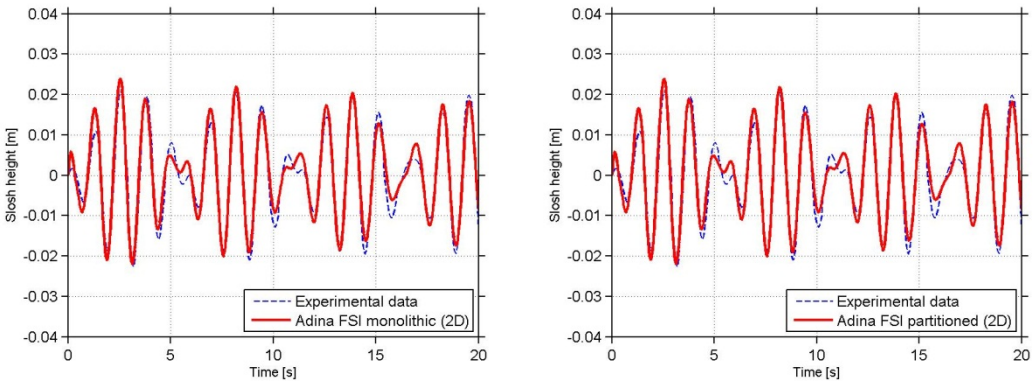

a) b)

Figure 6-11: Wave height from a) analysis method number 9 and b) analysis method number 10 compared with experimental results.

6.1.6 Other Results

To further compare the different analysis methods other results and aspects of the different simulations are shown and discussed in the following section.

Time history of the fluid pressure

The variation in the hydrodynamic fluid pressure is studied for all methods at a depth of 0.1 m below the surface close to the left wall. This should give an indication on how large load the fluid will exert on to the tank wall during the periodic motion. The hydrostatic pressure at this depth is approximately 1 kPa and that since no measurements are available on the fluid pressure the analytical solution will be included in all figures as a reference solution.

The hydrodynamic pressure for all acoustic simulations, method number 5 to 7, is shown in Figure 6-12 together with the result from the analytical solution. In all four analyses significant numerical noise is present in the first tenths of a second of the solution; this is probably due to numerical instability and inaccurate initial condition and is disregarded when discussing the solution. From the figures it can be seen that the maximum hydrodynamic pressure varies between 20-40 % of the hydrostatic pressure, i.e. 0.2-0.4 kPa. This magnitude is reasonable considering that the free surface varies with ± 2 cm, which correspond to a change in pressure calculated as $\rho gh = 1000 \cdot 9.81 \cdot 0.02 \approx 0.2$ kPa. The different time variation obtained from the various methods is probably due to the numerical treatment, in how the equations are solved and how the elements of the respective domain are coupled when setting up the equations. This is especially evident when comparing Figure 6-12a) and b), which are both based on almost identical linear velocity potential formulations. The result in Figure 6-12b) shows almost identical results as the analytical solution whereas the result from Figure 6-12a) shows slightly larger hydrodynamic pressures and also deviates in the beating phases. One significant difference between the analyses is that Figure 6-12a) uses the Newmark time integration, while Figure 6-12b) uses the Hilber-Hughes time integration, since Newmark time integration gave unstable results in Solvia. This could also help to explain the noise in the beginning of the signals in combination with the impulse that is exerted in both the fluid and the structure when the periodic motion starts. Since the noise is very high frequent, a filter could have been used to remove it, but this has not been done here since the purpose is to compare the different methods with each other. The non-linear version of the velocity potential formulation in Adina, Figure 6-12c), shows almost identical results as its linear counterpart in Figure 6-12a). The acoustic velocity formulation shown in Figure 6-12d) exhibits a hydrodynamic pressure variation that is in good agreement with the analytical solution, although significant noise is present in the beginning of the time history; as for the other methods.

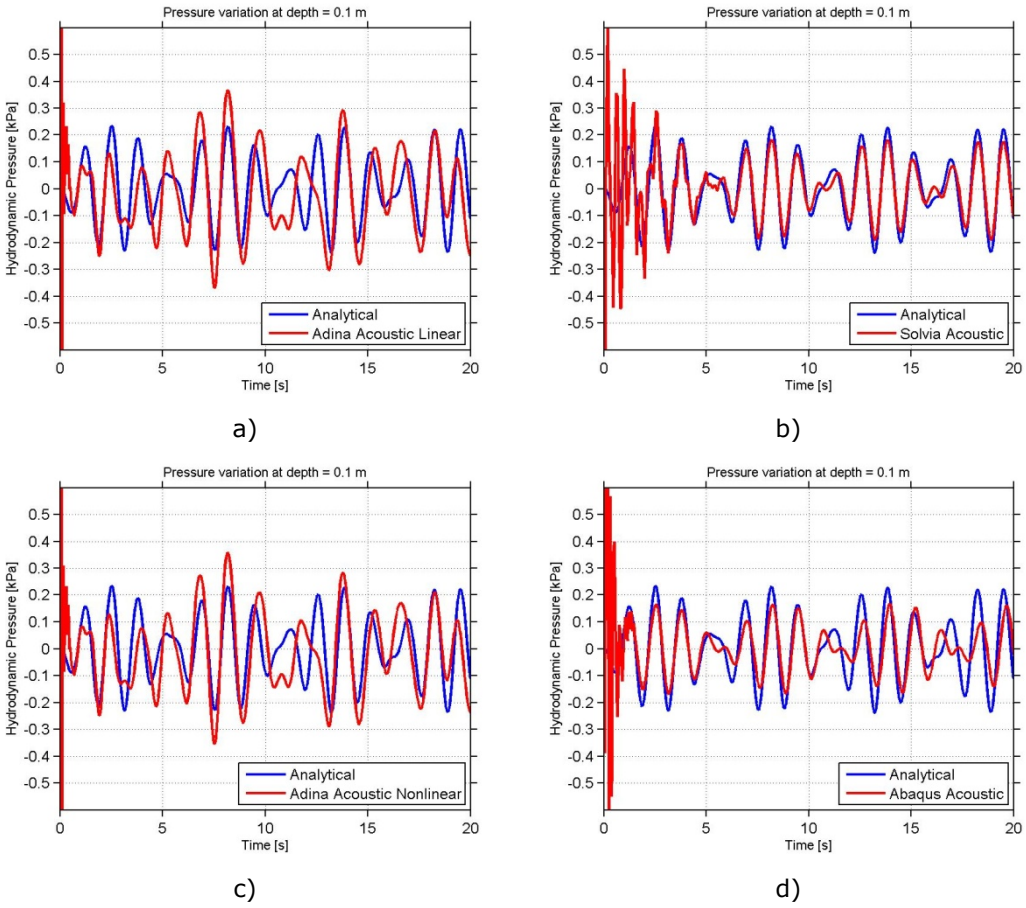

Figure 6-12: Hydrodynamic fluid pressure from acoustic simulations, a) and b) method number 5, c) method number 6 and d) method number 7. Results from the analytical solution included for comparison.

In all methods where the fluid domain is described with an ALE mesh, i.e. method 8 - 10, it is difficult to measure the hydrodynamic pressure at a specific depth since the nodes are not stationary in the vertical direction. This can be compared to the used acoustic methods and all Eulerian methods where the nodes are stationary at a specific depth. Hence, depending on the motion of the nodes, the nodal pressure will be almost constant in time for the ALE methods, since the nodes most often follows the vertical motion of the free surface.

This can for instance be observed in Figure 6-13, which shows the results from a monolithic analysis with explicit time integration and an ALE adaptive mesh in the fluid domain, method number 8. The result point is chosen so that its initial location is 0.1 m below the initial water surface. The red curve in the figure shows the variation of the nodal pressure at that result point. It can be observed that the variation in nodal pressure is significantly smaller than that predicted by the analytical solution, the blue curve, as expected. If, however, the pressure that corresponds to the vertical displacement of the result point is added to the nodal pressure, so that the pressure in the fluid at

a stationary depth is obtained, the green curve, very good agreement is achieved between the analytical solution and the numerical solution. From the figure it can also be observed that significant numerical noise is present in the beginning of the solution, which is probably due to difficulty in obtaining a stable initial condition in the fluid domain.

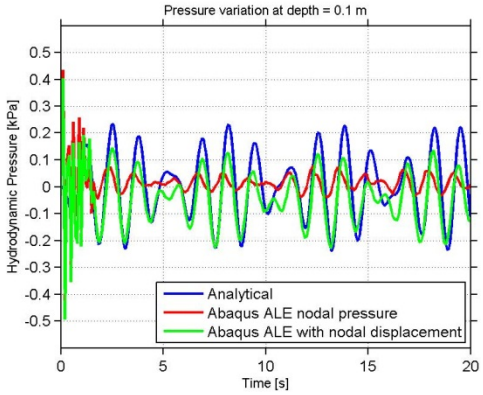

Figure 6-13: Fluid pressure from analysis method number 8 compared with results from the analytical solution.

The same can be observed from the implicit FSI formulations in Adina, method nr 9 and nr 10, in which the fluid domain is also described with an ALE mesh. Looking at the red curve, in Figure 6-14, which shows the variation in nodal pressure at a specific node, it can be seen that the pressure is almost constant when compared to the pressure variation from the analytical solution. If however, the variation in the vertical coordinate of the node is taken in to consideration and added to the nodal pressure, green curve, it can be observed that the numerical solution and analytical solution agrees very well. Further, it can be noticed that the monolithic, Figure 6-14 a), and partitioned method, Figure 6-14 b), give almost identical results.

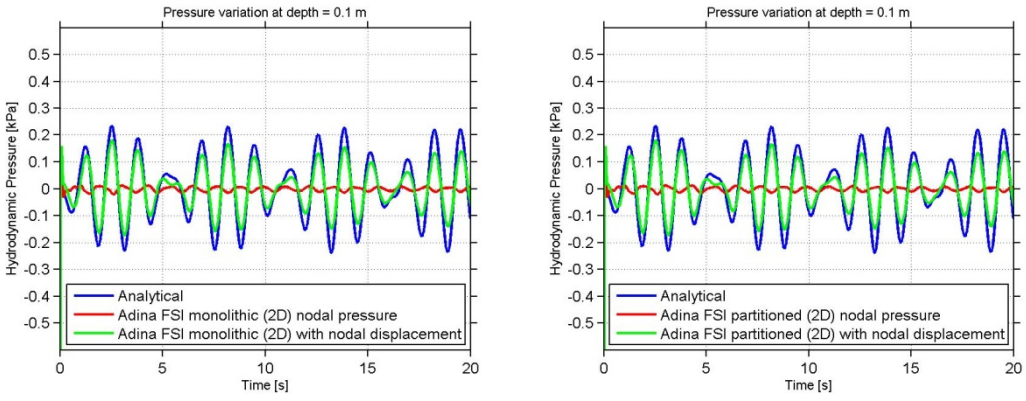

a) b)

Figure 6-14: Fluid pressure from a) analysis method number 9 and b) analysis method number 10 compared with results from the analytical solution.

To study how the hydrodynamic pressure varies over the height of the tank wall its vertical distribution is plotted over the height of the left tank wall in Figure 6-21. The pressure is shown for analysis method number 2, 5, 7, 8 and 9 at two time points, 13.1 and 13.8 seconds, which correspond to one maximum value and one minimum value in the above presented time histories, respectively. The distribution of the hydrodynamic pressure at 13.1 seconds is shown in Figure **6-21**a) and at 13.8 seconds in Figure **6-21**b). In the figures the hydrodynamic pressure is normalised against the hydrostatic pressure at the given depth. From both time points it can be observed that all methods give similar pressure profiles and that the largest relative increase in pressure is obtained close to the free surface. This indicates that most of the hydrodynamic pressure in this test setup comes from the convective pressure and only a small portion from the impulsive pressure, which tends to give a larger increase close to the bottom of the water body. It can also be observed that the acoustic method in Adina, method number 5, gives the highest increase in pressure and that the acoustic method in Abaqus, method number 7, give the lowest increase in pressure. As mentioned earlier, a significant difference between these two methods Adina includes the hydrostatic forces implicitly in its governing equations while Abaqus only considers the hydrodynamic pressure. This can be one cause of the different results, since this means that no impulsive part is included in Abaqus.

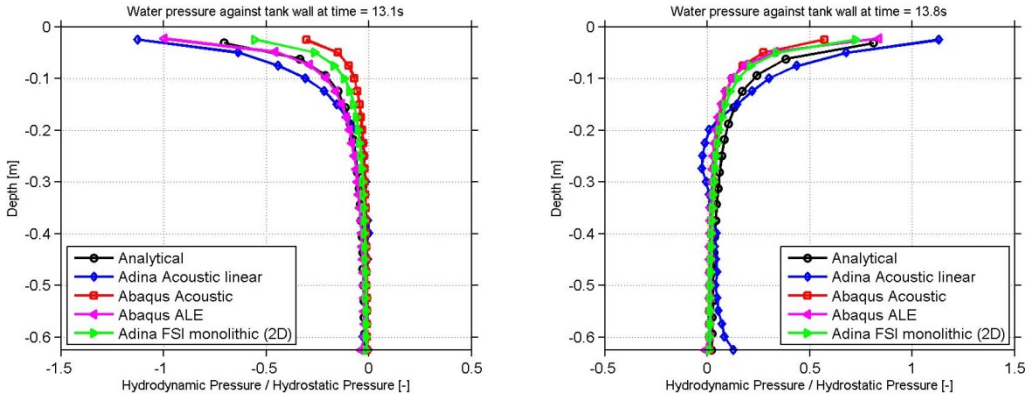

a) b)

Figure 6-15: Hydrodynamic pressure distribution against a side tank wall normalised with the hydrostatic pressure. At time a) 13.1 s and b) 13.8 s.

Response of the tank wall

To compare the effect that the fluid has on the structure, in this case the tank, time histories of the stress response will be compared for different methods. It is chosen to compare an effective stress, here chosen as the von Mises stress. From looking at the spatial variation of the von Mises stress in a static case, Figure 6-16, a point approximately 0.13 m from the bottom of the tank towards the symmetry plane is chosen for the comparison. This point is chosen since it is the location of the highest concentration of stresses in towards the symmetry plane of the left and right walls. The time histories are extracted at the gauss integration point closest to the outside surface of the

tank. This point is located at a relative thickness coordinate of 0.577, where 1 equals the outside surface and 0 the midsurface of the shell element.

Figure 6-16: Distribution of stress in the left tank wall, looking of the chosen result point is marked in the figure.

To compare all different methods, a reference solution is made in which only the hydrostatic water pressure is applied as a pressure load on the tank, i.e. method number 1. The variation of the von Mises stress with the periodic motion from the reference solution is presented in Figure 6-17. It can be seen that the dynamic contribution to the stress state is of a magnitude equal to 0.05 kPa, which can be compared to the static stress state in the result point that equals 108 kPa. Hence, the dynamic load increases the stress in the result point with 0.046%. In other words, the dynamics load has little effect on the stress state of the tank.

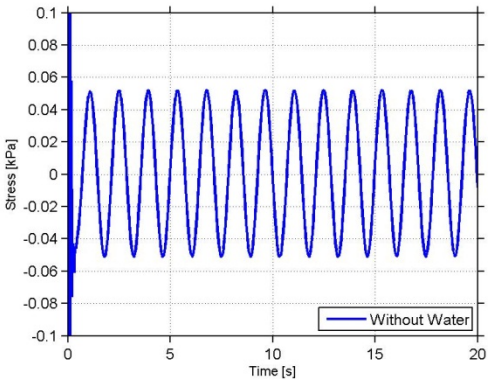

Figure 6-17: Dynamic part of the von Mises stress from the reference solution without water.

In addition to the different methods for including water in the analyses compared above, the two simplified methods number 3 and number 4 are also analysed when comparing the response of the tank. The properties of method number 3 and 4 are compared in Table 6-5. In the table the masses and spring stiffness are presented per meter in the thickness direction of the water body, z-direction, and the height is measured from the bottom of the tank. I can be noticed that the biggest difference between the two methods is the location of the convective mass. Further, the springs that connect the convective mass are distributed over half the height of the convective mass as prescribed by ASCE 4-98, see Section 3.1.1.

Table 6-5: Properties of the mass and spring system in method number 3 and 4.

Method number	Impulsive		Convective		
	Mass [kg/m]	Height [m]	Mass [kg/m]	Height [m]	Spring Stiffness [(kN/m)/m]
3. Housner	395.6	0.234	231.7	0.207	7.14
4. Epstein	391.1	0.234	235.0	0.389	7.35

The time history of the von Mises stress at the chosen result point from the two simplified FSI methods are presented in Figure 6-18 and compared to the analysis without water. It can be observed from the figure that both methods exhibit significant noise in the first second of the solution, as have been shown for most of the other simulations as well. The dynamic contribution now has a magnitude of 5-8 kPa compared to 0.05 kPa from the analysis without water. If the mass and spring system is defined according to Housner, Figure 6-18a), a dynamic increase of 7.4% is obtained if compared to the static load case. The analysis with a mass and spring system according to Epstein, Figure 6-18b), on the other hand only give a dynamic increase of 4.6% compared to the static load case. One possible explanation for this large difference is that the convective mass is closer to the chosen result point when Housner is used, which will lead to larger deformations of the tank wall and thus larger stresses at that location. Another interesting difference between the two methods is the response in the beating phases, which probably has the same explanation.

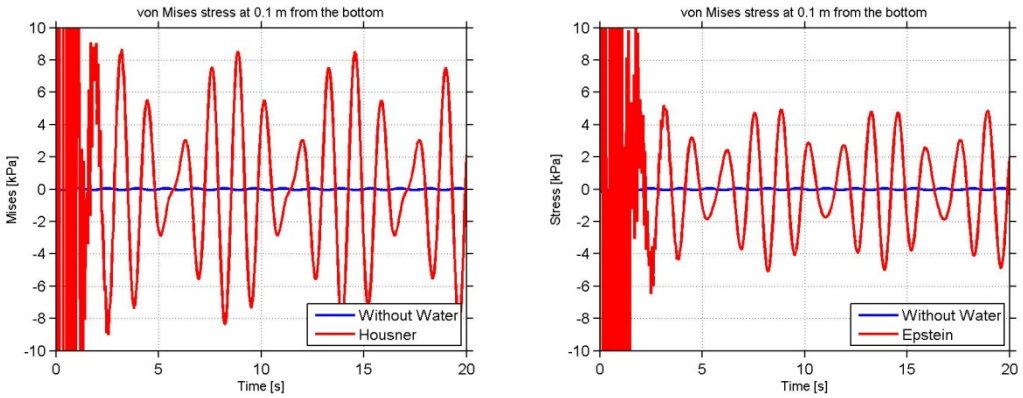

a) b)

Figure 6-18: Dynamic part of the von Mises stress the two simplified FSI methods a) number 3 and b) number 4. Results from analysis without water included for comparison

Time history results of the von Mises stress in the tank wall from the four acoustic simulations, method number 5 to 7, are shown in Figure 6-19, compared with the analysis without water. The dynamic contribution of the stress state when the signal has stabilised is now of a magnitude equal to 2 kPa for all four simulations. This means that the dynamic increase compared to the static load case is approximately 1.9%. It can be observed that all four simulations give almost identical results except for the amount of noise in the early parts of the simulation, where Figure 6-19b) exhibits most noise; which is consistent with previous observations. Further, it is interesting to note that the periodicity of the acoustic simulations corresponds very well with the results obtained in the simplified method according to Epstein in Figure 6-18b). However, the magnitude of the dynamic stress part is almost twice as large in the simplified method.

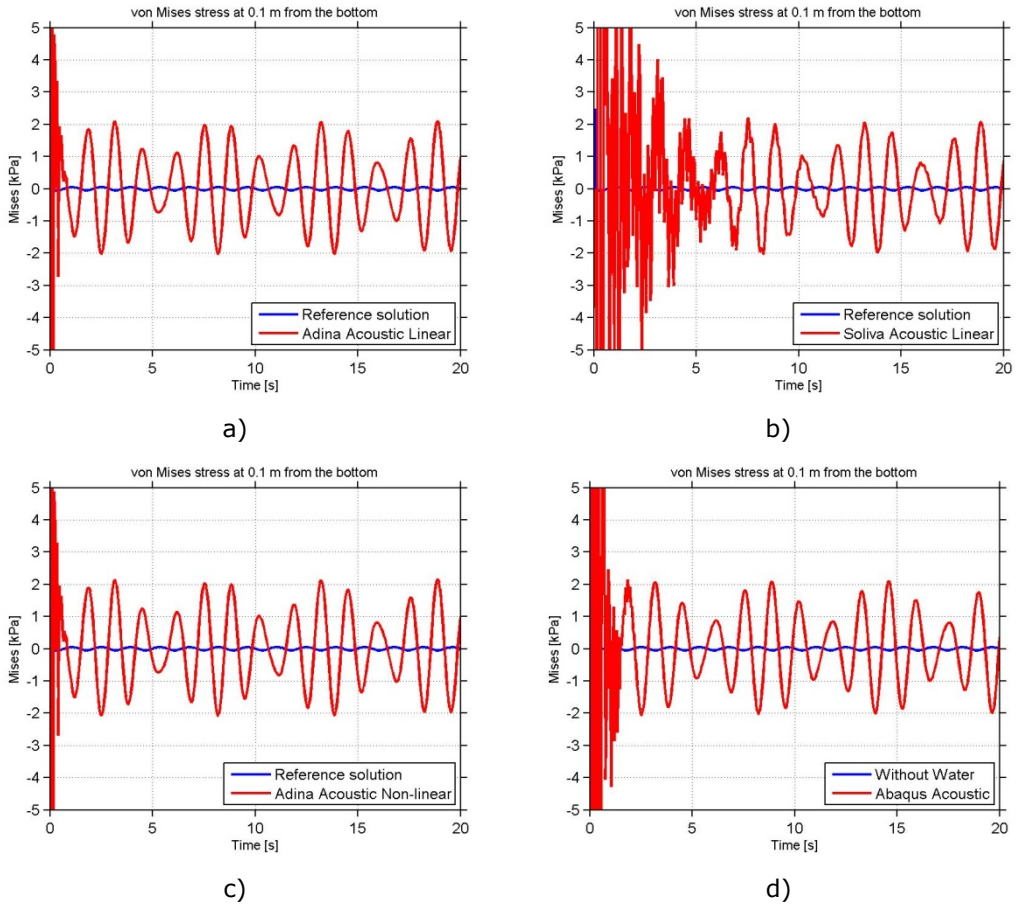

Figure 6-19: Dynamic part of the von Mises stress from acoustic simulations, a) and b) method number 5, c) method number 6 and d) method number 7. Results are compared with a reference solution with no fluid.

Looking at the results from the non-linear ALE method in Abaqus, method number 8, shown in Figure 6-20 it can be observed that a lot of high frequency noise is present throughout the entire solution. Disregarding these high frequencies it can be concluded that the dynamic part of the von Mises stress at the specified result point varies between -4 to 2 kPa, which is in good agreement with the acoustic methods presented above. Considering the maximum increase in stress obtained from the dynamic load, this means that the stress from the static load case is increased with approximately 2.0%.

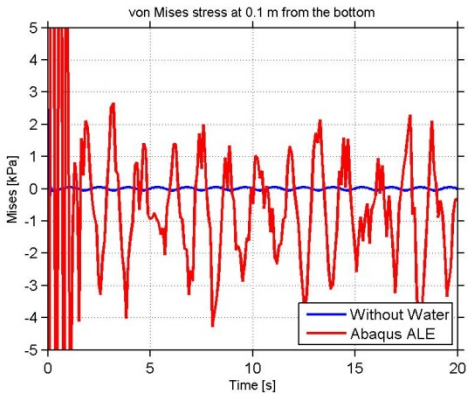

Figure 6-20: Dynamic part of the von Mises stress from analysis method number 8 compared with results from the simulation without water.

To further compare the results from the different methods presented above, the frequency content of the time histories presented in Figure 6-18 to Figure 6-20 is shown in Figure 6-21 as response spectrums. In Figure 6-21a) the entire time signal of the time histories is considered. From the figure it can be observed that a lot of energy is concentrated around 3 to 10 Hz, which originates from the noise seen in the beginning of each time history. It is also interesting to notice that the two simplified methods show a lot higher energy content than the rest of the simulations. In Figure 6-21b), only the results from 10 to 20 seconds is considered when calculating the response spectrums to exclude the high frequency noise in the early part of the time histories. Further, the figure is zoomed in between 0.5 to 2 Hz to focus on the frequencies of the driving motion and lower eigen modes of the water body. From the figure two distinct peaks are visible, the first at 0.7 Hz which coincides with the frequency of the driving motion. The second peak is located at 0.9 Hz which corresponds to the first natural frequency of the water body. Both peak values are included in all simulations which includes water, but for the simulation without water only the first peak at 0.7 Hz is included. As previously discussed it can also be observed that the magnitude is considerably higher for the simulations that include water. Further, it is again shown that the two simplified methods give higher stress values at both peaks compared with the more advanced methods for including the dynamic effects of water.

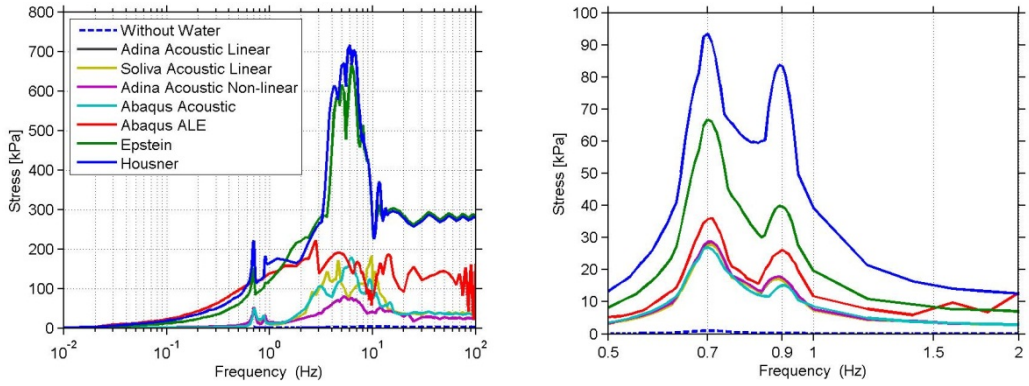

a) b)

Figure 6-21: Response spectres from a) entire signal, b) from 10 to 20 seconds zoomed in at 0.5 to 2 Hz.

To summarize the effect of including water on the response of a structure excited by periodic motion, the increase in stress due to the dynamic effect for all simulation presented in Table 6-6 as the increase in stress due to the dynamic load compared to the stress at static loading. When only including the structure (1) a very slight increase is obtained from the dynamic load. But when using the simplified methods (3 and 4) the increase in stress due to the dynamic load is to large, if compared to the more advanced methods. Hence, this shows the importance of first of all including hydrodynamic effects in dynamic analyses, and secondly of describing them as accurately as possible.

Table 6-6: Summary of the dynamic response in the tank wall compared with the static load case.

Method number	**1**	**3**	**4**	**5a**	**5b**	**6**	**7**	**8**
Increase	0.046%	7.4%	4.6%	1.9%	1.9%	1.9%	1.9%	2.0%

Computational efficiency

One important aspect that has to be taken into consideration when choosing a suitable method for including hydrodynamic effects in a seismic analysis of concrete structures at nuclear facilities is the computational efficiency of the method. This is important since the size of the model, when looking at an entire building, will be very large and that the time signal often spans between 10-50 seconds. Hence, if a too detailed method is chosen the computational time can be unreasonable considering the purpose of the analysis.

Since different software and hardware have been used for the different methods used in the presented example, it is difficult to compare exact computational times. But nonetheless, some conclusions can be drawn considering the level of detail in the used methods.

As a reference, if only the structure is analysed without any water the computational time is in order of minutes. If the mass and spring system of the simplified methods is added to the structure the computational time rises to a couple of minutes. This is due to the low stiffness of the springs which require smaller time increments to obtain a stable solution. The next level of detail is to include the water as a linear material, i.e. the linear acoustic methods number 5 and number 7. Since the entire fluid domain has to be modelled with continuum finite elements the number of equations that needs to be solved rises dramatically. But since all equations are linear the extra computational cost is relatively small and the overall computational time increase to an order of ten minutes. If non-linear terms are included in the equations of the acoustic fluid domain, i.e. method number 6, the computational time increases to around one hour.

If real fluid flow is to be included in the simulations, the computational time increases dramatically and can be above ten hours, perhaps even days. The reason is a combination of increased cost of solving the equations of the fluid domain and iterative process of coupling the structure and fluid. Apart from the extra cost for solving each equation, the non-linear methods most often also require that a smaller time increment is used to achieve stable and accurate solution, which further increases the computational time.

6.1.7 Comments

From the comparison of the numerical methods with experimental measurements of the sloshing wave it can be concluded that all methods agrees well with the experiments. Almost all methods seem to overestimate the wave height slightly, especially in the beginning of the simulation. The accuracy is good enough for all methods when compared to the experimental data. Further, it is also evident that the beating phases, when the driving frequency and the first natural frequency of the water body cancel each other out, is the most difficult phase to describe accurately. Many of the simulations miss both magnitude and the periodicity of the wave in these phases.

Looking at the hydrodynamic pressure of the fluid which constitutes the load that will be exerted on the structure it can be concluded that it is largest close to the free surface. This indicates that the hydrodynamic effects are dominated by convective pressures due to the sloshing waves. This can be explained by the low frequency and amplitude of the driving motion, which will lead to a maximum acceleration of approximately 0.1 m/s^2. If a simple control is made with the impulsive masses obtained from Housner (1963) and Epstein (1976), see Table 6-5, the maximum impulsive force is $F = ma = 395 \cdot 0.1 = 39.5\ N/m$. This resultant impulsive force is very small if compared to the resultant hydrostatic force that acts on each wall $F = \frac{\rho g h}{2} = \frac{(1000 \cdot 9.81 \cdot 0.624) \cdot 0.624}{2} = 1909\ N/m$. Since, the impulsive force is proportional to the acceleration and thus the frequency of the dynamic load the importance of the impulsive forces increases when the dynamic load contains higher frequencies. And consequently, as found in the current example, the convective forces are most important for low frequency loads.

It was also shown in the example that it is very important to include hydrodynamic effects when considering the response of the structure. These

will increase the load effect on the structure when subjected to a load of periodic nature. Further, it could also be concluded that the simplified methods, in which the hydrodynamic effects are included as a mass and spring system, resulted in significantly higher stresses in the structure then if the fluid was included with continuum elements; with either linear or non-linear material properties. Hence, it can be beneficial to include the hydrodynamic effects in a more realistic manner than the simplified methods, especially if a structure is found to be near failure.

It is, however, important to keep in mind the extra computational time that the more advanced methods will lead to and also the extra effort they require from the analyst setting up the simulation. For the most advanced method, even a slight error in the input to the analysis may give completely different and unrealistic results due to the non-linearity of the equations that are solved in the fluid domain and at the interface between the fluid and the structure. Considering the analysis of seismic loading of large concrete structures it is deemed unrealistic to use the non-linear methods, given the size of the model and length of the time signal. It is therefore recommended that primarily the linear fluid models are used. In some cases, it might be sufficient to use the simplified mass and spring models. However, according to the simulations performed in this report showed that the induced stresses may differ significantly. In addition, according to Epstein (1976), the model developed by Housner (1954) has showed to significantly underestimate the hydrodynamic forces due to seismic excitation in cases with flexible structures.

6.2 Simplified BWR containment

The main purpose with this example is to compare the different methods based on different seismic input. The structure will be subjected to a large and a small earthquake with mainly low and high frequency content, respectively. The larger earthquake corresponds to a typical earthquake on the US west coast while the smaller one corresponds to a typical Swedish earthquake. This also means that it is possible to judge if there is necessary to include FSI in the seismic analysis based on the size of the earthquake and the structural characteristics of the analysed structure. In this example, a simplified geometry of a Swedish BWR containment will be used. Further, the analyses will be performed with three different commercial FE-software's; SOLVIA, ADINA and ABAQUS. This in order to compare some of the different methods included in the software's for modelling FSI.

6.2.1 Geometry

The simplified geometry, of a typical Swedish BWR containment, used in this study is illustrated in Figure 6-22. The walls of the upper concrete pool have a thickness of 1.6 m. The containment has a diameter of 24.2 m and is 1.1 m thick; in the model, this part has been modelled as a beam element with a pipe cross section. Both horizontal and vertical tendons are used in the real

structure; these are, however, not modelled in this study in order to get a model which is as simple as possible.

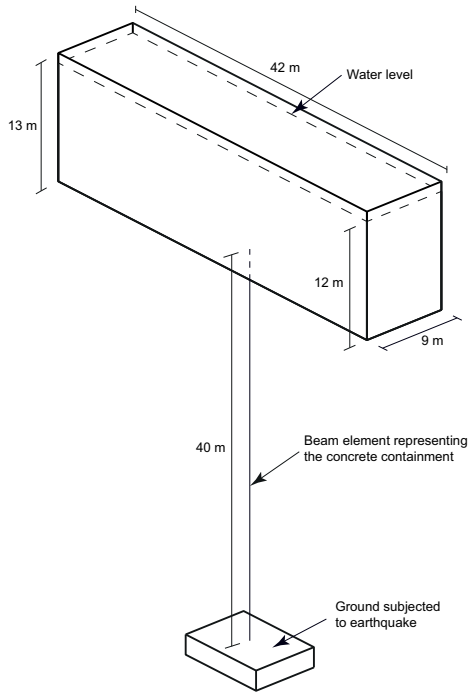

Figure 6-22: Geometry of a typical Swedish BWR containment model used in the analyses.

6.2.2 Material and material models

Only two materials are used in the model since the tendons are neglected, these two are concrete and water. All concrete in the containment and the upper pool has been modelled with the material properties presented in Table 6-7 and with a linear elastic material model.

Table 6-7: Material properties for the concrete.

Concrete	
Young's modulus	30 GPa
Poisson's ratio	0.2
Density	2400 kg/m^3

The water contained in the two upper pools has been modelled using the material properties shown in Table 6-8.

Table 6-8: Material properties for the water.

Water	
Bulk modulus	2.2 GPa
Dynamic viscosity	0.0013 Pa/s
Density	1000 kg/m^3

6.2.3 Mesh and modelling techniques

The mesh used in this study is shown in Figure 6-23; three different types of elements are used in the model. The concrete containment is modelled using beam elements with a pipe cross section. The avaerage element length is 4 m, i.e. a total of 10 elements along the height of the containment. Since the cross section is relatively large, transverse shear deformations (i.e. elements on Timoshenko beam theory) have to be considered in order to recieve reliable results. The concrete pool walls are modelled with 4-noded shell elements with full gauss integration. An average element length of 1 m is used, which is sufficiently fine in order to get converging results. The water is modelled with 8-noded fluid elements using full gauss integration, an average element length of 1 m is used for these elements as well.

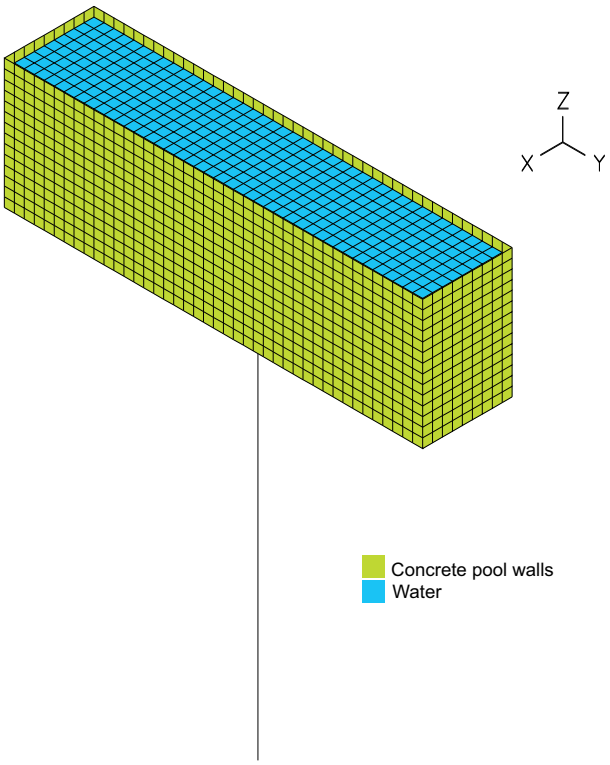

Figure 6-23: Mesh of the concrete pool walls and the fluid.

The beam elements, representing the containment, are connected to the bottom of the upper pool by rigid links. These rigid links are connected over an area on the bottom corresponding to the diameter of the containment. This is shown in Figure 6-24 a) and b) where the red area in b) shows the area that is connected to the beam with rigid links. The contact between the fluid and the pool walls is different and depends on the FSI method used, why no general information is given here. For more information regarding the contact definitions see ADINA (2011), SOLVIA (2011) and Dassault Systèmes (2012).

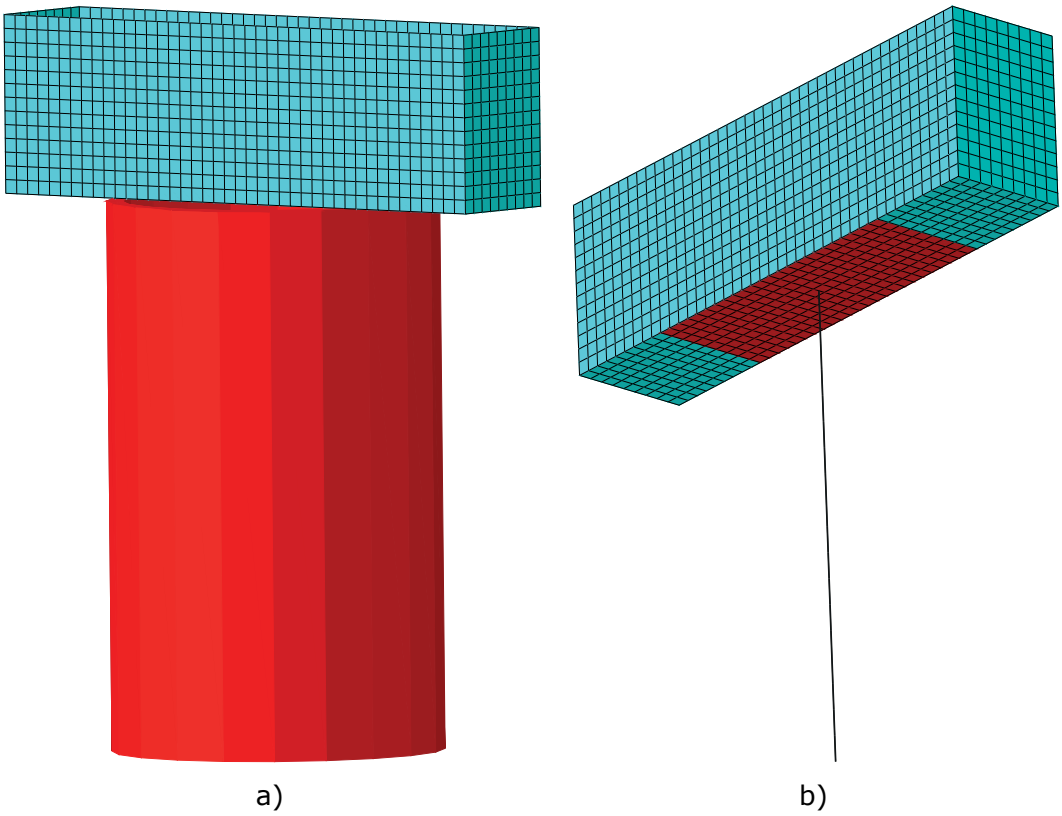

Figure 6-24: a) Shows a rendered version of the beam element (red part) representing the concrete containment. b) The red area shows where the rigid links from the top of the beam element connects to the concrete pool.

All rotational degrees of freedom are restrained at the bottom node of the beam element; the ground will be subjected to an earthquake and, therefore, needs to be able to move. However, to be able to do an eigenfrequency analysis of the structure, fix boundary conditions have to be applied. In this study, all translations and rotations at the ground node of the beam are locked in the eigenfrequency analyses.

Rayleigh damping have been applied to both the structure and the water in accordance to the recommendations given in ASCE (1998) and Regulatory

guide 1.61 (NRC, 2007), as presented earlier in Figure 2-1 and Figure 2-2 in Section 2.3

6.2.4 Loads

Two different kinds of seismic excitation loads have been applied to the structure in the performed analyses, as earlier presented in Section 2.5. These are time histories for two different earthquakes and self-weight from the structure and the water in the upper pool. The first applied earthquake corresponds to a typical Swedish earthquake, which is rather small and has a high frequency content. The second earthquake is the El Centro earthquake, which may be considered as a typical earthquake for the US west coast. This earthquake has, in contrast to the Swedish earthquake, a low frequency content and rather large amplitudes. The applied time histories for the Swedish earthquake are shown in Figure 2-3 to Figure 2-5 while the ground acceleration from the El Centro earthquake are shown in Figure 2-6 to Figure 2-8. In the figures, two horizontal directions are defined where the time history in Figure 2-3 and Figure 2-6 respectively correspond to the direction parallel with the longest side of the pool and the other horizontal direction is defined as perpendicular to the same side.

6.2.5 FSI methods

As mentioned above, the analyses have been performed in three different FE-software's. The methods used to account for the FSI differ slightly between the programs and are, therefore, summarised in Table 6-9.

Table 6-9: Summary of FSI methods used.

Nr.	Method	Integration scheme	Analysis type	Software
1	Structure only	Implicit	Frequency	Abaqus
2	Structure only	Implicit	Linear transient	Abaqus
3	Acoustic, potential based	Implicit	Linear transient	Solvia, Adina
4	Acoustic, velocity	Implicit	Non-linear transient	Abaqus

A more thorough explanation of the methods may be found in section 5 as well as in section 6.1.3.

6.2.6 Results and discussions

Natural frequency analysis

In this section, the results from the natural frequency analysis of the structure are presented. Since not all the used programs are able to include the water in an natural frequency analysis; it has been excluded in all the analyses in order to be able to compare the results from the different programs. The natural frequencies obtained from the three programs are shown in Table 6-10.

Table 6-10: Structural eigen frequencies obtained from the three FE-programs.

Mode	SOLVIA [Hz]	ADINA [Hz]	ABAQUS [Hz]
1	3.1169	3.5969	3.1531
2	3.1888	3.7287	3.2231
3	5.7594	5.7888	5.8207
4	7.0495	6.6625	7.1012
5	8.3671	8.6830	8.5587
6	9.8839	11.2565	10.3338
7	11.0694	11.4921	11.3907
8	11.2675	12.1006	11.5494
9	11.4676	12.3761	11.6425
10	11.9739	14.8250	11.9722
11	15.5848	15.4070	15.5473

As can be seen from the results, the difference between the obtained eigenfrequencies from SOLVIA and ABAQUS is rather small. However, it can also be observed that the eigenfrequency from ADINA differ rather much for some of the modes. This is due to the fact that a beam element with a pipe cross section in ADINA cannot account for transverse shear deformations (Adina, 2011), while this is included in both SOLVIA and ABAQUS. Because of this, the eigenfrequency of the modes which mainly involve bending of the beam will differ. At the same time, it is also possible for ADINA to find different mode shapes than the ones observed in SOLVIA and ABAQUS.

The eigenfrequency of the water can be estimated by using Eq. [3-10]; with the dimensions according to Figure 6-22 the eigenfrequency for the first mode is 0.72 Hz. As mentioned above, no eigenfrequencies will be determined with the FE-programs for the water.

Earthquake excitation analyses

In this section, the results from the earthquake excitation time-history analyses will be presented. In Figure 6-25 and Figure 6-26, the frequency

content at the bottom of the pool after excitation of structure with the Swedish and El Centro earthquake, respectively, are shown.

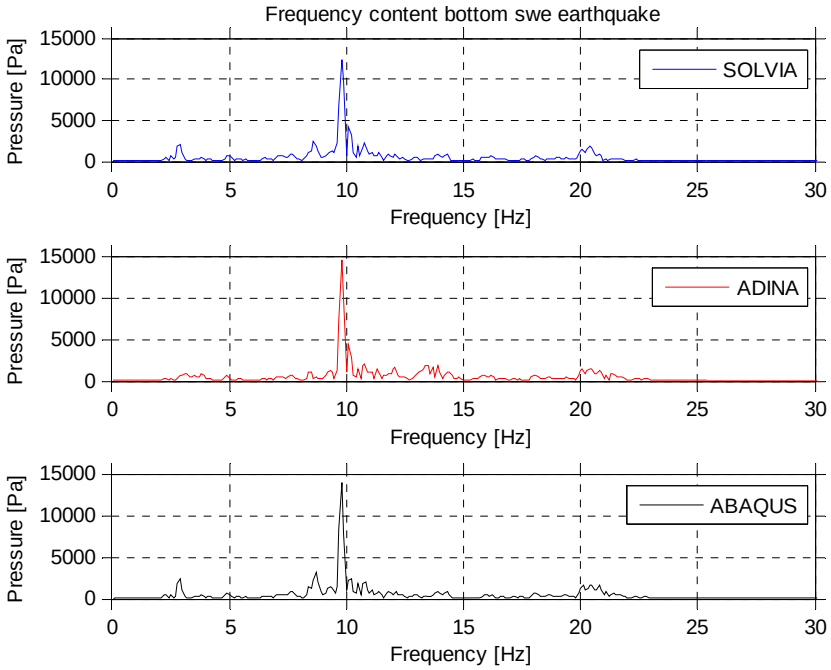

Figure 6-25 Frequency content at the bottom of the pool for the Swedish earthquake.

It can clearly be observed that the results for the Swedish earthquake just differ slightly between the three programs, i.e. the energy concentrations occur at the same frequencies and the amplitudes are rather similar.

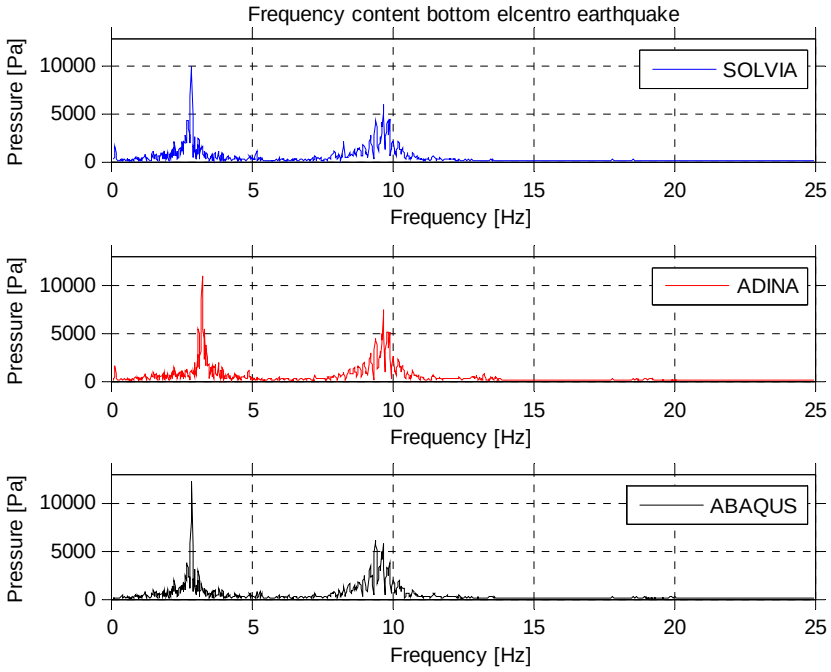

Figure 6-26 Frequency content at the bottom of the pool for the El Centro earthquake.

From Figure 6-26 it can be concluded that the frequency content distribution does not differ a lot between the programs. However, a small peak can be noted for a frequency between approximately 0 and 1 Hz in the result plots from SOLVIA and ADINA, while this peak is missing in the ABAQUS results. This can most likely be explained due to the difference in definition of the fluid elements used in ABAQUS from the ones used in SOLVIA and ADINA; the ABAQUS fluid elements does not have any mass. Since the eigenfrequency of the water often is rather small and depends on the dimensions of the pool and the mass of the water, the first peak, below 1 Hz, in the frequency content is missing in the ABAQUS results.

In Figure 6-27 and Figure 6-29, the hydrodynamic water pressure due to the Swedish earthquake at the bottom and the top of the pool, respectively, is shown. The results from the three programs are shown in the same figures. Further, Figure 6-28 and Figure 6-30 shows the same hydrodynamic water pressure but after the use of a Butterworth filter with a cutoff frequency of 11 Hz. The choice of 11 Hz is based on frequency content presented above, where it can be concluded that most of the energy is concentrated to frequencies below 11 Hz, see Figure 6-25.

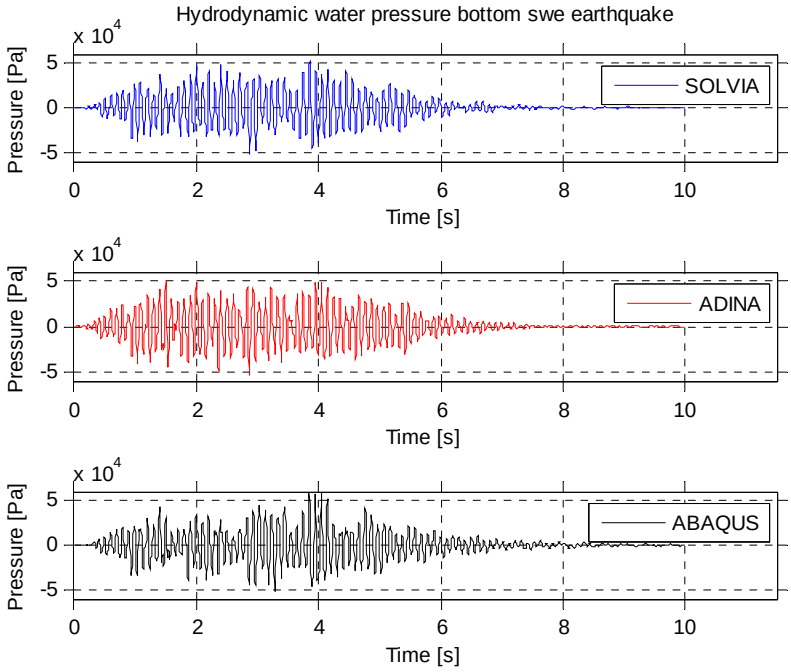

Figure 6-27 Hydrodynamic water pressure at the bottom of the pool due to the Swedish earthquake.

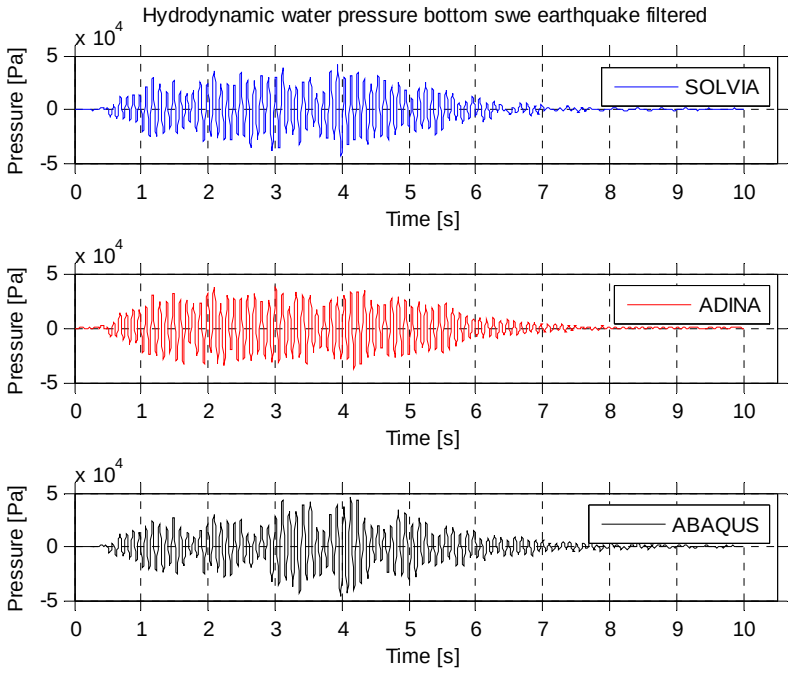

Figure 6-28 Filtered hydrodynamic water pressure at the bottom of the pool due to the Swedish earthquake.

The results for the bottom hydrodynamic water pressure are quite similar between the three FE-programs. However, a rather better compliance can be seen between the SOLVIA and ADINA results. This is most certainly, as mentioned before, due to the fact that these fluid elements include the mass of the water while ABAQUS does not.

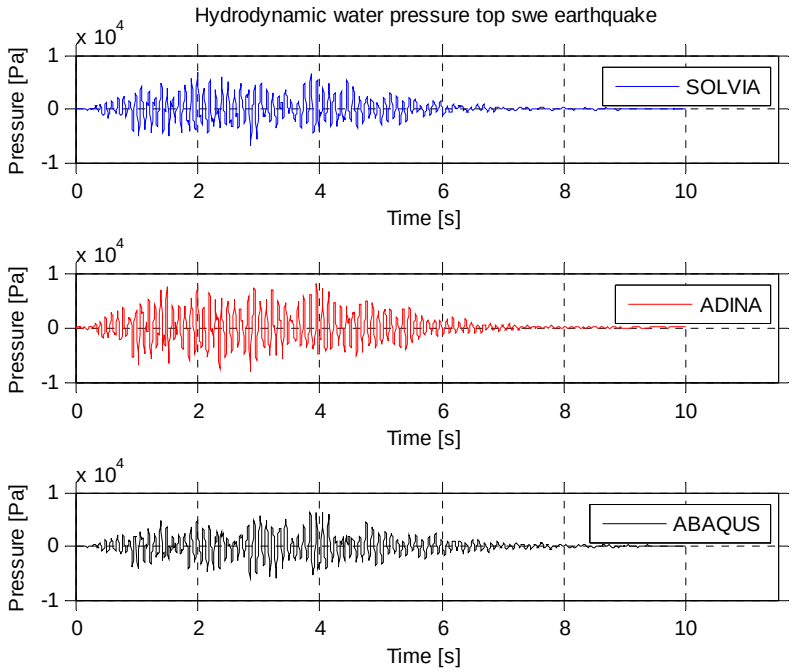

Figure 6-29 Hydrodynamic water pressure at the top of the pool due to the Swedish earthquake.

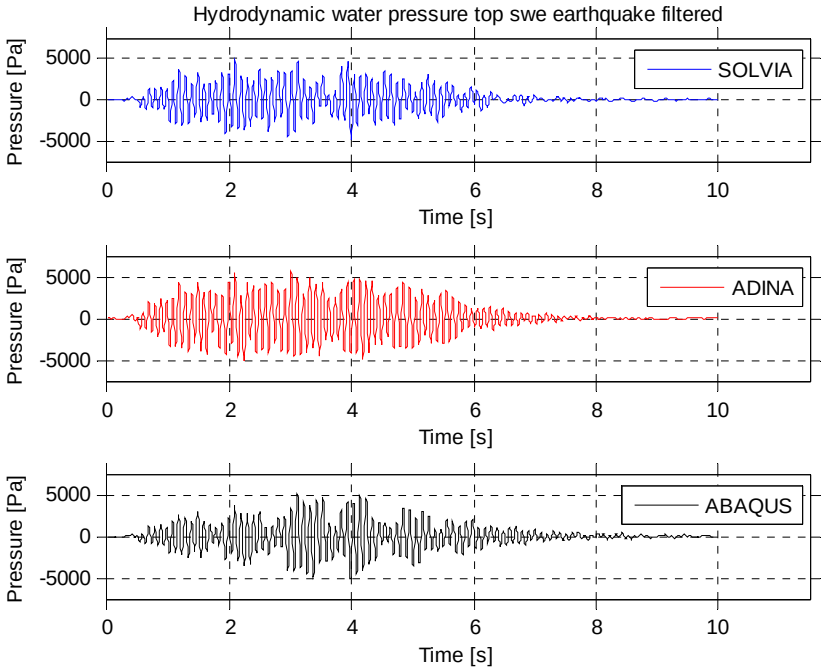

Figure 6-30 Filtered hydrodynamic water pressure at the top of the pool due to the Swedish earthquake.

As for the bottom hydrodynamic water pressure, the results for the top hydrodynamic water pressure agrees very well between the three programs. Nevertheless, there is a quite better compliance between the SOLVIA and ABAQUS results unlike the case for the bottom hydrodynamic water pressure. Since the total mass acting on the fluid element is much smaller on the top, it seems that the lack of masses in the ABAQUS fluid elements does not affect the results as in the bottom part of the pool.

The hydrodynamic water pressure at the bottom and the top of the pool due the El Centro earthquake is presented in Figure 6-31 and Figure 6-33, respectively. The results after using of a Butterworth filter with a cutoff frequency of 11 Hz are shown in Figure 6-32 and Figure 6-34. The cutoff frequency has been chosen based on the frequency content plots shown above, where it can be concluded that most of the energy is concentrated to the frequencies below 11 Hz, see Figure 6-26.

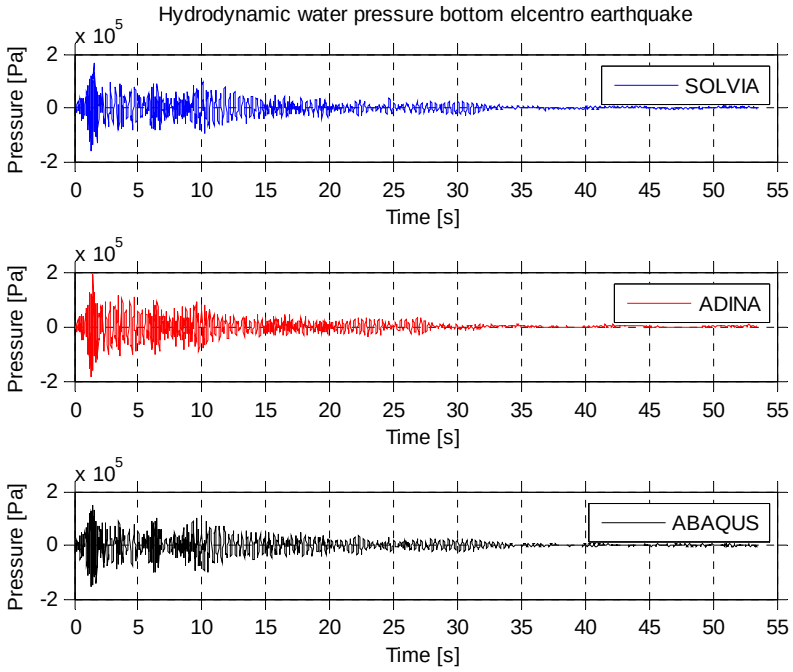

Figure 6-31 Hydrodynamic water pressure at the bottom of the pool due to the El Centro earthquake.

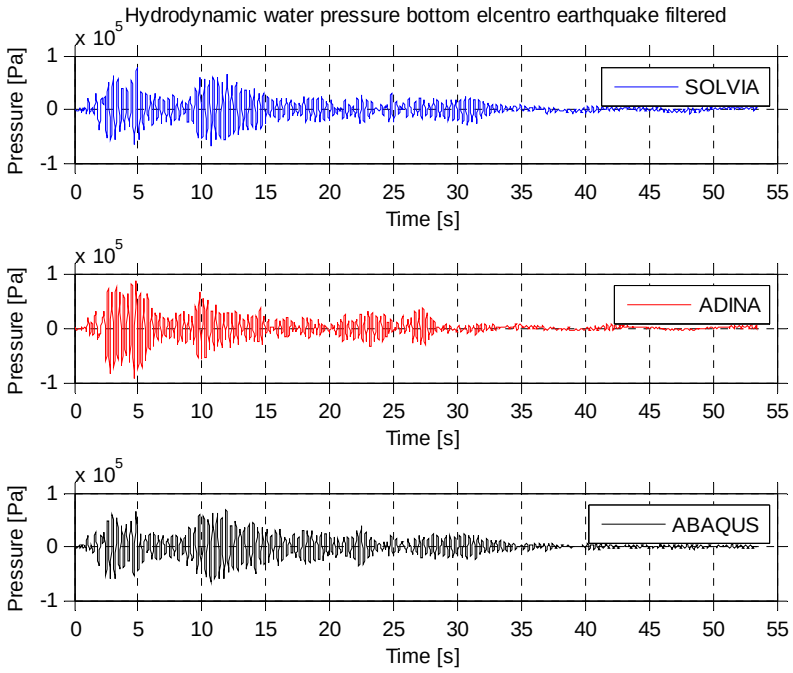

Figure 6-32 Filtered hydrodynamic water pressure at the bottom of the pool due to the El Centro earthquake.

The hydrodynamic water pressure due to the El Centro earthquake at the bottom obtained from the three FE-programs corresponds very well with each other. No significant differences can be observed in the results.

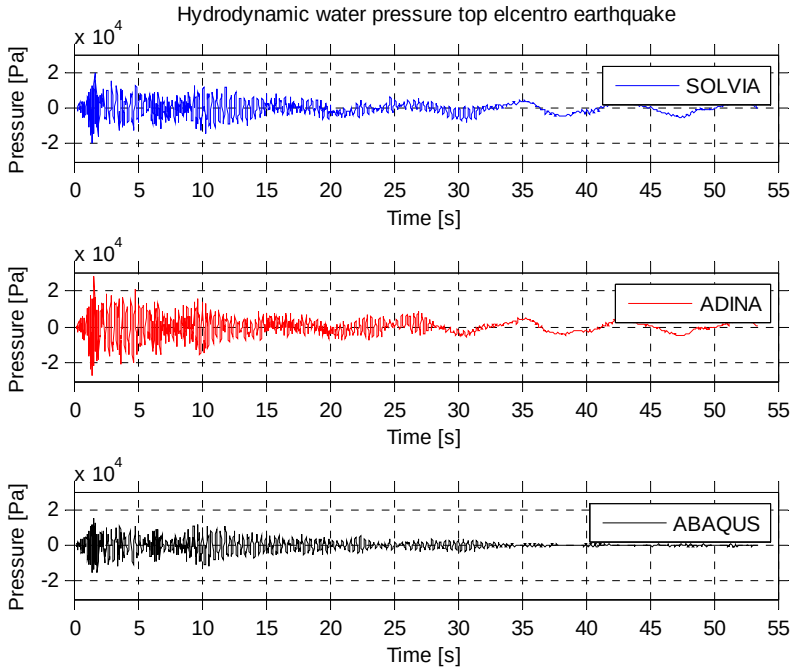

Figure 6-33 Hydrodynamic water pressure at the top of the pool due to the El Centro earthquake.

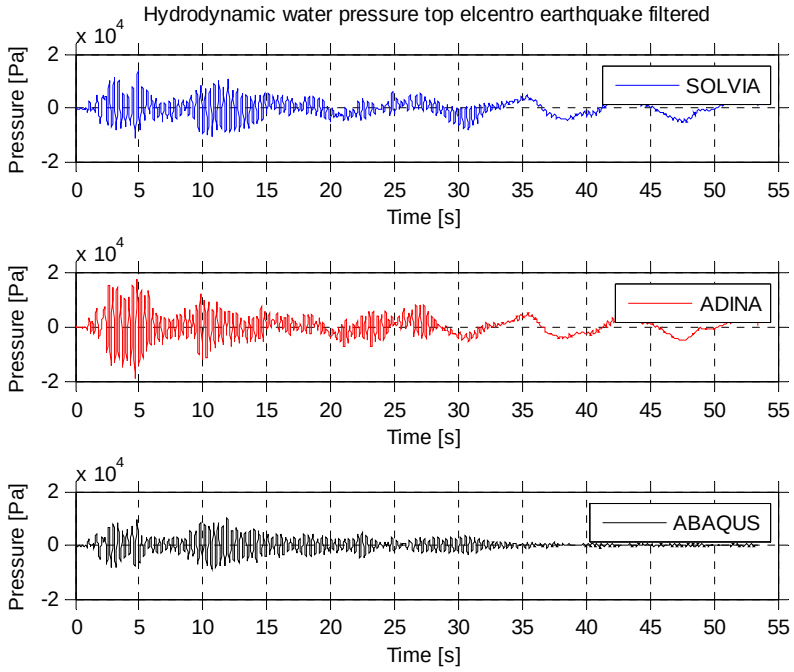

Figure 6-34 Filtered hydrodynamic water pressure at the top of the pool due to the El Centro earthquake.

As can be seen in Figure 6-33 and Figure 6-34, there is a quite large difference in the hydrodynamic water pressure between the programs. While SOLVIA and ADINA almost give the same results, the ABAQUS result deviates. The difference starts to occur at approximately 15 s and continues throughout the excitation. The hydrodynamic pressure varies with very low frequency in both SOLVIA and ADINA while it is almost zero in ABAQUS. This indicates that a standing wave has developed in the pool which cannot be described by ABAQUS due to the definition of the fluid elements without mass. This can also be seen in Figure 6-26, where the peak at very low frequency observed in both SOLVIA and ADINA is missing in the ABAQUS results.

During the post-process of the result data from the FE-programs, it was observed that the ADINA results were decreasing linearly. This can be seen in the middle plot in Figure 6-35. The reason to this behavior is that the applied accelerations result in a vector which moves the structure approximately 6 m from its original position, while the surface of the water remains at this position due to its boundary conditions. This is also the case for the ABAQUS analysis, but because of the missing mass in the fluid element definition the same effects does not occur. In SOLVIA, the accelerations are applied with a different method and this does not become a problem. Even though the results look wrong at first, they are correct and just needs to be a bit more post-processed. By removing the linear trend from the ADINA results they comply very well with the SOLVA results.

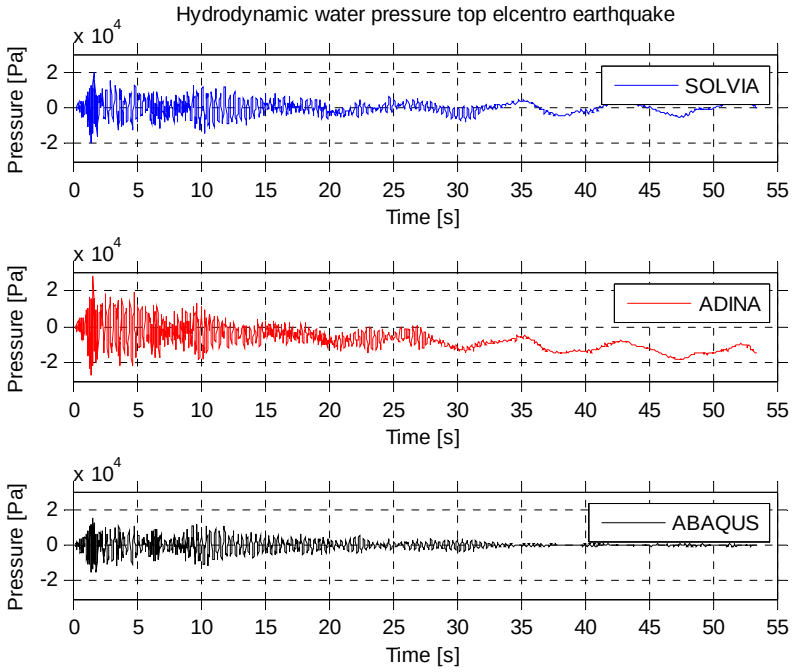

Figure 6-35 Hydrodynamic water pressure at the top of the pool due to the El Centro earthquake without removing linear trend for the ADINA results.

Figure 6-36 to Figure 6-39 shows the SXX and SZZ stresses obtained in the concrete pool wall due to the Swedish and the El Centro earthquake. The stresses are measured at an element located 3 m above the bottom and at the middle at the short side of the pool located at the most negative y-position in Figure 6-23. A comparing analysis without fluid elements, performed in ABAQUS, is also included in the figures. The SXX stresses are located in the x-direction defined by the coordinate system in Figure 6-23 while the SZZ stresses are located in the z-direction according to the same coordinate system. The results presented in the figures have been filtered with a Butterworth filter; the cutoff frequency used for the Swedish and the El Centro earthquake is 11 Hz.

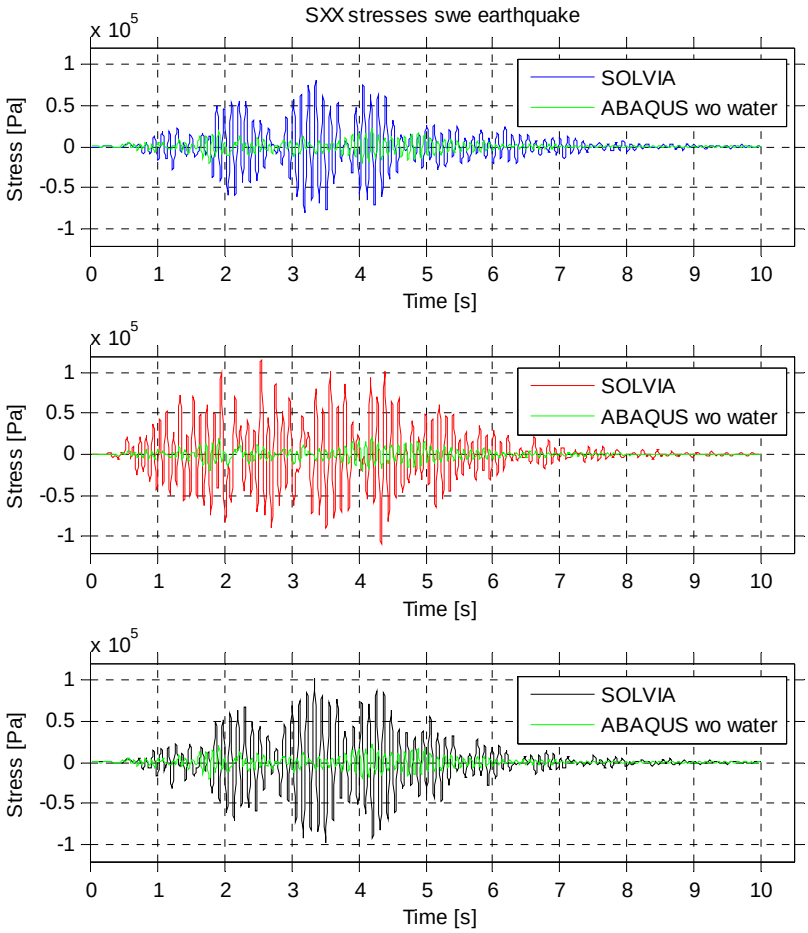

Figure 6-36 SXX stresses due to the Swedish earthquake.

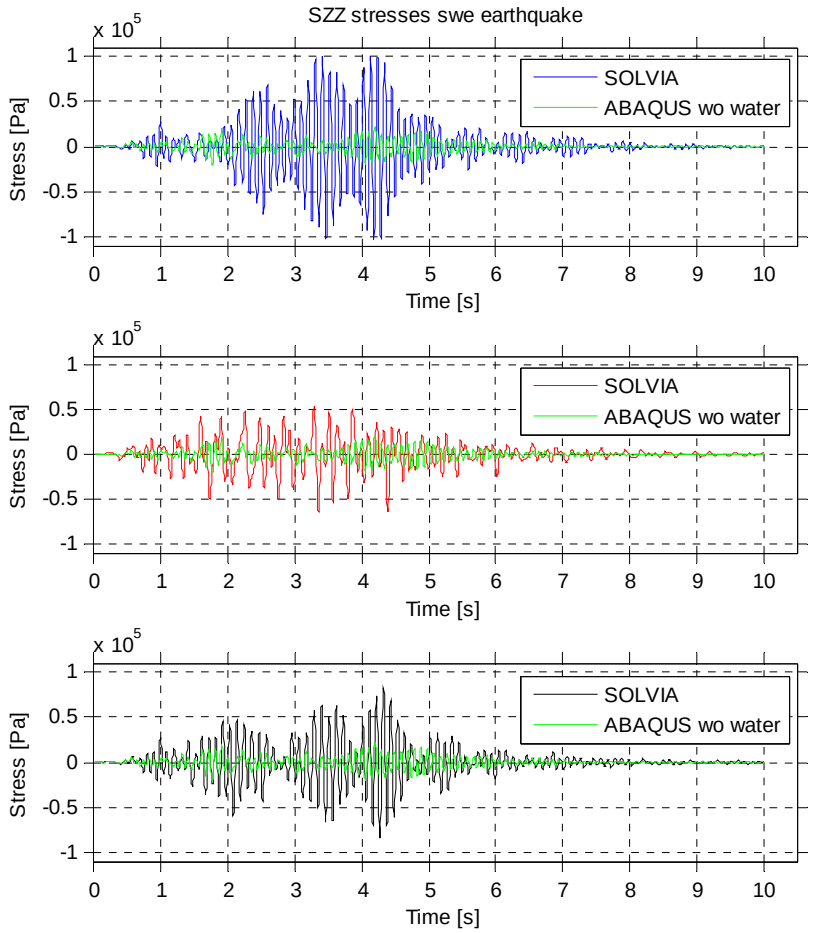

Figure 6-37 SZZ stresses due to the Swedish earthquake.

As can be seen in Figure 6-36 and Figure 6-37 the obtained SXX and SZZ stresses differs a bit between the FE-programs. One reason is that the pipe elements in ADINA lack the influence of shear deformations which also influence the stress state in the walls of the tank. There may be several other reasons for these differences, but the most important conclusion from the figures is that the comparing analysis without the water generates a lot smaller stresses in the structure. This means that it seems very important to include the water in the analysis when performing an earthquake analysis.

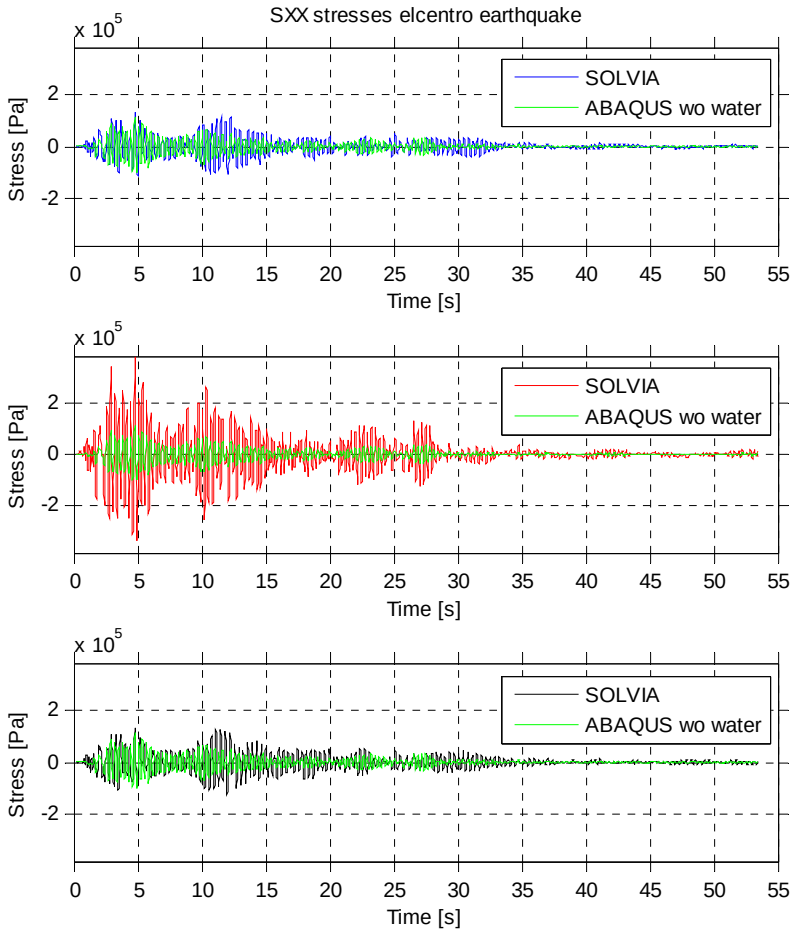

Figure 6-38 SXX stresses due to the El Centro earthquake.

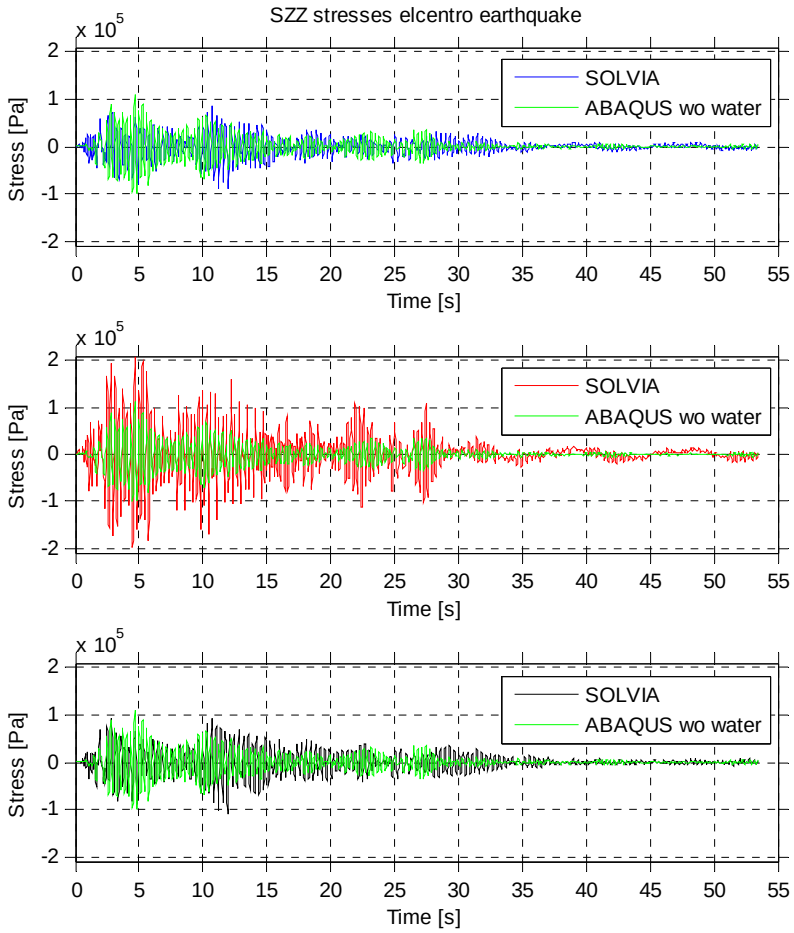

Figure 6-39 SZZ stresses due to the El Centro earthquake.

As for the Swedish earthquake excitation, the obtained stresses differ a bit between the three FE-programs. The difference to the reference analysis without the water is smaller than for the Swedish earthquake, but the stresses obtained from the analyses including the water is almost always larger. Therefore, also these analyses imply that it is important to include the water when analysing structures containing large amounts of water.

7 Discussion

7.1 Fluid-structure interaction

The area of numerical analysis of the interaction between fluids and solids is a huge area with a lot of on-going research. The area is further of interest to a variety of engineering problems, ranging from flow in blood vessels, aero-dynamics and of course the interaction between water and civil engineering structures, which has been the focus of this report. Apart from this, many of the numerical techniques that have to be employed in an FSI analysis can also be used in other categories of multiphysic applications, which further increases the research area. Due to the different interests of the numerous disciplines engaged in the research area a large amount of methods have been developed, each with different strengths and weaknesses suited for the problem in mind when developing the method. It has been impossible to cover all these available methods in the scope of this project, so instead the focus has been to describe the most important numerical techniques and the categories of methods that are of most interest for civil engineering problems.

To a large extent, the problem of coupling a fluid computational domain with a structural computational domain is a numerical issue which has to be resolved using specially developed numerical techniques. The difficulty of this task can be realised if considering the differences between the two computational domains that are to be coupled. In the fluid domain, the unknown field variables are usually taken as the fluid velocity and the fluid pressure, whereas in the structural domain, the unknown field variables are normally the displacements. When coupling these two domains, the different field variables can for example make it difficult to transfer the right amount of momentum between the two domains so that the momentum of the entire problem is conserved. This can lead to extra iterative steps and extra computational time and possible convergence problems. Another aspect that needs to be considered is the different computational frameworks that are usually employed when solving the respective domains separately. Where especially the Eulerian frame typically used in fluid dynamics makes it difficult to include a moving boundary such as a deforming structure. As a result several special techniques have been developed, such as:

- A new computational frame for the fluid, which can incorporate a moving boundary and still handle the large deformations associated with fluid dynamics. This is typically referred to as an Arbitrary Lagrangian-Eulerian (ALE) frame.
- Another way is to develop methods in which each element in the Eulerian frame of the fluid need not be occupied with the same fluid, a so called volume of fluid (VOF) method. In such a method the deforming structure can constitute a moving boundary which moves through the Eulerian frame and defines the amount of fluid in each Eulerian element. Examples of such methods are the immersed

boundary methods and the coupled Eulerian-Lagrangian (CEL) methods.

The consequence of employing these special techniques is of course partly that extra computational effort is needed and partly an increased risk of unconverging solution and thus unrealistic results, since new non-linear equations are introduced. The last major aspect that needs to be considered when developing a FSI method is how to numerically couple the two domains, this can be done in several different ways:

- Assemble all equations in a single system and one solver, a monolithic coupling.
- Use separate solvers for each domain and a specially developed algorithm to transfer loads and boundary effects between the two domains. Two main alternatives are typically used:
    - A sequential algorithm where one domain leads the solution.
    - A parallel algorithm where each increment is conducted in an iterative manner between the domains.

The monolithic approach is perhaps the most accurate, especially for problems with a strong physical coupling, but it also leads to a very large and often ill-conditioned equation system. As a consequence these types of methods are often computationally demanding to solve. The other principal method used where each domain is solved separately is in its nature more computationally efficient, however, of course depending on the efficiency of the used coupling algorithm. However, many of these algorithms become unstable when the physical coupling between the two domains is strong. As a general rule, it can be approximated that the accuracy of the algorithms is reduced for analyses including large deformations of the structure when the densities of the two domains are of similar order; which is the case for concrete and water.

The numerous possibilities of defining and combining the above mentioned techniques has, as mentioned earlier, lead to a vast amount of different numerical methods for fluid-structure interaction. If looking at the focus of this project, the global response of the structure, most are unnecessary complicated when it comes to describing the fluid domain. Generally, when determining the effect that the fluid has on the global response of the structure, phenomenons such as splashing against and above walls and turbulence are of little interest. The main aspects which influence the structure are the mass and inertia of the fluid as well as the surface waves, i.e. sloshing, which contributes to the hydrodynamic pressure. Considering this, simplified methods such as elements with acoustic equations and even mass and spring systems to represent the fluid will often suffice in describing the effect that the fluid has on the response of the structure. It should, however, also be known that these simplified acoustic methods also exist in many different versions, with different assumptions to simplify the non-linear N-S equations. Thus, before using an acoustic fluid element, one should make sure that the assumptions do not conflict with the problem statement. When it comes to the mass and spring systems, there also exist different theories to determine the location and properties of the system. This can depend on whether the water body is rectangular or circular, if the water body is deep or shallow or if the structure is to be considered to be rigid or flexible. Another

aspect that can affect which theory to choose is if the water body is of finite or infinite length, this, however, is normally not an issue when it comes to the water in nuclear facilities.

7.2 Numerical examples

In the second part of the report, two different examples were analysed to study some of the different numerical methods described in the report.

- Sloshing in a partially filled rectangular water tank
- Seismic analysis of a simplified BWR containment with the used fuel pool (elevated pool).

The aim of the first example was to study numerical methods for including FSI, from simple mass and spring models to advanced methods solving complete N-S equations. It was chosen, even though it does not necessarily resemble a pool at a nuclear facility, since some experimental measurements were available in the literature. Thus, making it possible to not only compare different analysis methods, but also to validate them against both experimental data and linear analytical solutions.

From this example it was found that most analysis methods give accurate results for the sloshing wave height when compared with the experimental data. It should here be mentioned that the tank was only excited by a simple harmonic motion with a frequency that does not give rise to any resonance waves in the water body. Also when it comes to fluid pressure good agreement between the different analysis methods was found, although no experimental data was available for this parameter. It was also noticed that most of the change in pressure occurred close to the free surface of the water, which indicates that it mainly consists of a convective pressure, i.e. from the sloshing.

When the response of the tank wall is examined, it was concluded that the inclusion of water in the analysis has a major impact on the dynamic response. Apart from using different methods for including water in the simulation, a reference simulation was also performed in which the water was only included as a hydrostatic pressure, that is no mass or hydrodynamic pressures. It was found that since the tank is relatively stiff, the harmonic load only lead to an increase/decrease less than one per mille of the static state. If, however, the water mass and, for this problem especially, the hydrodynamic effects of the water was included, the dynamics effects increased significantly. The magnitude of the dynamic effect now ranged from 2-7%, depending on which numerical method that was used.

When studying the response of the tank wall, the results differed significantly between different categories of numerical methods. Using the simplified approach of including the effects of the water with a mass and spring system gave results in the tank wall that were significantly higher than the methods which included the water as continuum elements, i.e. both acoustic and the more advanced methods. Comparing the acoustic methods with the more advanced methods it could be observed that these gave similar results for the stresses in the tank wall. But, one important aspect here is that a lot more

effort was needed to achieve these results with the more advanced methods, both regarding the input from the user and the computational time needed.

Another important finding is therefore that it is very important to choose which numerical method to use with care and with the requirements of the given problem in mind. When performing an analysis in which the deformation of the structure is moderate and the main interest is the response of the structure, acoustic or even more simplified methods is often sufficient and will save significant computational time. If, however, the problem is of a more highly dynamical nature and with larger structural deformations it is probably necessary to consider using a more advanced method which solves the complete N-S equations.

The aim of the second example was to, based on the findings from the first example, use appropriate methods to analyse the response of a simplified BWR containment structure subjected to seismic loading. The focus was on the response of the spent fuel pool placed above the containment, i.e. the structure resembles an elevated pool structure. Furthermore, the example also aimed at studying the difference between different earthquakes and if the frequency content and magnitude of the time signals influence the importance of including water in the analysis. The first earthquake was a large US west coast earthquake with high magnitude and a wide range of frequencies, typically from 1 to 20 Hz. The second is a typical Swedish earthquake used in design, which has much lower amplitude but a concentration on higher frequencies, typically from 10 to 30 Hz. From the findings from the first example it was decided to only use different acoustic methods in this example, since they seemed to show most promise in this type of application.

Considering that the model consists of an elevated structure with a ground loading, the structural deformations even without water will be larger than in the first example. With large structural deformation it was found that it is important whether body forces are included in the governing equations of the acoustic fluid, this is often not the case. Especially for the large US earthquake it was found that the inclusion of body force in the equations resulted in that a standing wave formed in the pool after the earthquake, which was not the case for the acoustic method without body forces. It can also be noticed that no standing waves were observed for any of the methods when simulating the smaller Swedish earthquake.

In acoustic methods that do not include body forces in the governing equations the hydrostatic pressure needs to be applied as a pressure load on the pool walls. However, if the structural deformations are large, the size of the hydrostatic pressure might change during the simulation, as the undisturbed water level changes with the deformation. If body forces are included, this change will be taken care of automatically. But if not the pressure load needs to be adjusted to take the structural deformation in to account, which can be problematic as it also has to be related to the hydrodynamic pressure due to for example sloshing.

Regarding the response of the concrete wall all used acoustic methods gives similar results. As for the first example, a simulation was also performed without including any water, except hydrostatic pressure. If the results of the acoustic simulation are compared with this reference simulation, it can be concluded that the inclusion of the dynamic properties of water has a

significant impact on the response of the concrete wall, as was also found in the first example. What is also a very interesting finding is that the relative increase obtained when including water compared to the reference solution is significantly larger for the smaller Swedish earthquake than for the US earthquake. One possible reason might be that the Swedish earthquake is not large enough to excite the relatively stiff structure without any water, but it will induce significant dynamic effects in the water which give rise to higher stresses in the concrete as well. However, this shows that it is very important to include water in seismic analyses, even in Swedish conditions where earthquakes are not considered when normally designing a conventional building.

One last aspect that needs to once again be mentioned is the computational expense of performing an FSI simulation. Since in the application of seismic analysis of buildings at nuclear facilities the structural model will inevitably be quite large and this also results in large volumes of water. If the resolution of the water often required by the more advanced method is to be met this will result in very large models with computational times possibly spanning several days, of course depending on the available hardware. Using for instance an acoustic method will allow for lower resolution of the fluid domain and perhaps also larger time increments as well as lower cost of solving each equation, since they are often linear. Using this method will probably reduce the computational time to a few hours instead of several days, without losing too much accuracy in the solution, as pointed out earlier. One further advantage is of course also the often simpler numerical techniques used for the coupling which also reduces the effort and time needed to be put in by the analyst. However, including FSI even with an acoustic method will increase the analysis time and effort required, but as shown in the two examples must be considered as a necessary step when performing a dynamic analysis of a structure which includes water.

7.3 Further studies

Since it was concluded in this report that the acoustic methods are most suitable when analysing seismically loaded structures, a more thorough literature study is necessary of these methods. A reason for this is so that the limitations of the methods are better understood, but also to look in to the different formulations which are available.

To further study and confirm the conclusions from this report regarding the influence of including water in seismic analysis of buildings at nuclear facilities, some sort of experimental measurements are required. This can for instance be obtained by performing scale tests on a structure similar to the simplified BWR model used in the second example in this report. Most experiments that can be found in the literature mainly concerns liquid storage tanks placed on ground level, either excited with a simple harmonic motion or a seismic load. One such example can be found in (Odemir and Souli, 2010) which concerns a scale test of a cylindrical liquid storage tank loaded with the El Centro earthquake also used in this report. However, the liquid storage tanks does not really resemble the properties of the large concrete buildings found at nuclear facilities, they are both smaller and especially more slender.

Thus it would be interesting to conduct a scale model test on for instance a simplified BWR containment. Doing so would help in validating numerical methods for FSI and also in determining the importance of water to the dynamic response of the structure.

Such an experiment could also be used as a benchmark example for other organisations interested in numerical analysis to increase the knowledge and competence of FSI simulations within the civil engineering community in Sweden. Today the normal way of including FSI, if included at all, is to use the simplified methods of mass and spring system which in this report was shown to give very conservative results. However this may not always be the case and they may just as well underestimate the hydrodynamic forces. According to Epstein (1976), the model developed by Housner (1954) has showed to significantly underestimate the hydrodynamic forces due to seismic excitation in cases with flexible structures. Increasing the understanding of how water behaves when loaded dynamically and how it should be properly included in a numerical analysis can therefore result in better and more accurate results.

8 References

Adina (2011). *ADINA System 8.7.* ADINA R&D Inc. Watertown. MA. USA.

Antoci C., Gallati M., Sibilla S., (2007). *Numerical simulation of fluid–structure interaction by SPH.* Computer and Structures 85 (2007) 879-890.

ASCE (1998). *Seismic Analysis of Safety-Related Nuclear Structures and Commentary.* ASCE Standard 4-98. American Society of Civil Engineers.

Bathe K. J., Zhang H. (2002). *A flow-condition-based interpolation finite element procedure for incompressible fluid flows*. Computer & Structures. vol. 80. pp. 1267–1277.

Belytschko T. B., Kam Liu W., Moran B. (2000). *Nonlinear Finite Elements for Continua and Structures*. John Wiley & Sons Ltd. England.

Belytschko T. B., Kennedy J. M. (1976). *A fluid-structure finite element method for the analysis of reactor safety problems.* Nuclear Engineering and Design. vol. 38. pp. 71-81.

Benson D. J. (1992a). *Momentum Advection on a Staggered Mesh.* Journal of Computational Physics. vol. 100. pp. 143–162.

Benson D. J. (1992b). *Computational Methods in Lagrangian and Eulerian Hydrocodes.* Computer Methods in Applied Mechanics and Engineering. vol. 99. pp. 235-394.

Bessette G., Vaughan C., Bell R., Attaway S. (2003) *Zapotec: A Coupled Methodology for Modeling Penetration Problems.* Fluid Structure Interaction II. Wessex Institute of Technology Press. pp. 273-282.

Brown K.H., Burns S. P., Christon M.A. (2002) *Coupled Eulerian-Lagrangian Methods for Earth Penetrating Weapons*. SAND2002-1014. Sandia National Laboratories. USA.

Bøckman A., Shipilova O., Skeie G. (2012). *Incompressible SPH for free surface flows.* Comp. and Fluids. vol. 67. pp. 138-151.

Chopra A. K. (2007). *Dynamics of Structures: Theory and Applications to Earthquake Engineering.* 3rd Edition. Pearson Prentice Hall.

Cook R. D., Malkus D. S., Plesha M. E., Witt R. J. (2002). *Concepts and Applications of Finite Element Anlysis.* 4th Edition. John Wiley & Sons Inc.

Courant R., Friedrichs K., Lewy H. (1967) [1928]. *On the partial difference equations of mathematical physics.* IBM Journal of Research and Development. vol. 11. pp. 215-234.

CREA Consultant (2007). *Suite of ASCE 4-98 Compliant Time-Histories to Swedish 5% Spectra.* CREA Consultants, 2007.

Dassault Systèmes (2012). *Abaqus 6.12 Online Documentation.* Dassault Systèmes Simulia Corp. Providence. RI. USA.

Donea J., Giuliani S., Halleux J. P. (1982). *An arbitrary Lagrangian-Eulerian finite element methods for transient dynamic fluid-structure interaction.* Computer Methods in Applied Mechanics and Engineering. vol 33. pp. 689-723.

Donea J., Huerta A., Ponthot J., Rodriguez-Ferran A. (2004). *Chapter 14: Arbitrary Lagrangian-Eulerian Methods.* Encyclopaedia of Computational Mechanics, Volume 1: Fundamentals. John Wiley & Sons.

Epstein H. I. (1976). Sesimic desing of liquid-storage tanks*.* ASCE Journal of Structural Division. vol. 102. pp. 1659- 673.

Faltinsen O. M. (1978). *A numerical non-linear method of sloshing in tanks with two-dimensional flow.* Journal of Ship Research. vol. 22. pp. 193-202.

Farhat C., Lesoinne P. (2000). *Two efficient staggered algorithms for the serial and parallel solution of three-dimensional nonlinear transient aeroelastic problems.* Computer methods in applied mechanics and engineering. vol. 182. pp. 499-515.

Felippa C. A., Park K. C. (1980). *Staggered transient analysis procedures for coupled-field mechanical systems.* Computer methods in applied mechanics and engineering. vol. 24. pp. 61-111.

Felippa C. A., Park K. C., Farhat C. (2001). *Partitioned analysis of coupled mechanical systems.* Computer methods in applied mechanical engineering. Vol. 190, pp. 3247-3270.

Giannopapa C. G., (2004), *Fluid structure interaction in flexible vessels*. PhD thesis. King's College London. London.

Gingold R.A., Monaghan J.J. (1977). *Smoothed particle hydrodynamics: theory and application to non-spherical stars.* Mon. Not. R. Astron. Soc. vol. 181. pp. 375–89.

Goudarzi M. A., Sabbagh-Yazdi S. R. (2012). *Investigation of nonlinear sloshing effects in seismically excited tanks.* Soil Dynamics and Earthquake Engineering. vol. 43. pp. 355-365.

Hirt C. W., Amsden A. A., Cook J. L. (1974). *An arbitrary Lagrangian-Eulerian computing method for all flow speeds.* Journal of computational physics. vol. 14. pp. 227-253.

Hirt C. W., Nichols B. D. (1981). *Volume of fluid (VOF) method for the dynamics of free boundaries,* Journal of Computational Physics. vol. 39 pp. 201-225.

Hou G., Wang J., Layton A. (2012). *Numerical Methods for Fluid-Structure Interaction - A Review*. Communications in Computational Physics. Vol. 12. No. 2. pp. 337-377.

Housner G.W. (1963). *The Dynamic Behavior of Water Tanks.* Bulletin of the Seismological Society of America. vol. 53. no. 2. pp. 381-387.

HSE. (2007). *Fluid structure interaction effects on and dynamic response of pressure vessels and tanks subjected to dynamic loading. Part 1: State-of-the-art review.* Research report RR527. Health and Safety Executive

Hübner B., Wahlhorn E., Dinkler D. (2004). *A monolithich approach for fluid-structure interaction using space-time finite elements.* Computer methods in applied mechanics and engineering. vol. 193. pp. 2087-2104.

Hughes, T. J. R., Liu W. K., Zimmerman T. K. (1981). *Lagrangian-Eulerian finite element formulation for incompressible viscous flow.* Computer Methods in Applied Mechanics and Engineering. vol. 29. pp. 329-349.

Iaccarino G., Verzicco R. (2003). *Immersed boundary technique for turbulent flow simulations.* Appl. Mech. Rev. vol. 56(3) pp. 331–347.

Ibrahim R. A. (2005). *Liquid sloshing dynamics: theory and applications.* Cambridge University Press. USA.

Idelshon S. R., Oñate E., del Pin F., Calvo N. (2006). Fluid Structure Interaction Using the Particle Finite Element Method. Computer Methods in Applied Mechanics and Engineering. vol. 195. pp. 2100-2123.

Lucy L.B. (1977). *A numerical approach to the testing of the fission hypothesis.* Astron. J. vol. 82, pp. 1013–1024.

Noh W. F. (1964). *CEL: A time-dependent, two-space-dimensional, coupled Eulerian-Lagrangian code.* Methods in Computational Physics. pp. 117-179. Academic Press. New York.

Matthies H. G., Niekamp R., Steindorf J. (2006). *Algorithms for strong coupling procedures.* Computer methods in applied mechanics and engineering. vol. 195. pp. 2028-2049.

Mittal R., Iaccarino G (2005). *Immersed boundary methods.* Annu. Rev. Fluid Mech. vol. 37. pp. 239–261.

Monaghan J. J. (2005). *Smoothed particle hydrodynamics*. Rep. Prog. Phys. vol. 68. pp. 1703-1753.

Odemir Z., Souli M., Fahjan Y. M. (2010). *Application of nonlinear fluid-structure interaction to seismic analysis of anchored and unanchored tanks.* Engineering Structres. vol. 32. pp. 409-423.

Olovsson L. (2000). *On the Arbitrary Lagrangian-Eulerian Finite Element Method.* Linköping Studies in Technology, Dissertation No. 635, Linköping University, Sweden.

Oñate E., Idelshon S. R., del Pin F., Aubry R. (2004). *The Particle Finite Element Method. An Overview.* International Journal Computational Methods, vol 1. pp. 267-307.

Oñate E., Idelshon S.R., Celigueta M.A., Rossi R., Marti J., Carbonell J.M., Ryzhakov P., Suárez B. (2011). *Advances in the particle finite element method (PFEM) for solving coupled problems in engineering.* Computational Methods in Applied Sciences. vol. 25. pp. 1-49.

Peskin C. S. (1977). *Numerical analysis of blood flow in the heart.* Journal of computational physics. vol. 25. pp. 220-252.

Peskin C. S. (2002). *The immersed boundary method.* Acta numerica. vol. 11. pp. 479-517.

Pope S. B. (2000). *Turbulent flows.* Cambridge University Press. Cambridge. UK.

Reynolds D. D. (1981). *Engineering principles in acoustics: noise and vibration control.* Allyn and Bacon Inc. Boston. USA.

Ross M. R. (2006). *Coupling and Simulation of Acoustic Fluid-Structure Interaction Systems Using Localized Lagrange Multipliers.* PhD thesis. University of Colorado.

Roth T., Silfwerbrand J., Sundquist H. (2002). *Betonginneslutningar i svenska kärnkraftverk.* (In Swedish). SKI Report 02:59. Statens kärnkraftinspektion SKI.

Rugonyi S., Bathe K. J. (2001). *On finite element analysis of fluid flows fully coupled with structural interactions.* Computer Modeling in Engineering and Sciences. vol. 2. pp. 195-212.

Ryzhakov P. B., Rossi R., Idelsohn S. R., Oñate E. (2010). *A monolithic Lagrangian approach for fluid–structure interaction problems.* Computational mechanics. vol. 46. pp. 883-899.

Tenneked H., Lumley J. L. (1972). *A First course in Turbulence.* MIT Press. USA.

Tritton D. J. (1988). *Physical Fluid Dynamics.* Oxford University Press. New York. USA.

Tseng Y. H., Ferziger J.H. (2003). *A ghost-cell immersed boundary method for flow in complex geometry.* Journal of Computational Physics, vol. 192(2). pp. 593–623.

Seyoum S. (2005). *Dynamic Analysis of Liquid Containing Cylindrical tanks.* M.Sc. thesis, Addis Ababa University.

SKI (1992). *Characterization of seismic ground motions for probabilistic safety analysis of nuclear facilities in Sweden*. SKI Technical Report 92:3. Statens Kärnkraftsinspektion, 1992.

Spraque M. A., Geers T. L. (2004). *A spectral-element method for modeling cavitation in transient fluid-structure interaction.* International Journal for Numerical Methods in Engineering. vol. 62. pp. 2467-2499

SOLVIA (2011). *SOLVIA Finite Element System Version 03*, SOLVIA Engineering AB. Västerås. Sweden

Souli M., Benson D. J. (2010). *Arbitrary Lagrangian-Eulerian and Fluid-Structure Interaction: Numerical Simulation.* Wiley-ISTE. London. UK

Souli M., Zolesio M. P. (2001). *Arbitrary Lagrangian-Eulerian and free-surface methods.* Computer methods in applied mechanics and engineering. vol. 191. pp. 451-466.

Sussman T., Sundqvist J. (2003). *Fluid-Structure interaction analysis with a subsonic potential-based fluid formulation.* Computers and Structures. vol. 81 pp. 949-962.

USACE 1110-6051 (2003*). Time-history dynamic analysis of concrete hydraulic structures.* US Army Corps of Engineers. Engineering manual, EM 1110-6051.

US NRC (2007)**.** *Damping values for seismic design of nuclear power plants*. Regulatory Guide 1.61. U.S. Nuclear Regulatory Commission.

van Leer B. (1977). *Towards the ultimate conservative difference scheme. IV. A new approach to numerical convection.* Journal of Computational Physics. vol. 23. pp. 276-299.

Versluis M. (2010). *Hydrodynamic pressures on large lock structures*. MS.c. thesis. TU Delft.

Westergaard H. M. (1931). *Water Pressures on Dams during Earthquakes.* ASCE Transactions, 98 (November), pp 418-433.

Zhang H. Zhang X., Ji S., Gou Y., Ledezma G., Elabbasi N. deCougny H. (2003). *Recent development of fluid-structure interaction capabilities in the ADINA system.* Computer and Structures. vol. 81. pp. 1071-1085.

ELFORSK

SVENSKA ELFÖRETAGENS FORSKNINGS- OCH UTVECKLINGS - ELFORSK - AB

Elforsk AB, 101 53 Stockholm. Besöksadress: Olof Palmes Gata 31
Telefon: 08-677 25 30, Telefax: 08-677 25 35
www.elforsk.se